

AD-A080 037

UNITED TECHNOLOGIES RESEARCH CENTER EAST HARTFORD CONN
BEAMED ENERGY COUPLING STUDIES.(U)

F/G 21/8

JAN 80 M C FOWLER, L A NEWMAN, D C SMITH

F04611-77-C-0039

UNCLASSIFIED

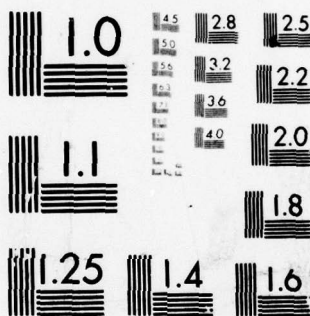
UTRC/R79-922895-25

AFRPL-TR-79-51

NL

1 of 2
AD
A080 037





MICROCOPY RESOLUTION TEST CHART
NATIONAL BUREAU OF STANDARDS-1963-A

① LEVEL II

BEAMED ENERGY COUPLING STUDIES

Final Technical Report

UNITED TECHNOLOGIES
RESEARCH CENTER
EAST HARTFORD, CONNECTICUT 06108

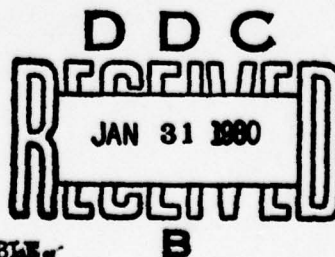
AUTHORS: M.C. FOWLER
L.A. NEWMAN
D.C. SMITH

FOR PERIOD COVERING 1 JUNE 1977 TO MAY 31, 1979

J A N U A R Y 1 9 8 0

Approved for Public Release;
Distribution Unlimited.

AIR FORCE ROCKET PROPULSION LABORATORY
DIRECTOR OF SCIENCE AND TECHNOLOGY
AIR FORCE SYSTEMS COMMAND
EDWARDS AFB, CALIFORNIA 93523



THIS DOCUMENT IS BEST QUALITY PRACTICABLE.
THE COPY FURNISHED TO DDC CONTAINED A
SIGNIFICANT NUMBER OF PAGES WHICH DO NOT
REPRODUCE LEGIBLY.

80 1 31 085

AD A 080037

DDC FILE COPY



NOTICES

When U.S. Government drawings, specifications, or other data are used for any purpose other than a definitely related government procurement operation, the government thereby incurs no responsibility nor any obligation whatsoever and the fact that the government may have formulated, furnished, or in any way supplied the said drawings, specifications, or other data, is not regarded by implication or otherwise, or in any manner licensing the holder or any other person or corporation, or conveying any rights or permission to manufacture, use or sell any patented invention that may in any way be related thereto.

FOREWORD

This final report was submitted by United Technologies Research Center, East Hartford, CT under Contract F04611-77-C-0039, Job Order Number 2308M1QQ, with the Air Force Rocket Propulsion Laboratory, Edwards AFB, CA. The authors wish to gratefully acknowledge the valuable technical assistance of L. Muldrew, B. Doyle, J. Nycz, R. Basilica, and W. New in carrying out the experimental portion of this program.

This report has been reviewed by the Information Office and is releasable to the National Technical Information Service (NTIS). At NTIS it will be available to the general public, including foreign nations.

This technical report has been reviewed and is approved for publication; it is unclassified and suitable for general public release.

Vincent N. Berlan
for CURTIS C. SELPH
Project Manager

FOR THE COMMANDER

Edward E. Stein
EDWARD E. STEIN
Deputy Chief, Liquid Rocket Division

DISCLAIMER NOTICE

**THIS DOCUMENT IS BEST QUALITY
PRACTICABLE. THE COPY FURNISHED
TO DDC CONTAINED A SIGNIFICANT
NUMBER OF PAGES WHICH DO NOT
REPRODUCE LEGIBLY.**

19 REPORT DOCUMENTATION PAGE		READ INSTRUCTIONS BEFORE COMPLETING FORM
1. REPORT NUMBER AFRPL-TR-79-51	2. GOVT ACCESSION NO.	3. RECIPIENT'S CATALOG NUMBER
4. TITLE (and Subtitle) BEAMED ENERGY COUPLING STUDIES.	5. TYPE OF REPORT & PERIOD COVERED FINAL-Jun 77 - May 79	
6. AUTHOR(s) M. C./Fowler, L. A./Newman D. C./Smith	7. AUTHORING ORG. REPORT NUMBER R79-922895-25	8. CONTRACT OR GRANT NUMBER(s)
9. PERFORMING ORGANIZATION NAME AND ADDRESS United Technologies Research Center East Hartford, Connecticut 06108	10. PROGRAM ELEMENT, PROJECT, TASK AREA & WORK UNIT NUMBERS F04611-77-C-0039	11. REPORT DATE January 1980
12. CONTROLLING OFFICE NAME AND ADDRESS Air Force Rocket Propulsion Laboratory Edwards AFB, California 93523	13. NUMBER OF PAGES 136	14. SECURITY CLASS. (of this report) Unclassified
15. MONITORING AGENCY NAME & ADDRESS (if different from Controlling Office)	16. DISTRIBUTION STATEMENT (of this Report) Approved for public release Distribution Unlimited	17. DISTRIBUTION STATEMENT (of the abstract entered in Block 20, if different from Report) Final technical rept. 1 Jun 77-31 May 79
18. SUPPLEMENTARY NOTES		
19. KEY WORDS (Continue on reverse side if necessary and identify by block number) Laser propulsion, molecular coupling, CO ₂ lasers, CO lasers, laser supported plasmas, laser supported flames, absorption coefficient, H ₂ , H ₂ O, D ₂ O, NH ₃ .		
20. ABSTRACT (Continue on reverse side if necessary and identify by block number) This report describes the analytical and experimental results of a study to determine the feasibility of using molecular seeds to couple CO ₂ laser radiation and CO laser radiation to the working fluid, H ₂ , of a high performance rocket thruster. The gas mixtures studied experimentally were H ₂ /H ₂ O, H ₂ /D ₂ O, and H ₂ /NH ₃ at CO ₂ laser wavelengths. The promise of CO as an absorber of CO laser radiation was established analytically. To attain the high temperatures, 1000-6000°K, desired, these mixtures were placed in a cell positioned in a		

409252 gW

UNCLASSIFIED

SECURITY CLASSIFICATION OF THIS PAGE(When Data Entered)

diagnostic apparatus which determined the spatial variation of the mixture absorption coefficient and temperature about the axis of a hot, dense plasma sustained by focused high power CW CO₂ laser radiation. The measurements on these mixtures indicated their performance as couplers to exceed expectations created by the analytical study. In addition, it was found that in the absence of plasma, the temperature of the mixtures could be raised to temperatures as high as 2000-4000°K simply by absorption by the mixture of laser energy at the high power beam focal spot to create the observed laser sustained flame. Further work is needed to determine the conditions under which this flame can be sustained in the laser energized rocket thruster.

ACCESSION for	
NTIS	White Section <input checked="" type="checkbox"/>
DDC	Buff Section <input type="checkbox"/>
UNANNOUNCED	<input type="checkbox"/>
JUSTIFICATION	
BY	
DISTRIBUTION/AVAILABILITY CODES	
Dist. AVAIL. and/or SPECIAL	
A	23P

UNCLASSIFIED

SECURITY CLASSIFICATION OF THIS PAGE(When Data Entered)

TABLE OF CONTENTS

	<u>Page</u>
SECTION I - INTRODUCTION	6
SECTION II - ANALYTICAL RESULTS	8
Introduction	8
Analytical Methods	9
Wavelength Region: $5\mu\text{m}$	13
Wavelength Region: $10.6\mu\text{m}$	37
Conclusions	59
SECTION III - EXPERIMENTAL METHOD	60
Introduction	60
The High Pressure Cell	60
The Gas Handling System	62
Diagnostic Apparatus	64
Detector Signal Conditioning and Storage	67
Data Processing	68
SECTION IV - EXPERIMENTAL RESULTS	74
Refraction Effects	74
The Laser Sustained Flame	74
Example of Data Reduction	79
Measured $k_u(T)$ Curves	86
Coupling Measurements	92
SECTION V - DISCUSSION	96
REFERENCES	98
APPENDIX A - CARBON MONOXIDE LASER LIGHT SOURCE	102
APPENDIX B - COMPUTER PROGRAM "STOR2"	104
APPENDIX C - COMPUTER PROGRAM "RED5"	107
APPENDIX D - COMPUTER PROGRAM "DAL1"	110

TABLE OF CONTENTS (Cont'd)

	<u>Page</u>
APPENDIX E - COMPUTER PROGRAM "P".	112
APPENDIX F - COMPUTER PROGRAM "DRED4".	114
APPENDIX G - COMPUTER PROGRAM "CHOOS2"	117
APPENDIX H - COMPUTER PROGRAM "MASAG5"	120
APPENDIX I - COMPUTER PROGRAM "ABEL8"	125

ILLUSTRATIONS

	<u>Page</u>
1. Equilibrium Chemistry at 10 atm H_2 and one atm CO vs Temperature.	14
2. Absorption Spectra-One atm CO in 10 atm H_2	15
3. CO Absorption Coefficient vs Temperature	17
4. Absorption per cm vs Temperature One atm CO in 10 atm H_2	18
5. Absorption Cross Section for Ground State CO	21
6. CO Saturation Intensity vs Temperature	22
7. Equilibrium Chemistry of 10 atm H_2 and One atm H_2O vs Temperature	23
8. Absorption Spectra-One atm H_2O in 10 atm H_2	26
9. Absorption Coefficient Function $g(W)$ vs W for H_2O ($T=600$ K).	28
10. Absorption Coefficient Function $g(W)$ vs W for H_2O ($T=3000$ K)	29
11. H_2 C and W^* Parameters for ν_2 R Branch vs Temperature	30
12. $\bar{k}(2000\text{ cm}^{-1})$, $\alpha(2012.5\text{ cm}^{-1})/u$ and $\bar{\alpha}(2000-2020\text{ cm}^{-1})$ for one atm H_2O in 10 atm H_2 vs Temperature	31
13. Absorption per cm ($\bar{k}(2000\text{ cm}^{-1})u$) For One atm H_2O in 10 atm H_2 vs Temperature.	33
14. Absorption Spectra-One atm OD in 10 atm H_2	35
15. Absorption per CM for One atm OD in 10 atm H_2 vs Temperature . .	36
16. Equilibrium Chemistry of 10 atm H_2 and One atm D_2O vs Temperature	38
17. Absorption Spectra-One atm H_2O in 10 atm H_2	40
18. Absorption Spectra-One atm HDO in 10 atm H_2	41

ILLUSTRATIONS (Cont'd)

	<u>Page</u>
19. Absorption Spectra-One atm D ₂ in 10 atm H ₂ tm	43
20. Absorption Spectra-One atm D ₂ O in 10 atm H ₂ (D ₂ O Data Base Augmented)	45
21. H ₂ O C and W* Parameters for ν_2 P Branch vs Temperature	47
22. H ₂ O C' and W* Parameters for Rotational Transitions vs Temperature	48
23. \bar{k} (950 cm ⁻¹) and α (945 cm ⁻¹)/u for One Atm H ₂ O in 10 Atm H ₂ vs Temperature	50
24. Absorption per cm (\bar{k} (950 cm ⁻¹)u) for One Atm H ₂ O in 10 Atm H ₂ vs Temperature	51
25. \bar{k} (950 cm ⁻¹) and α (945)/u for One Atm HDO in 10 Atm H ₂ vs Temperature	52
26. \bar{k} (950) and α (945)/u for One Atm D ₂ O in 10 Atm H ₂ vs Temperature	53
27. Absorption per cm (\bar{k} (950 cm ⁻¹)u) for One Atm D ₂ O in 10 Atm H ₂ vs Temperature	55
28. Equilibrium Chemistry of 10 Atm H ₂ and One Atm NH ₃ vs Temperature	56
29. Absorption Spectra-One Atm NH ₃ in 10 Atm H ₂	57
30. Absorption per cm(α (945.94 cm ⁻¹)) for One Atm NH ₃ in 10 Atm H ₂ vs Temperature	58
31. High Pressure Plasma Containment Cell	61
32. Gas Handling System	63
33. Diagnostic Apparatus	65
34. Measured Profiles I_r^* and I_c^* Along with I_r and I_c in the Presence of Laser Sustained Plasma in 11 Atm H ₂	75

ILLUSTRATIONS (Cont'd)

	<u>Page</u>
35. Measured Spontaneous Emission Profiles I_n and I_n'	76
36. Profiles of I_r° , I_c° , I_r , and I_c After Being Processed Through "RED5"	77
37. Beam Profiles in the Absence of Plasma	80
38. Beam Profiles in the Presence of Plasma	81
39. Calculated Values of ΔP and $\Delta\phi$	82
40. Least Squares Fit of ΔP Data	83
41. Least Squares Fit of $\Delta\phi$ Data	84
42. Measured Absorption Per cm vs Temperature (T) - H_2/H_2O	85
43. Measured Absorption Per cm vs Temperature (T) - H_2/D_2O	89
44. Measured Absorption Per cm vs Temperature (T) - N_2/NH_3	91
45. Effect of Power on Coupling	94
46. Effect of P_{D_2O} on Coupling	95

SECTION I

INTRODUCTION

This report deals with the results of an investigation to determine the feasibility of using molecular seeds in high performance working fluids such as hydrogen to absorb energy incident from a distant laser source and utilize this energy to raise the heat content of the working fluid which provides thrust for a rocket. The ultimate objective of a laser thruster program is to generate a high temperature-high pressure gas which is predominantly hydrogen in order to utilize the low mass and therefore high specific impulse of a high temperature hydrogen rocket propellant. The seed molecules are required to absorb the laser energy and thereby increase the gas temperature to the 5000 to 6000°K range. The study is thus part of the beamed energy concept, a highly attractive approach to several rocket applications.

In this study, focus was placed first on calculating analytically and then measuring experimentally the absorption per cm of several molecular seeds at temperatures up to 6000°K. The analytical study considered molecular seed candidates for both the CO (CO, H₂O and OD seed candidates) and CO₂ (H₂O, HDO, D₂O and NH₃ seed candidates) lasers, and the results of that study are presented in the present report. Obtaining temperatures as high as 6000°K in a molecular gas such as hydrogen by conventional methods such as shock tubes is extremely difficult, so a novel heat source was used. This source was a hot dense plasma created in the gas mixture under study by pulsed laser induced gas breakdown and then sustained by the focused output of 7 kW CW CO₂ laser for a time interval on the order of ten seconds. This time limit was set by cell and window heating and is not a fundamental limit to the laser sustained plasma lifetime. The cell containing the mixture under study had been placed in one arm of an interferometer modified in such a way as to permit simultaneous determination of the phase shift and power loss for radiation passing through the heated region of the cell from the interferometer light source, a third CO₂ laser operating at a wavelength of interest to this study. Processing the phase shift and power loss information resulted in obtaining both the magnitude and the temperature dependence of the absorption per cm of the mixture.

The results of the analytical investigation are briefly summarized for 9% mixtures of the candidate in H₂ at 11 atmospheres pressure. Of the candidate molecules for coupling to CO laser radiation, the CO molecule performed the best, exhibiting an absorption per cm of 10^{-2} at temperatures as low as 300°K and a chemical stability which permits this magnitude to be maintained to temperatures in excess of 6000°K. Optical saturation of CO was found not to be a problem at laser intensities of interest to the beamed energy concept. The molecule D₂O was found to be the most effective coupler to CO₂ laser radiation, having an absorption per cm in excess of 10^{-2} in the temperature

interval between 400°K and 4800°K. The molecule H_2O was found to couple effectively to both the CO and CO_2 laser, its absorption per cm 10^{-2} over the temperature range between 400°K to 3800°K in the former case and 1300°K to 4800°K in the latter. The ammonia molecule is a very effective coupler only at temperatures below about 1000°K due to thermal decomposition.

The experimental investigation was carried out only at CO_2 laser wavelengths although a high performance CO probe laser was constructed for measurements at $5\mu\text{m}$.

In carrying out the experimental investigation at CO_2 laser wavelengths, two interesting results were obtained: First, for the binary mixtures $\text{H}_2/\text{H}_2\text{O}$ and $\text{H}_2/\text{D}_2\text{O}$ the measured magnitude of the absorption per cm was significantly higher than calculated analytically while exhibiting a temperature dependence consistent with that determined in the analytical study. Second, it was found that in the absence of any plasma whatsoever, the degree of energy absorption by the $\text{H}_2/\text{H}_2\text{O}$, $\text{H}_2/\text{D}_2\text{O}$ and H_2/NH_3 mixtures from the focused high power CW CO_2 laser was sufficient to heat the mixture locally to temperatures as high as 3900°K, producing a visible discharge of light from the high power laser focal region. The first of these results indicates that H_2O and D_2O are indeed very attractive molecular seeds for coupling laser radiation to rocket thruster working fluids, being even more attractive than was indicated by the analytical study. The second result indicates the possibility that there exists a set of (seed concentration and composition)/(laser incident intensity) conditions for which the laser powered rocket thruster can self activate, that is, bring itself up to a temperature region of high absorptivity to the incident laser radiation without the need of any mixture preheating with electric sparks or any energy adding device other than the incident laser radiation itself.

In the following sections, this investigation is described in detail, beginning in Section II with a description of the analytical results. Section III is a description of the experimental set up, the method of data gathering, and the process of data reduction. The results of the measurements are presented in Section IV, and conclusions drawn from these measurements as well as recommendations for future work are given in Section V.

SECTION II

ANALYTICAL RESULTS

Introduction

This section summarizes the results of the analytical study to determine the optical absorption properties of several molecules at two wavelengths, namely 5.0 μm and 10.6 μm , in the electromagnetic spectrum. The molecules considered were CO, H₂O, HDO, D₂O, NH₃ and OD. For any molecule, the absorption per unit length is the product of the absorption coefficient of the molecule, k , and the molecules' concentration u . This study considered mixtures of the above named molecules in hydrogen at temperatures extending from 300°K to 6000°K, and therefore resolved itself into considering separately the temperature variation of both k , due to molecular energy level positions, partition function values, induced emission, and collisional pressure broadening, and u due to density decrease and shifting chemical equilibria with increasing temperature.

The following subsection is a general discussion of the analytical techniques used to study the temperature dependence of both k and u . In the former case two general approaches are used: 1) a line by line summation over the known optical transitions of the molecule in the wavelength region of interest and 2) an empirical method useful for those situations in which the transitions are too numerous and too complicated to permit rapid line-by-line calculation of k . The former method is amenable to all the molecules studied at temperatures below about 1500°K as both CO and OD are simple enough in structure to permit an easy all inclusive treatment of the transitions of interest while for the other three molecules, tables of transitions and/or energy levels permit calculation of k so long as the temperature is not so high that transitions not attainable from the table become important. The line-by-line calculation is relatively useful at the lower temperatures as it provides a detailed description of the wavelength dependence of k , permitting selection of an effective laser line for coupling energy into the molecule. At higher temperatures, the increase in spectral line density due to excited state transitions and band overlap causes an increase in the accuracy of the empirical band formulae which provide the average value of k , denoted \bar{k} , over a specified wavelength interval.

The results of the application of these techniques to the above mentioned molecules are described. In each case the equilibrium concentration of the molecule is calculated and combined with the calculated value of k . Where warranted, a discussion of the degree to which equilibrium is established in the mixture under practical conditions is included. In addition, for CO, the extent of optical bleaching of the molecule by the coupled radiation field is calculated.

The findings of the study indicate CO as the coupling molecule of choice at 5 μm wavelength and D₂O the molecule of choice at 10.6 μm .

Analytical Methods

Equilibrium Chemistry

For each of the candidate molecules, calculation was made of the equilibrium chemical composition in a mixture initially containing ten atmospheres of hydrogen on one atmosphere of the candidate molecule. The calculations were carried out for constant total pressure, eleven atmospheres, at temperatures up to 6000°K. The calculations were made using a computer program described in detail elsewhere.¹

The density unit used throughout this report, the amagat, is the density of an ideal gas of one atmosphere pressure at 273°K, 2.69×10^{19} molecules per cubic centimeter.

Absorption Coefficient Computation

Line-By-Line Calculation

In this method, the value of the absorption coefficient, k , at frequency ω is expressed as a sum over the contributions at ω of optical transitions centered at frequencies ω_i

$$k(\omega) = \sum_i k_i(\omega, \omega_i) \quad (1)$$

where ω_i the frequency of the i th transition and $k_i(\omega, \omega_i)$ is the contribution of this transition to $k(\omega)$. The value of $k_i(\omega, \omega_i)$ is the product of the line intensity, S_i , for the transition and its associated line factor, L_i , which for the high (10 atmospheres hydrogen) pressures of interest to this study, takes the form peculiar to collisional line broadening:

$$L_i(\omega, \omega_i, \gamma_i) = \gamma_i / (\pi(\gamma_i^2 + (\omega - \omega_i)^2)) \quad (2)$$

In this Expression γ_i is the line width of the transition due to collisions both with other absorbing molecules and with other molecules in the mixture.

For a molecule possessing a permanent dipole moment M_0 and undergoing a transition from a rotational angular momentum state characterized by the quantum number J'' to one characterized by J' the value of S_i , denoted by $S_i(J'', J', \omega)$ for this pure rotational transition is given by ²

$$S_i(J'', J', \omega) = \frac{8\pi^3 M_0^2 \omega_i}{3hcQ(T)} S_{J''}^{J'} \exp(-E_{J''}/kT)(1 - \exp(-hc\omega_i/kT)) \quad (3)$$

where $E_{J''}$ is the energy of the molecule relative to J'' equaling zero in the lowest vibrational state, $Q_i(T)$ is the internal energy partition function of the molecule, and $S_{J''}^{J'}$ is the line strength of the transition and depends on the values of J'' and J' . Where the molecule changes its vibrational as well as its rotational level, S_i is denoted by $S_i(J'', J', v'')$:³

$$S_i(J'', J', v'', \omega) = \frac{S_B \omega_i (v''+1) S_{J''}^{J'}}{\omega_0 Q(T)} \exp(-E_{J''}/kT)(1 - \exp(-hc\omega_i/kT)) \quad (4)$$

where v'' is the lower level vibrational quantum number, ω_0 is the energy separation between the levels (v'' , $J'' = 0$) and ($v'' + 1$, $J' = 0$) and S_B , called the band strength, is the sum of $S_i(J'', J', v'', \omega)$ over all J'' and v'' . For the simple molecules CO and OD the quantities ω_i , $E_{J''}$ and $S_{J''}^{J'}$ are calculated relatively easily and the use of the line by line method to calculate $k(\omega)$ for these molecules will be described. Also, tabulations of ω_i , $E_{J''}$ and $S_{J''}^{J'}$ exist for H_2O , HDO , D_2O and NH_3 so that highly resolved absorption spectra were calculated and the results of those calculations will be given. The fractional power loss per unit length calculated by line-by-line calculations is denoted by α .

Band Model Calculations

As can be seen from the above discussion, line by line calculations are particularly useful when there are either relatively few transitions contributing to the value of $k(\omega)$ or, if this is not the case, the values of S_i and L_i are readily calculable from simple formulas. As will be seen, the latter proves to be the case for simple molecules as CO and OD but not for more complex ones as H_2O , HDO and D_2O and NH_3 . For the latter, line by line calculations may be done at relatively low temperatures using values of $E_{J''}$, ω_i and $S_{J''}^{J'}$ obtained from experimental data and compiled in tabular form by a number of workers. At higher temperatures however, transitions, originating from higher lying energy levels not appearing in the tables become important and the value of $k(\omega)$ calculated using the line by line method is too small. Since for these molecules the necessary additional information needed can not be readily obtained, resort is made to band models in which the

measured absorption coefficient centered at ω and extending over a given frequency interval to either side of ω is set equal to the average of $k(\omega)$ over the interval inside which the line intensity and the interline spacing are assumed to have given mathematical forms. This study uses the work of Ludwig^{3,4} in which the spectral lines of H_2O in both wavelength regions of interest are assumed to be randomly spaced, and the probability of a line having intensity S_i is assumed to have the form

$$P(S_i) = S_0^{-1} \exp(-S/S_0) \quad (5)$$

inside the spatial interval, 25 cm^{-1} in Ludwig's case, for which measurements were made. For this model the experimentally measured value of transmittance, T , takes on a particularly simple form

$$-\ln(T) = \bar{k}ul(1 + \bar{k}ul/4a)^{-1/2} \quad (6)$$

where \bar{k} is the value of k_i averaged over the experimental frequency interval, l is the experimental pathlength and a is the ratio of the line width γ_i to the line density d , the number of absorption lines per cm^{-1} . By determining T at a given temperature over a range of u , one can determine both \bar{k} and d , assuming a knowledge of γ_i .

From his measurements on H_2O , Ludwig⁴ provides values of \bar{k} and d for the frequencies of interest to this study for temperatures up to 3000°K . As the temperature range of interest in the present study extends to 6000°K and the species HDO and D_2O are also of interest, scaling laws were developed to extend Ludwig's results to higher temperatures and the other isotopic species of water, and these scaling laws are now described in general terms with the detailed results presented in following sections.

The scaling laws to be developed are derived from a treatment of \bar{k} given by Penner.⁵ In this treatment, the local average absorption coefficient $k(J'', J', v', \omega)$ is expressed as the ratio of $S(J'', J', v'', \omega)$ to the spacing between adjacent absorption lines which for a simple diatomic molecule is simply $2B$ where B is the molecule's rotational energy constant. For a diatomic molecule in a $^1\Sigma$ electronic state the quantities S_J^{J+1} and S_J^{J-1} and the associated values of ω are given by

$$S_J^{J+1} = J + 1 \quad (7)$$

$$\omega_J = \omega_0 + 2B(J+1)$$

and

$$S_J^{J-1} = J \quad (8)$$

$$\omega_J = \omega_0 - 2BJ$$

For a pure rotational transition, ω_0 is replaced by zero in Eqs. 7 and 8. The partition function Q is factored into its vibrational, Q_v , and rotational Q_r , parts

$$Q_v = (1 - \exp(-hc\omega_0/kT))^{-1} \quad (9)$$

$$Q_r = kT/hcB$$

and functions, defined as $\bar{k}(J'', J', v'', \omega)$ divided by $(1 - \exp(-hc\omega/kT))$ and summed over v'' , can be written in the following form for rotational, $f_r(\omega)$, and rotation-vibration, $f_{rv}(\omega)$ transitions respectively

$$f_r(\omega) = \left(\frac{8\pi^3 M_0^2}{3hc} \right) \left(\frac{\omega^2}{\omega^*{}^2} \right) \exp(-\omega^2/\omega^*{}^2) \quad (10)$$

$$g(\omega) \equiv f_{rv}(\omega) \left(\frac{\omega - \omega_0}{\omega} \right) = \frac{S_B Q_v(T)}{\omega_0} \left(\frac{\omega_0 - \omega}{\omega^*} \right)^2 \exp(-(\omega_0 - \omega)^2/\omega^*{}^2) \quad (11)$$

where

$$\omega^* \equiv (4kTB/hc)^{1/2} \quad (12)$$

Thus it is seen that for either type of transition, the absorption coefficient data can be transformed to a function of frequency which exhibits a maximum at ω or $\omega - \omega_0$ equaling ω^* , which is seen to scale as $(BT)^{1/2}$. Furthermore, in the case of $f_r(\omega)$, its magnitude at ω^* is seen to be independent of both temperature and isotopic species to the extent that M_0 is species independent. In contrast $g(\omega^*)$ is expected to increase with temperature as $Q_v(T)$ does, but, since S_B itself scales with ω_0 , is dependent on isotopic species only to the extent that $Q_v(T)$ is.

In the following subsections it is assumed that $\bar{k}(\omega)$ for a given transition exhibits the same general behavior as described above for $\bar{k}(J'', J', v'', \omega)$ so that $\bar{k}(\omega)$ may be scaled as described for temperature and isotopic species in order to obtain \bar{k} for H_2O , HDO and D_2 at temperatures up to $6000^\circ K$.

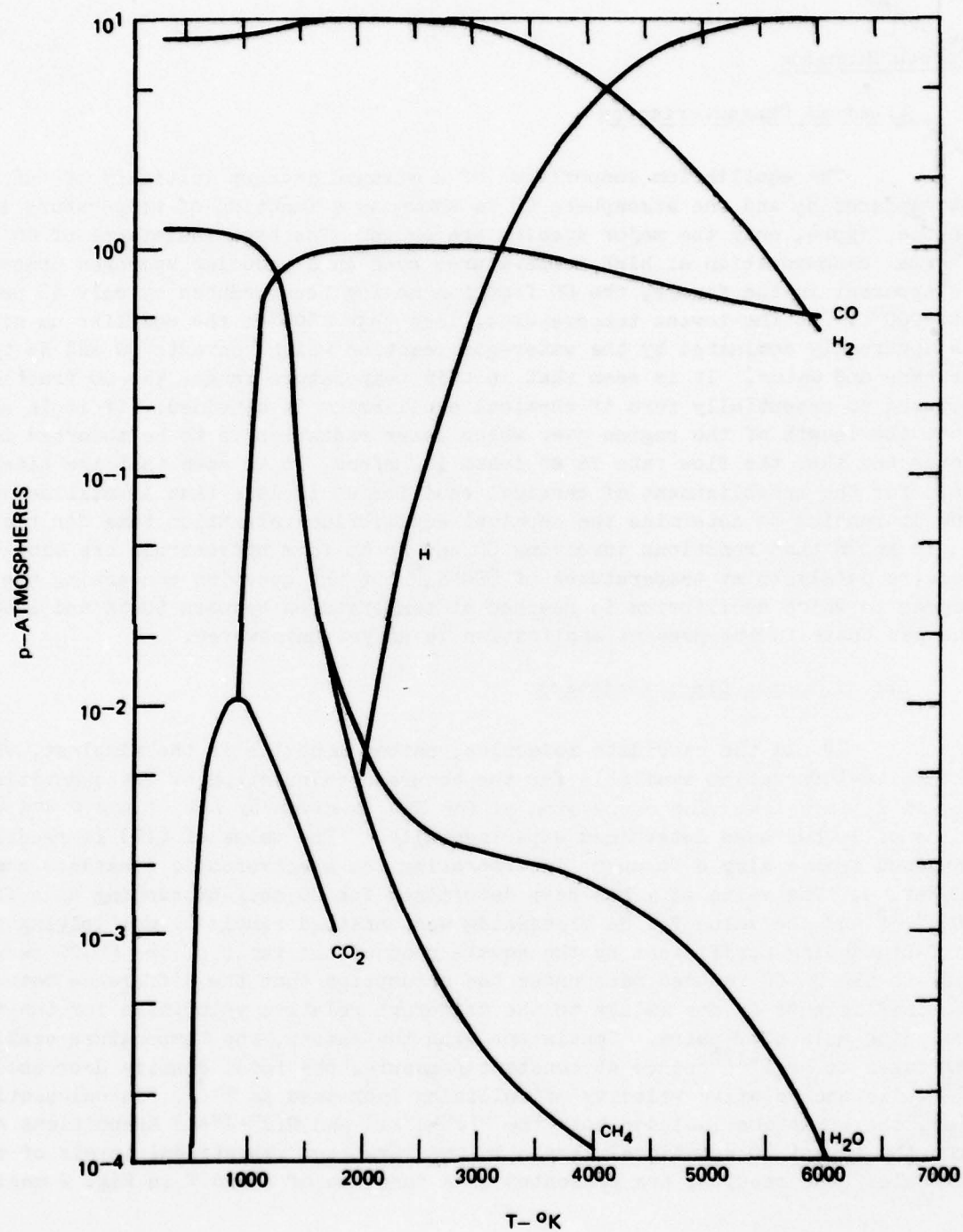
Wavelength Region: 5 μ mCarbon MonoxideChemical Characteristics

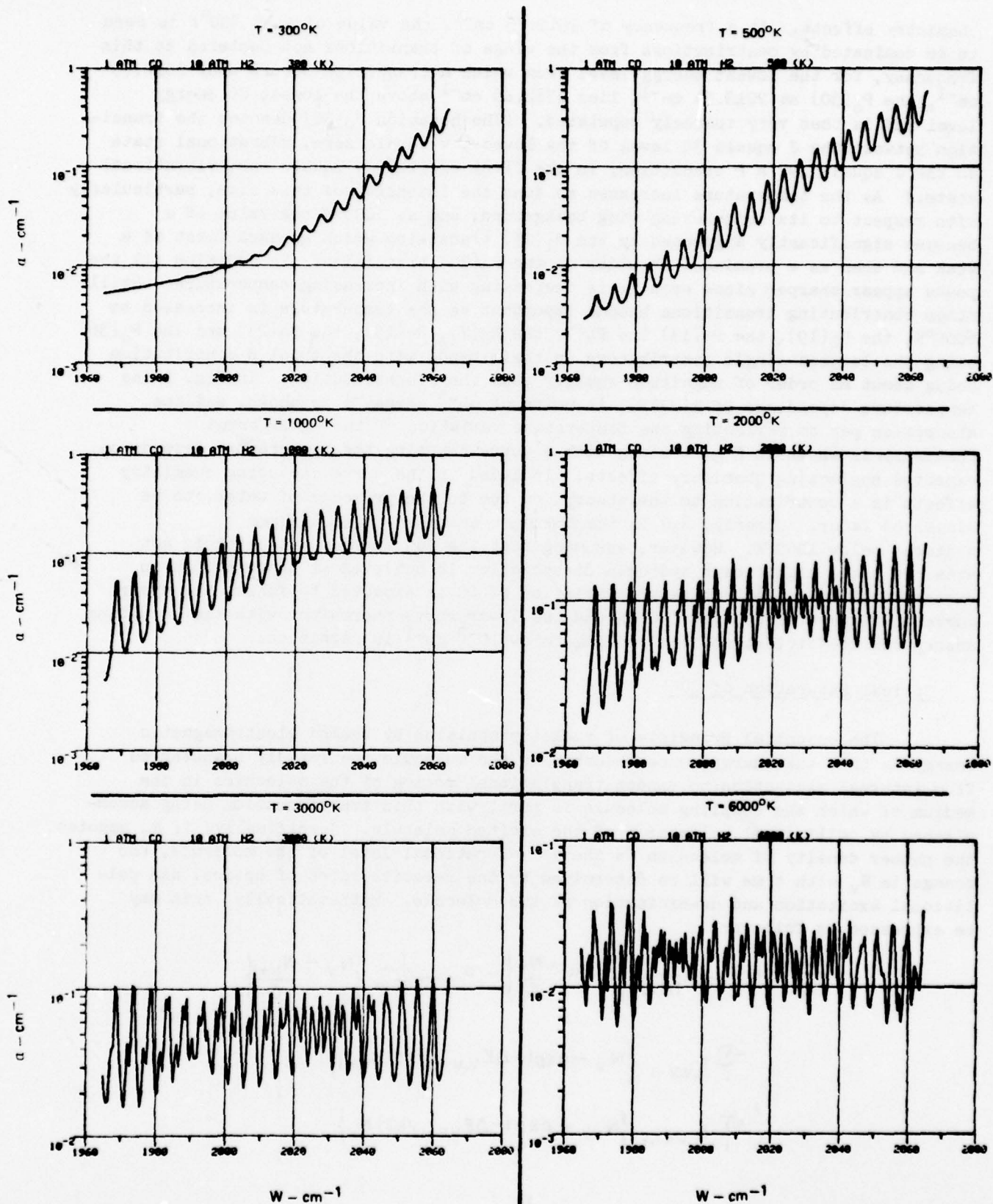
The equilibrium composition of a mixture made up initially of ten atmospheres H_2 and one atmosphere CO is shown as a function of temperature in Fig. 1. In the figure, only the major species are shown. The high resistance of CO to thermal decomposition at high temperature, even in a reducing hydrogen atmosphere, is apparent in the figure, the CO fraction having been reduced by only 50 percent at 6000°K. At the lowest temperatures, less than 1500°K, the equilibrium situation is apparently dominated by the water-gas reaction which converts CO and H_2 to methane and water. It is seen that in this temperature range, the CO fraction is reduced to essentially zero if chemical equilibrium is attained. If it is assumed that the length of the region over which laser radiation is to be absorbed is one meter and that the flow rate is at least 100 m/sec, it is seen that the time available for the establishment of chemical equilibrium is less than 10 milliseconds, and it remains to determine the chemical equilibrium relaxation time for the system. It is known that reactions involving CO and H_2 to form hydrocarbon are slow and require catalysts at temperatures of 600°K,⁶ but the question concerning the degree to which equilibrium is reached at temperatures between 500°K and 1500°K in the gas phase in the present application is as yet unanswered.

Spectroscopic Characteristics

Of all the candidate molecules, carbon monoxide is the simplest, with extensive information available for the accurate calculation of the quantities ω_i , ω_0 and E_0 in Eq. 4. The expression for $S_B^{J''}$ is given by Eqs. 7 and 8 and the value of S_B has been determined experimentally.⁷ The value of $Q(T)$ is readily obtained from a simple formula⁸ incorporating the spectroscopic constants contained in Ref. 9. The value of γ has been determined for CO self-broadening as a function of J'' ,¹⁰ and the value for H_2 broadening was obtained simply by multiplying the self-broadening coefficient by the square root of the ratio of the CO-CO reduced mass to the H_2 -CO reduced mass under the assumption that the difference between the two coefficients is due mainly to the different relative velocities for the two colliding molecular pairs. Consistent with the latter, the temperature scaling of γ was taken to be $T^{-1/2}$ since at constant pressure, the total density decreased as T^{-1} while the relative velocity of collision increased as $T^{1/2}$. In calculating $k(\omega)$, the summation included both the $P(J'' \rightarrow J''-1)$ and $R(J'' \rightarrow J''+1)$ transitions arising from the lowest 40 rotational levels in the first ten vibrational levels of the molecule. The results, are presented as a function of ω and T in Fig. 2 neglecting

EQUILIBRIUM CHEMISTRY OF 10 ATM, H_2 AND 1 ATM CO
VS
TEMPERATURE



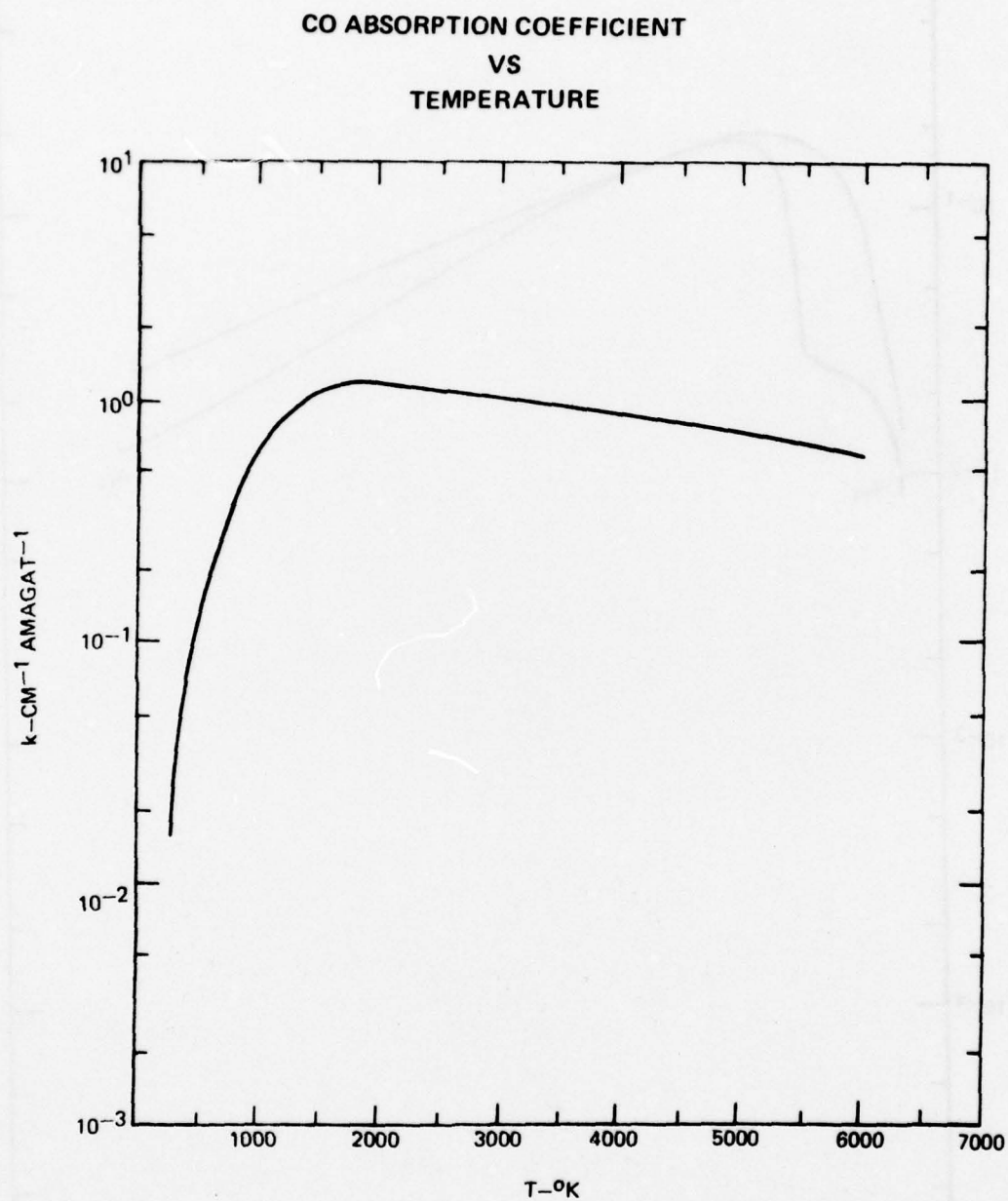


chemistry effects. At a frequency of 2012.73 cm^{-1} , the value of α at 300°K is seen to be dominated by contributions from the wings of transitions not centered at this frequency, for the lowest energy level from which a transition occurs near 2012.73 cm^{-1} , the $P_0(30)$ at 2013.34 cm^{-1} , lies 1782.65 cm^{-1} above the lowest CO energy level and is thus very sparsely populated. (The notation $P_0(30)$ denotes the transition between the J equals 30 level of the lowest, v equals zero, vibrational state to the J equals 29, a P transition, in the first excited, v equals one, vibrational state.) As the temperature increases so does the intensity of this line, particularly with respect to its neighboring wing background, and at 1000°K the value of α becomes significantly augmented by the $P_1(25)$ transition which appears first as a weak and then as a prominent shoulder on the $P_0(30)$ transition. In addition all the peaks appear sharper since each γ_i is decreasing with increasing temperature. Still other contributing transitions become important as the temperature is increased to 6000°K , the $P_2(19)$, the $P_3(13)$ the $P_4(7)$ the $R_6(7)$, $R_7(15)$, the $R_8(25)$ and the $R_9(36)$ being the largest single contributors in their bands with the total R contribution being about an order of magnitude smaller than the P contribution. In Fig. 3 the temperature dependence of $k(2012)$, in units of $\text{cm}^{-1} \text{ amagat}^{-1}$ is shown, and the absorption per cm reflecting the temperature variation of the equilibrium chemistry, is shown in Fig. 4 along with a curve denoting the temperature dependence expected neglecting chemistry effects. Included in the curve including chemistry effects is a contribution to the absorption due to the presence of water, to be discussed later. Clearly, H_2O is the dominant absorber in equilibrium mixtures below 1000°K . However, assuming that the equilibrium situation is not attained until significant hydrogen dissociation is achieved at temperatures in excess of 1500°K , the temperature variation of CO is expected to follow the upper curve at temperatures below 1500°K and the lower curve thereafter with the resulting absorption coefficient nowhere falling below 10^{-2} cm^{-1} in magnitude.

Optical Saturation of CO

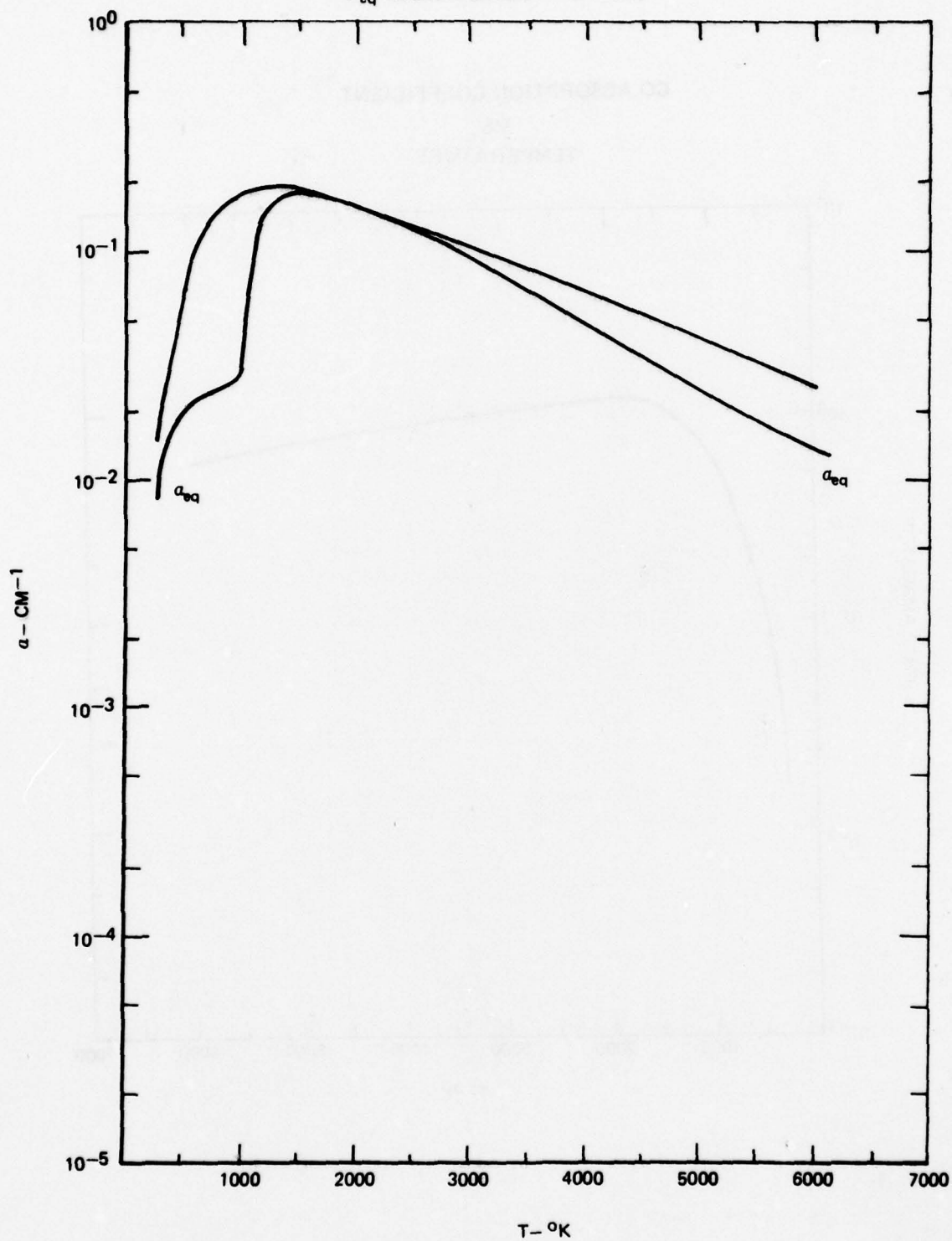
The essential principle of rocket propulsion by beamed electromagnetic energy is that the energy, once absorbed by the molecule, be rapidly transferred from internal excitation to random translational motion of the molecules in the medium of which the coupling molecule is part, with this transformation being accomplished by collisional relaxation of the excited molecule. Specifically, if N_v denotes the number density of molecules in the v^{th} vibrational level of the molecule, the change in N_v with time will be determined by the relative rates of optical and collisional excitation and de-excitation of the molecule. Mathematically, this may be expressed as follows:

$$\begin{aligned} \frac{dN_v}{dt} = & \sigma_{v-1,v} \frac{I}{hc\omega} \left\{ N_{v-1} - \frac{N_v}{C} \right\} - \sigma_{v,v+1} \frac{I}{hc\omega} \left\{ N_v - \frac{N_{v+1}}{C} \right\} \\ & - \sum_i r_{i,v,v-1} \left\{ N_v - \exp(-\Delta E_{v,v-1}/kT) N_{v-1} \right\} \\ & + \sum_i r_{i,v+1,v} \left\{ N_{v+1} - \exp(-\Delta E_{v,v+1}/kT) N_v \right\} \end{aligned} \quad (13)$$



77-12-30-2

ABSORPTION PER CM
VS
TEMPERATURE 1 ATM CO IN 10 ATM H₂
(a_{eq} INCLUDES CHEMISTRY EFFECTS)



77-12-30-8

where the first and second terms represent transitions between the v^{th} and $(v-1)^{\text{th}}$ and $(v+1)^{\text{th}}$ levels respectively caused by the presence of a radiation field of frequency ω and intensity I interacting with molecular absorption cross sections $\sigma_{v-1,v}$ and $\sigma_{v,v+1}$. For a P branch transition¹¹

$$C = \exp(-2JBhc/kT)$$

The second pair of terms in Eq. 13 represents transitions caused by collisions with other molecules. In the above, T represents the gas kinetic temperature, while for the purpose of this calculation, an effective vibrational temperature T_v is defined such that

$$\frac{N_v}{N_{v-1}} = \frac{N_{v+1}}{N_v} \equiv A^{-1} = \exp(\Delta E_{v+1,v} / kT_v)$$

where $\Delta E_{v+1,v}$ is the energy difference between the two vibrational levels, neglecting rotation. Invoking the harmonic oscillator approximation,

$$\sigma_{v,v+1} = (v+1) \sigma_{0,1}$$

$$\sigma_{v-1,v} = v \sigma_{0,1}$$

Landau-Teller selection rules

$$k_{v,v-1} = v k_{1,0}$$

$$k_{v+1,v} = (v+1) k_{1,0}$$

and making the substitution

$$B \equiv \exp(\Delta E_{v+1,v} / kT),$$

Eq. 13 can be written to express the steady state in the form

$$0 = \frac{I \sigma_{0,1}}{hc \omega} \left\{ Av - \frac{v}{C} \right\} - \frac{I \sigma_{0,1}}{hc \omega} \left\{ \frac{(v+1) - \frac{(v+1)}{AC}}{AC} \right\} \quad (14)$$

$$- r_{10} \left\{ v - \frac{Av}{B} \right\} + r_{10} \left\{ \frac{(v+1)}{A} - \frac{v+1}{B} \right\}$$

and the problem becomes one of solving this equation for A , thereby obtaining T_v and the sensitivity of the latter upon I . In the limit of zero intensity T_v and T are seen to be identical while in the limit of infinite intensity, T_v/T is seen to equal $\omega/(2JB)$ a quantity greater than unity, reflecting the fact that without the thermalizing effect of collisions, the molecule becomes vibrationally hot in which case the rate of stimulated emission tends to equal that of absorption, and the molecule thus ceases to couple to the radiation field. At intermediate values of I the degree of decoupling is less and the saturation intensity, I_s is defined as the value of I for which the degree of optical coupling between the v^{th} and $(v-1)^{\text{th}}$ levels is half its value at zero intensity. That is, I_s is the value of I at which

$$A - 1/C = (B - 1/C)/2$$

The value of r_{10} used in the calculation was that reported by Millikan and White¹² for ten atmospheres of H_2 relaxant. The value of $\sigma_{0,1}$ is the value of $k(\omega)$, in units

of cm^2 and calculated for CO using Eqs. 4 and 2 for $L_i(\omega_i, \omega_i, \gamma_i)$, divided by the stimulated emission factor $(1 - \exp(-hc\omega_i/kT))$,

$$\sigma_{01} = \frac{S_i(J'', J', 0, \omega_i)}{\pi \gamma_i (1 - \exp(-hc\omega_i/kT))} \quad (15)$$

and σ_{01} is presented in Fig. 5 as a function of ω_i and T . It is seen that over the entire temperature range of interest to this study the value of the maximum value of σ_{01} is essentially 10^{-19} cm^2 , and this value was used in the calculation, making the calculated value of I_s a lower bound on the true value in the case where the true value of σ_{01} is smaller than 10^{-19} cm^2 .

Considerable physical insight is gained by making several simplifying approximations with the resulting value of I_s being essentially identical to that obtained by solution of Eq. 14 by computer. These approximations are first the setting of C equal to unity and second the removal of the v dependence of each term in Eq. 14. With this done it is found that I_s is the laser intensity for which the rate of excitation of the first vibrational level by the radiation field equals the rate of deexcitation of that level by collisions:

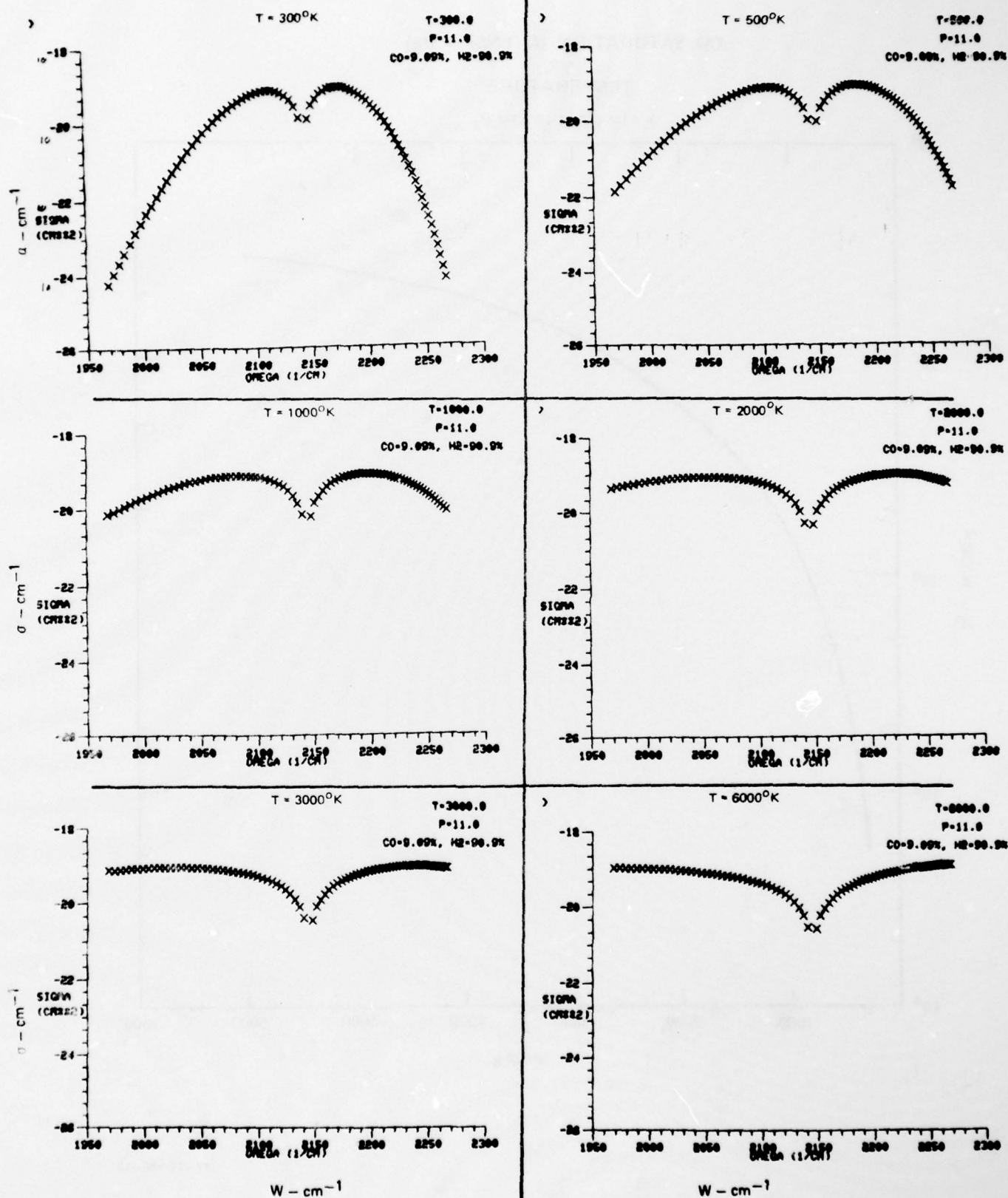
$$I_s = r_{10} hc\omega / \sigma_{01} \quad (16)$$

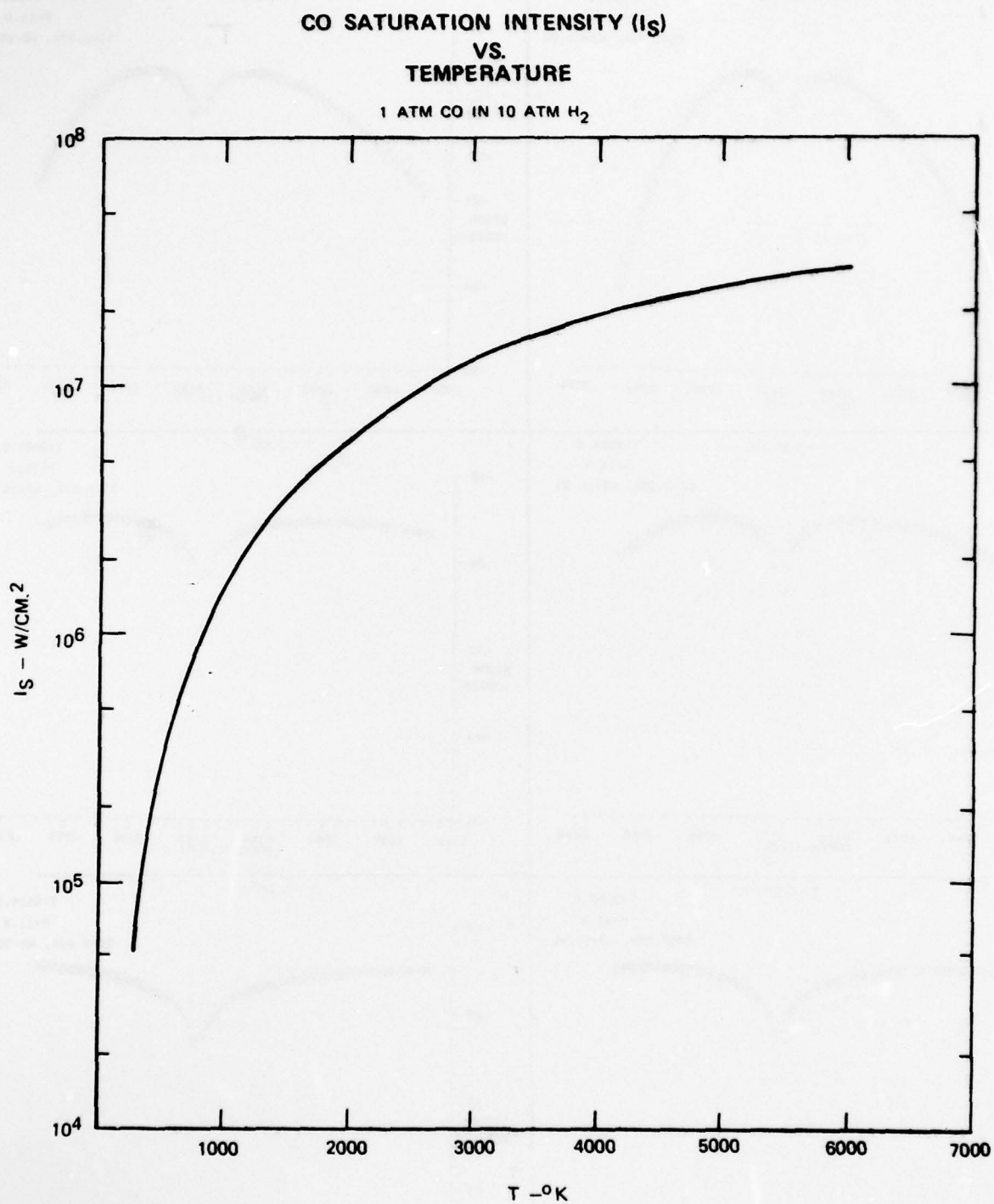
In Fig. 6 the temperature dependence of I_s for a mixture of one atmosphere CO in ten atmospheres H_2 is shown for the σ_{01} value discussed above. It is seen that for the gas mixture considered, I_s greatly exceeds 10^4 W/cm^2 , an intensity of interest to the beamed energy application, over the entire temperature range. It is noted that the large values of I_s obtained are due entirely to the effectiveness of H_2 as a CO vibrational quencher. Were He is to be used in place of H_2 , the value of I_s can be expected to be reduced by nearly two orders of magnitude at 300°K and approximately a factor of 2 at 6000°K .

H_2O

Chemical Characteristics

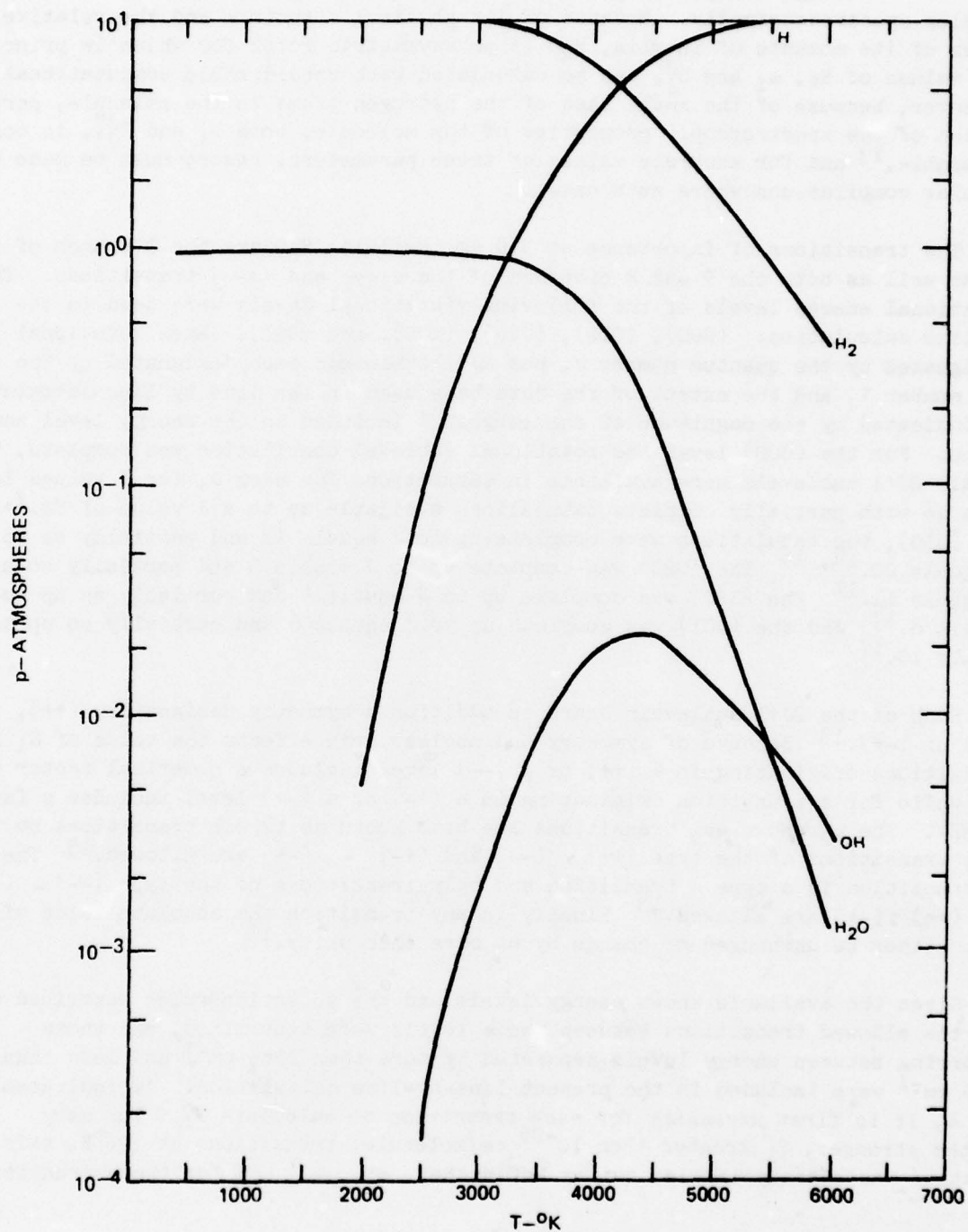
The chemical composition of a preequilibrium mixture of one atmosphere H_2O and ten atmospheres H_2 is shown in Fig. 7 as a function of temperature. It is seen that the H_2O mixture retains its initial composition until a temperature of about 4000° is attained at which point dissociation of the molecule occurs.

ABSORPTION CROSS SECTION (σ) FOR GROUND STATE CO 1 ATM CO IN 10 ATM H₂



77-12-30-15

EQUILIBRIUM CHEMISTRY OF 10 ATM H_2 AND 1 ATM H_2O
VS
TEMPERATURE



77-12-30-9

Spectroscopic Characteristics

Although being chemically quite simple, the H_2O molecule is extremely complex spectroscopically. Because of its physical structure and the relative sizes of its moments of inertia, H_2O is an asymmetric rotor for which in principle the values of E_J , ω_i and S_J'' , can be calculated with considerable computational effort.¹³ Moreover, because of the small mass of the hydrogen atoms in the molecule, perturbation of the spectroscopic properties of the molecule, both ω_i and S_J'' , is considerable,¹³ and for accurate values of these parameters, resort must be made to tabular compilations where such exist.

The transitions of importance at $5.0 \mu m$ involving H_2O are the R branch of the ν_2 as well as both the P and R branches of the $\nu_1-\nu_2$ and $\nu_3-\nu_2$ transitions. The rotational energy levels of the following vibrational levels were used in the line by line calculation: (000), (010), (020), (100), and (001). Each rotational level, designated by the quantum number J , has $2J+1$ sublevels each designated by the quantum number τ , and the extent of the data base used in the line by line calculation is indicated by the magnitude of the largest J included in the energy level compilation. For the (000) level the rotational sublevel compilation was complete, that is all $2J+1$ sublevels were available in tabulations for each J , for J values less than 16 with partially complete tabulations available up to a J value of 22.7,^{14, 15, 16} For (010), the tabulations were complete up to J equals 13 and partially so up to J equals 20.^{14, 16} The (020) was complete up to J equals 6 and partially so up to J equals 11.¹⁴ The (100) was complete up to J equals 4 and partially so up to J equals 8.¹⁷ And the (001) was complete up to J equals 6 and partially so up to J equals 10.¹⁷

Each of the $2J+1$ sublevels bears in addition a symmetry designation ($++$), ($--$), ($+-$) or ($-+$).¹³ Because of symmetry and nuclear spin effects the value of S_i for transitions originating in a ($++$) or a ($--$) level includes a numerical factor of $1/4$ while for a transition originating in a ($+-$) or a ($-+$) level includes a factor of $3/4$. The ν_2 and $\nu_1-\nu_2$ transitions are both known as type b transitions so that only transitions of the type ($++$) - ($--$) and ($+-$) - ($-+$) are allowed.¹³ The $\nu_3-\nu_2$ transition is a type a transition and only transitions of the type ($--$) - ($+-$) and ($++$) - ($-+$) are allowed.¹³ Finally in any transition the absolute value of J must either be unchanged or change by no more than unity.¹³

Given the available known energy levels and the selection rules described above, all the allowed transitions between these levels were determined, and those occurring between energy levels separated by more than 1965 cm^{-1} and less than 2065 cm^{-1} were included in the present line-by-line calculation. As indicated by Eq. 4, it is first necessary for each transition to calculate S_i . For many of the stronger, S_i greater than $10^{-25} \text{ cm/molecule}$, transitions at $296^\circ K$, this calculation was already carried out by McClatchey, et. al,⁷ and for those transitions

$S_i(T)$ was calculated from the expression

$$S_i(T) = \frac{S_i(296)Q(296)}{Q(T)} \exp \left[\frac{E_\ell(T-296)}{296T} \right] \left(\frac{1 - \exp(hc\omega_i/kT)}{1 - \exp(hc\omega_i/296K)} \right) \quad (17)$$

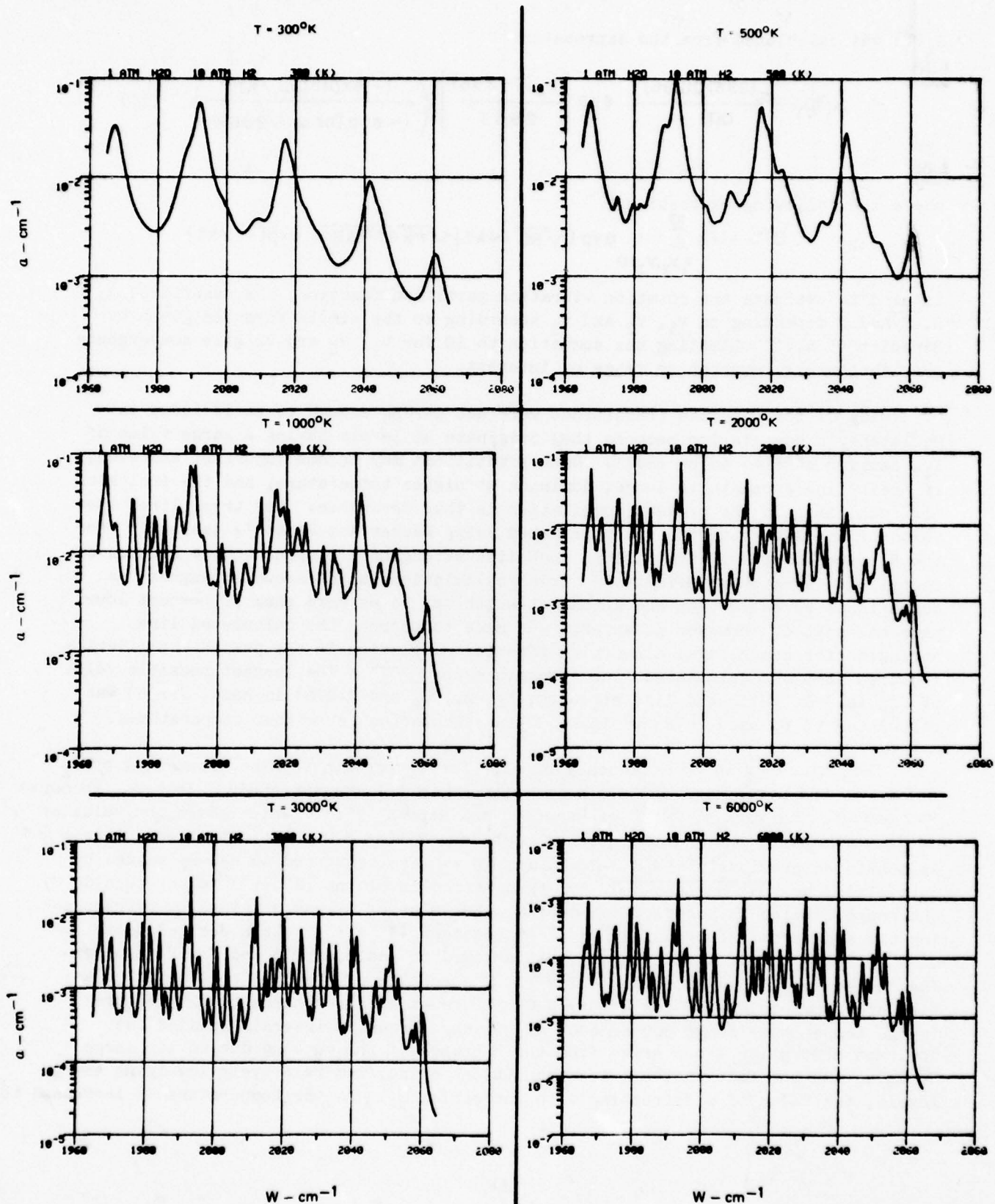
where the following expression¹⁸

$$Q(T) = 1/2 \sum_{v_1, v_2, v_3=0}^{10} \exp(\sqrt{BC}/4kT) \sqrt{\pi k^3 T^3 / ABC} \exp(-E/kT)$$

is used to evaluate the rotation vibration partition function, the quantities A, B, C and E depending on v_1 , v_2 and v_3 according to the simple formulae given by Benedict et al.¹⁹ Limiting the summation to 10 for v_1 , v_2 and v_3 gave convergence over the entire temperature range of interest.

Many of the possible transitions were not strong enough to be included in McClatchey's compilation because they originate at levels having a large value of E_ℓ , causing $e^{-E_\ell/kT}$ to be small. Such transitions may become important and even, if their line strength is large, dominant at higher temperature, and the inclusion of such lines in the present compilation is thus desirable. For these lines the value of the line strength was calculated using Wacker and Pratto's tables.²⁰ For the R branch of the v_2 transition, such line strengths are upper bounds because of centrifugal stretching effects.²¹ Trial calculations using known strengths⁷ as comparisons revealed that the actual strength may be as more than 50 percent lower than calculated. However no attempt was made to correct the calculated line strengths for centrifugal distortion effects. Inclusion in the present compilation required that the calculated line strength exceed 10^{-4} . The largest possible value of $S_{J''}$ is $J+1$. With the line strength, E_ℓ , ω_i , S_B and $Q(296)$ in hand, $S(296)$ was calculated to be used as shown in Eq. 17 in calculations at higher temperatures.

The values given by McClatchey et al.⁷ for γ_i pertain to line broadening by N_2 and O_2 in the atmosphere and are not relevant to the present study. Instead, recourse was made to the work at 298°K of Benedict and Kaplan^{22,23,24} which gives the value of γ_i in terms of J'' and τ'' , the quantum numbers defining H_2O rotational energy levels. As mentioned previously the H_2O-N_2 values of γ_i were converted to H_2O-H_2 values by multiplying by $\sqrt{\mu_{N_2-H_2O}/\mu_{H_2-H_2O}}$. For transitions involving (J'' , τ'') values outside the range studied by Benedict and Kaplan, the value of γ_i was obtained by extrapolating the appropriate curve of γ_i vs J'' at constant ($J'' + \tau''$) to the desired value of J'' . For H_2O self broadening, γ_i was assumed to scale as T^{-1} and for H_2 broadening the scaling was assumed to be $T^{-0.7}$. The results of the line by line calculation are shown in Fig. 8 for a 10:1 H_2O mixture at 11 atmospheres total pressure in the temperature range 300 to 6000°K. In the frequency interval studied the dominant absorption lines arise from the R branch of the v_2 band due to its large S_B value and the fact that all its transitions arise from relatively low lying energy levels, the value of α decreasing with increasing ω_i . As the temperature is increased to



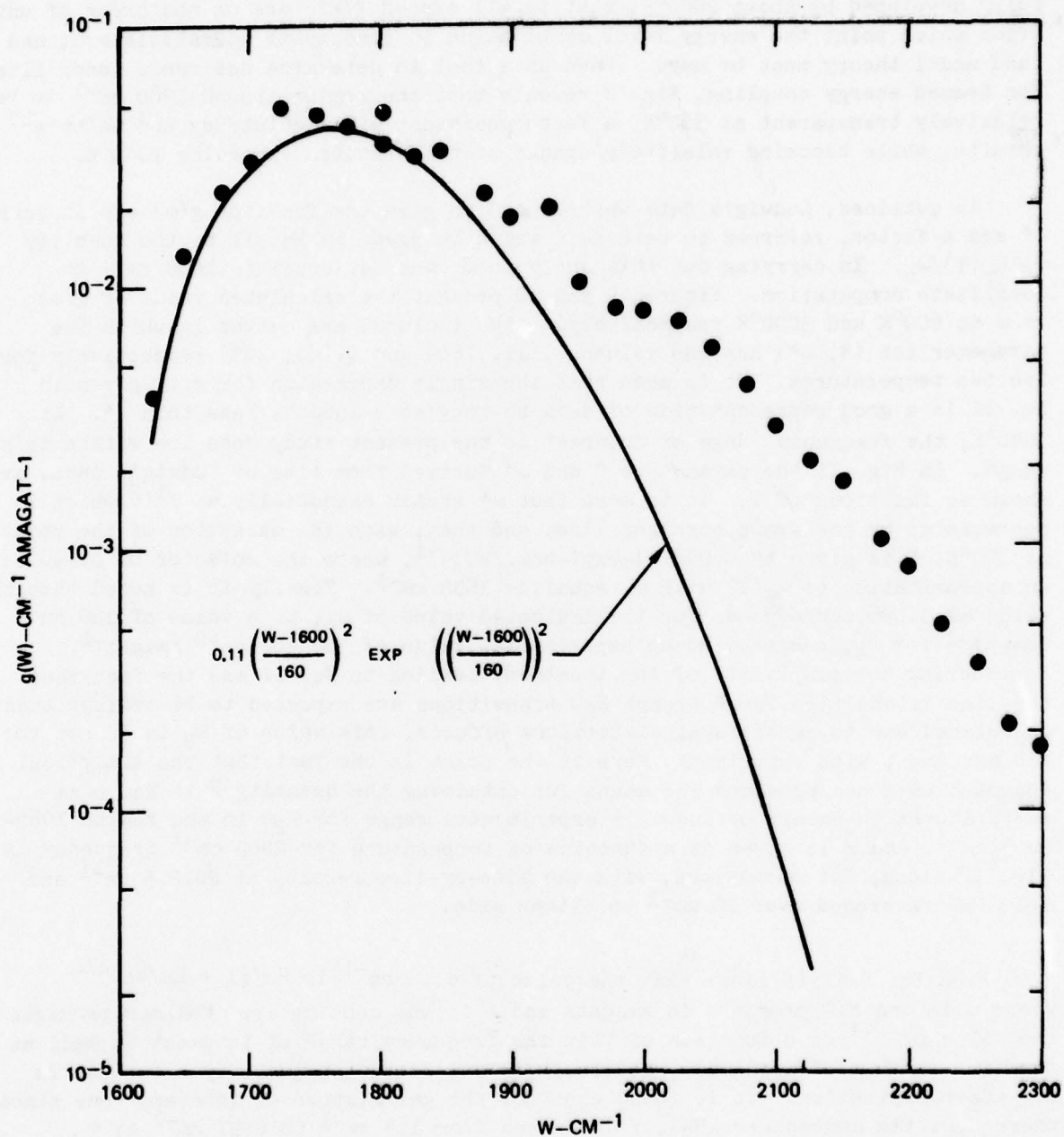
about 2000°K additional transitions become important and more fine structure appears. Apparently the spectrum calculated from the energy level data base is fully developed by about 2000°K, that is, all $\exp(-E/kT)$ are on the order of unity, after which point the energy level compilation is inadequate to calculate α , and band model theory must be used. Used as a tool to determine desirable laser lines for beamed energy coupling, Fig. 8 reveals that the region around 1980 cm^{-1} to be relatively transparent at 300°K, a fact consistent with McClatchey and Selby's²⁵ results, while becoming relatively opaque at temperatures exceeding 1000°K.

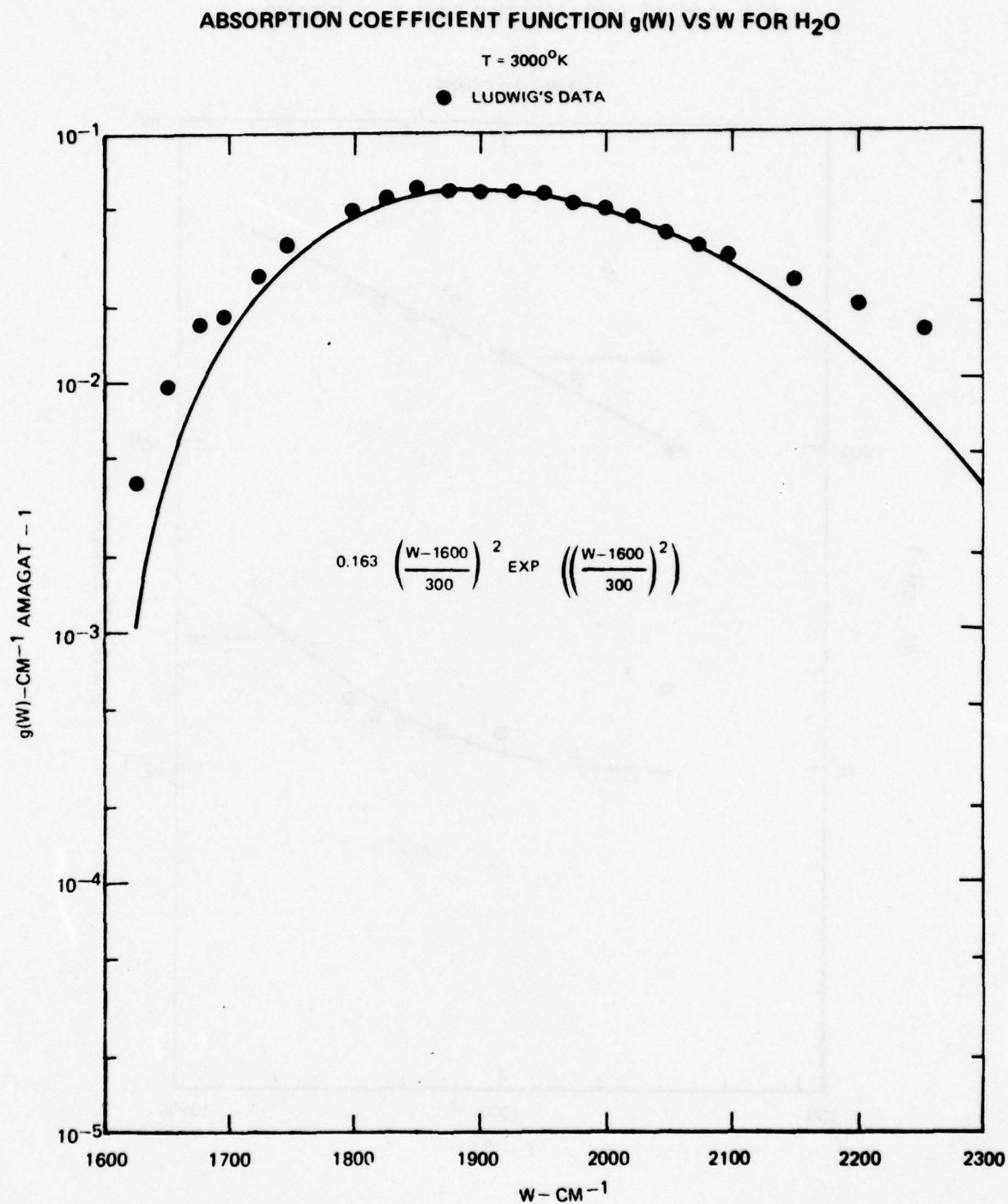
As outlined, Ludwig's data was reduced to give the function $g(\omega)$ and in turn ω^* and a factor, referred to here as C which is given in Eq. 11 by the quantity $S_B Q_V(T)/\omega_0$. In carrying out this analysis ω_0 was set equal to 1600 cm^{-1} to facilitate computation. Figures 9 and 10 present the calculated value of $g(\omega)$ vs ω at 600°K and 3000°K respectively. Also included are curves in which the parameter set (C, ω^*) has the values (.111, 160) and (.163, 300) respectively for the two temperatures. It is seen that the single expression for $g(\omega)$ given in Eq. 11 is a good representation of data so long as $\omega - 1600$ is less than ω^* . At 3000°K, the frequency range of interest to the present study does lie within this range. In Fig. 11 the parameters C and ω^* derived from fits of Ludwig's data, are shown as functions of T . It is seen that ω^* scales essentially as $T^{1/2}$ which is represented by the drawn straight line, and that, with the exception of the point at 300°K, C is given by $0.098 (1 - \exp(-hc\omega_0/kT))^{-1}$, where the cofactor of 0.098 is an approximation to $Q_V(T)$ with ω_0 equaling 1600 cm^{-1} . Finally it is noted that the value of 0.098 corresponds for the indicated value of ω_0 , to a value of 160 cm^{-2} amagat $^{-1}$ for S_B , compared to an experimental value of 300 ± 60 cm^{-2} amagat $^{-1}$. Considering the simplicity of the treatment leading to Eq. 11 and the fact that the line intensities for R branch H_2O transitions are expected to be smaller than calculated due to centrifugal distortions effects, this value of S_B is in not too bad agreement with experiment. More to the point is the fact that the analytical approach used has provided the means for obtaining the quantity \bar{k} in Eq. 6 at temperatures in excess of Ludwig's experimental range for H_2O in the region 1965-2065 cm^{-1} , and \bar{k} is given as a function of temperature for 2000 cm^{-1} frequency in Fig. 12 along, for comparison, with the line-by-line results at 2012.5 cm^{-1} and 2010 cm^{-1} averaged over 10 cm^{-1} to either side.

From Eq. 6 it is clear that the value of α in cm^{-1} is $\bar{k}u/(1 + \bar{k}u/4a)^{1/2}$ where u is the H_2O pressure in amagats and l is one centimeter. Malkmus provides the value of d^{-1} as a function of T in the frequency range of interest as well as the line width coefficients γ_i necessary to calculate the quantity a for use in the above expression. It is found that for the gas mixture of interest (one atmosphere H_2O , ten atmospheres H_2), γ decreases from 1.3 cm^{-1} to 0.21 cm^{-1} as T increases from 300°K to 6000°K while d^{-1} increases from .16 cm to 4400 cm over this temperature range at 2000 cm^{-1} so that $(1 + \bar{k}u/4a)^{1/2}$ is essentially unity throughout the temperature range, and α corresponds to $\bar{k}u$.

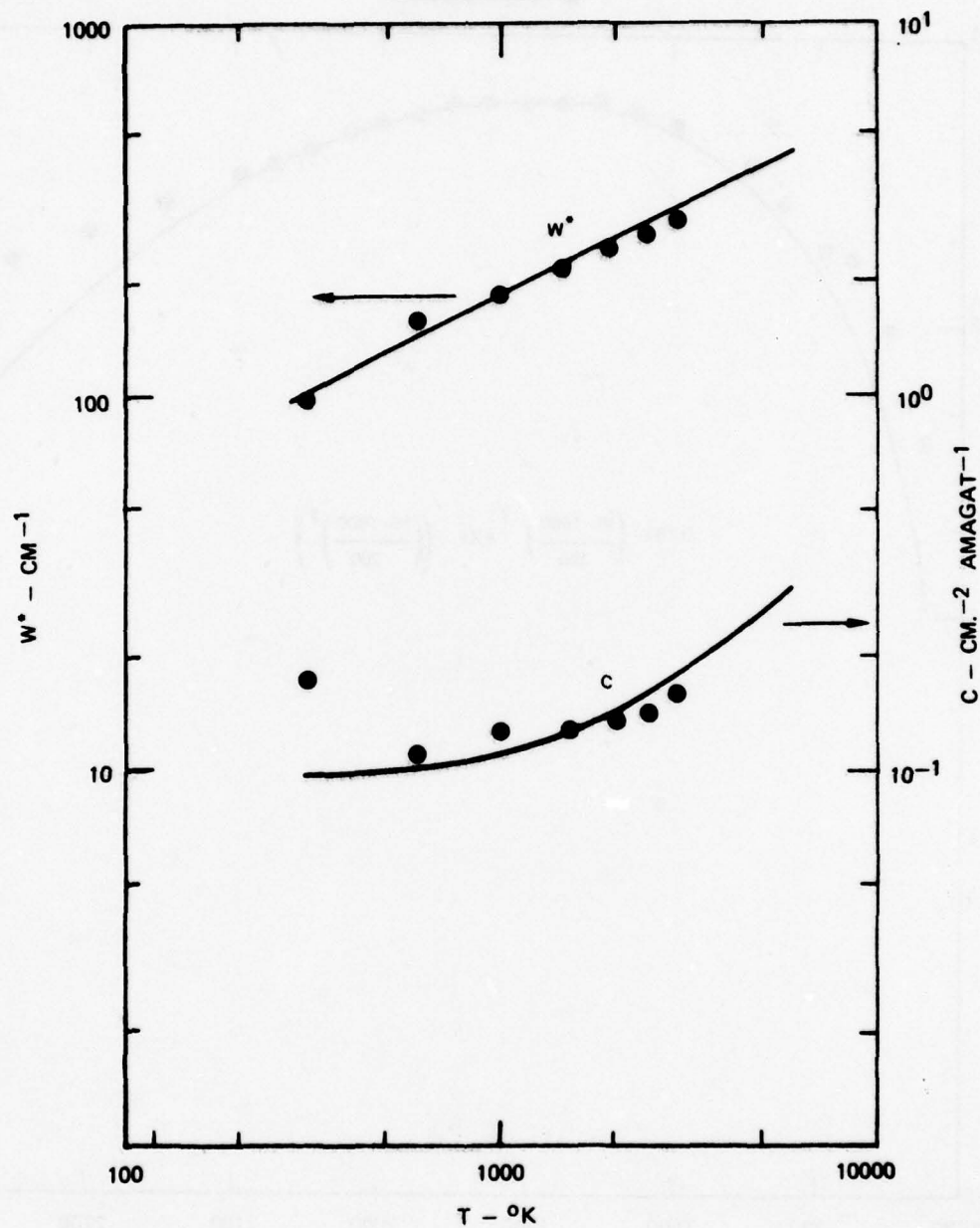
ABSORPTION COEFFICIENT FUNCTION $g(W)$ VS W FOR H_2O

● $T = 600^\circ K$
LUDWIG'S DATA

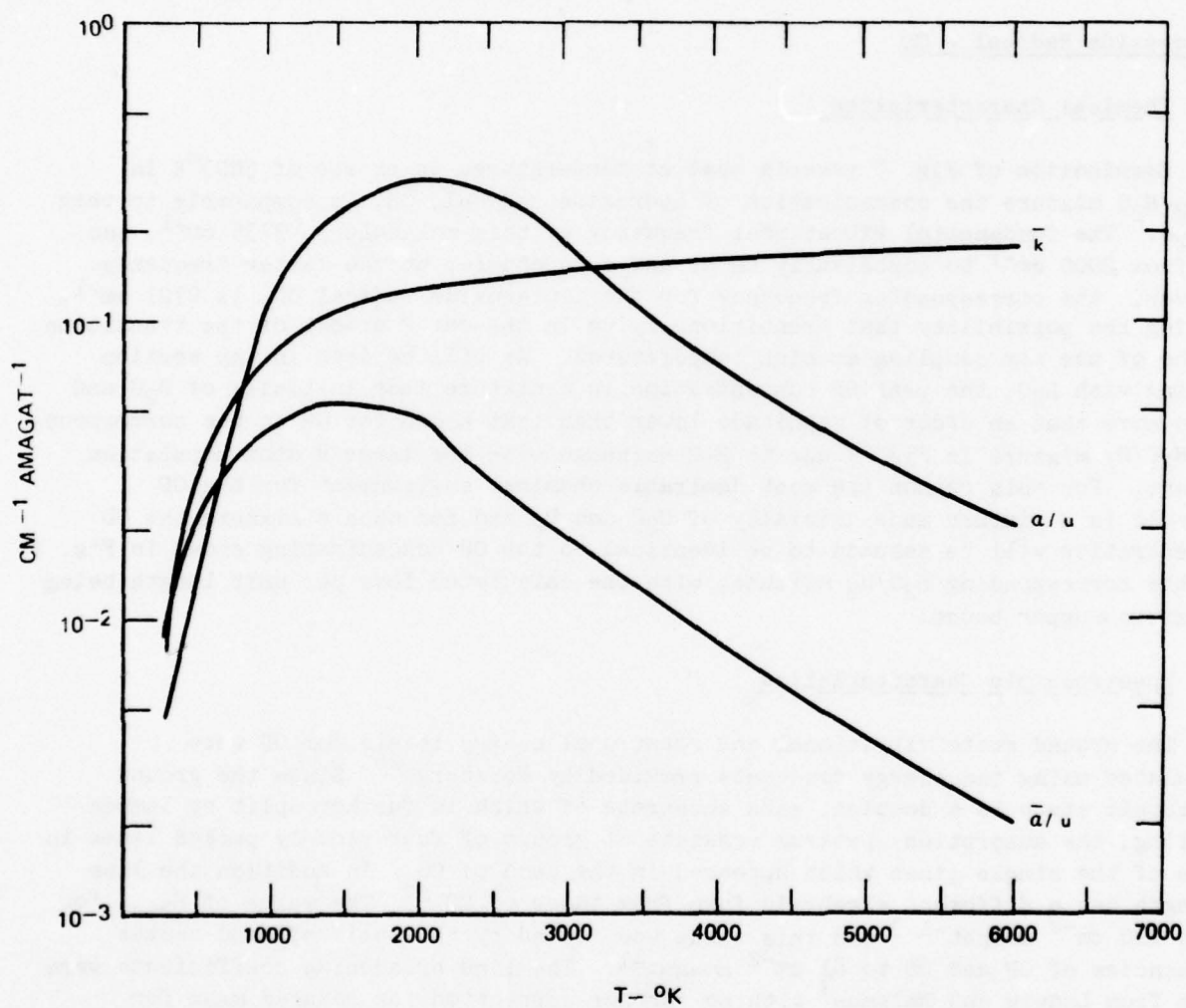




H₂O C AND W* PARAMETERS FOR ν_2 R BRANCH
VS.
TEMPERATURE



\bar{k} (2000 CM^{-1}), a ($2012.5 \text{ CM}^{-1}/u$), AND \bar{a} ($2000-2020 \text{ CM}^{-1}$) FOR 1 ATM H_2O IN 10 ATM H_2
VS
TEMPERATURE



In Fig. 13 \bar{k} is given as a function of temperature at 2000 cm^{-1} for both the case in which no chemical decomposition of H_2O is assumed to occur and the case in which the H_2O pressure is assumed to be the equilibrium value shown in Fig. 7. Examining Figs. 12, 13 and 8 and recalling that \bar{k} is derived from measurements which are essentially an average over a 25 cm^{-1} interval, the results of the two calculations seem consistent at temperatures below 2000°K above which the data base of the line by line calculation becomes inadequate for accurate calculation of α . It is seen that the absorption per unit length for H_2 is on the order of 10^{-2} cm^{-1} , for a desirable CO laser line such as those near 1980 cm^{-1} until temperature in excess of 4000°K are reached in which case the establishment of an unfavorable chemical equilibrium situation renders H_2O essentially useless as a CO laser coupler.

Deuterioxide Radical - OD

Chemical Characteristics

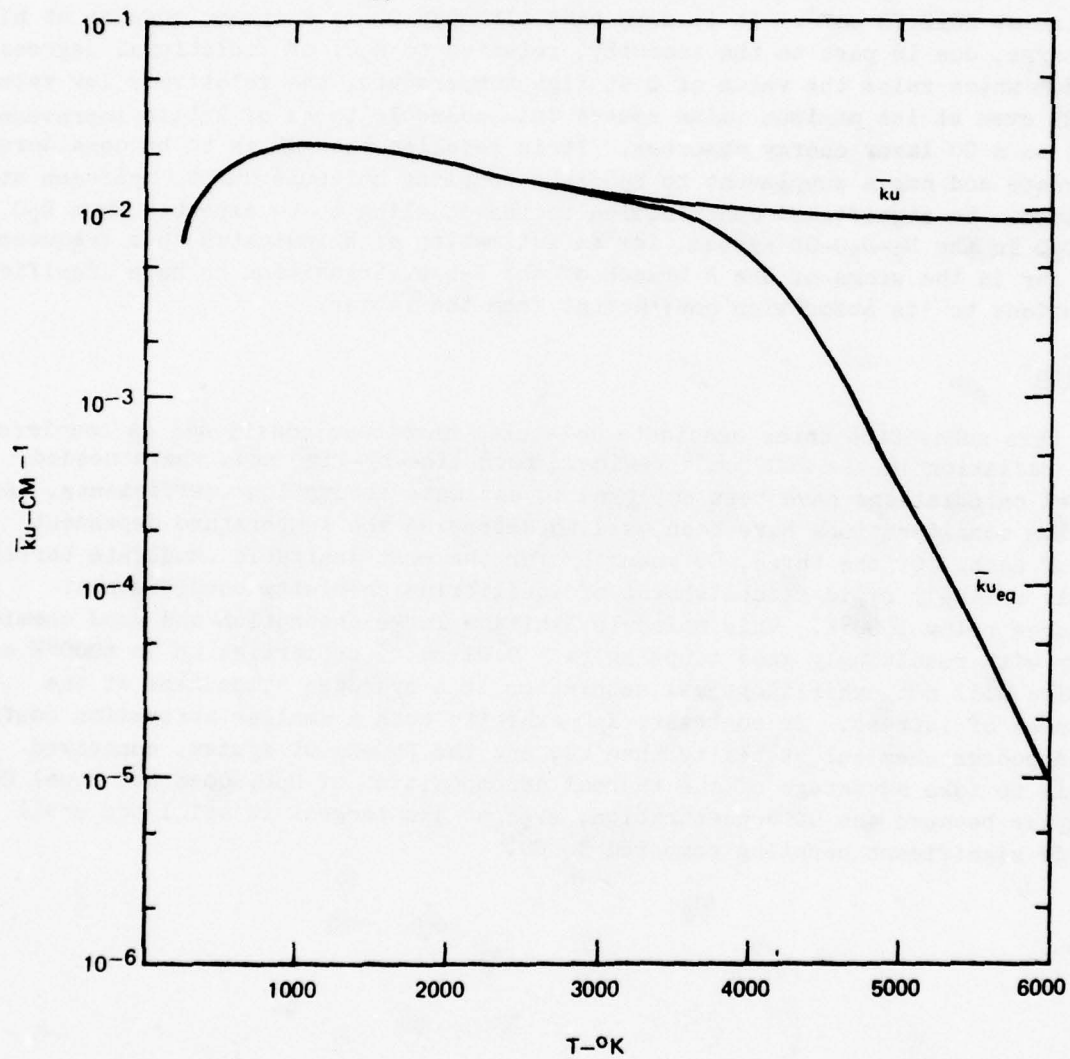
Examination of Fig. 7 reveals that at temperatures in excess of 5000°K in an $\text{H}_2\text{-H}_2\text{O}$ mixture the concentration of hydroxide radical, OH, is comparable to that of H_2O . The fundamental vibrational frequency of this molecule is 3735 cm^{-1} , too far from 2000 cm^{-1} to conceivably be of use as a coupler at the latter frequency. However, the corresponding frequency for the deuterioxide radical OD, is 2721 cm^{-1} , raising the possibility that transitions lying in the far P branch of the transition may be of use for coupling at high temperatures. As will be seen in the section dealing with D_2O , the peak OD concentration in a mixture made initially of D_2O and H_2 is more that an order of magnitude lower than that shown for OH in the corresponding $\text{H}_2\text{O}/\text{H}_2$ mixture in Fig. 7 due to H-D exchange with the large H atom population present. For this reason the most desirable chemical environment for the OD molecule is a mixture made initially of D_2O and D_2 and for such a mixture the OD concentration will be assumed to be identical to the OH concentration shown in Fig. 7 for the corresponding $\text{H}_2\text{O}/\text{H}_2$ mixture, with the calculated loss per unit length being therefore an upper bound.

Spectroscopic Characteristics

The ground state vibrational and rotational energy levels for OD were calculated using the energy constants provided by Herzberg.²⁶ Since the ground electronic state is a doublet, each substrate of which is further split by lambda doubling, the absorption spectrum consists of groups of four closely packed lines in place of the single lines which appeared in the case of CO. In addition the line strength has a different algebraic form from those of CO.²⁷ The value of S_{Band} for OH is $110\text{ cm}^{-2}\text{ amagat}^{-1}$ ³ and this value was scaled by the ratio of band center frequencies of OH and OD to $81\text{ cm}^{-2}\text{ amagat}^{-1}$. The line broadening coefficients were taken from Ludwig and Malkmus³ with no further correction for reduced mass for broadening by D_2 . The value of $Q(T)$ was calculated by summation over the first 60 rotational levels and first 11 vibrational levels of the four electronic sublevels.

ABSORPTION PER CM (\bar{k} (2000 CM.⁻¹)_u) FOR 1 ATM H₂O IN 10 ATM H₂
VS.
TEMPERATURE

(_{u_{eq}} INCLUDES CHEMISTRY EFFECTS)



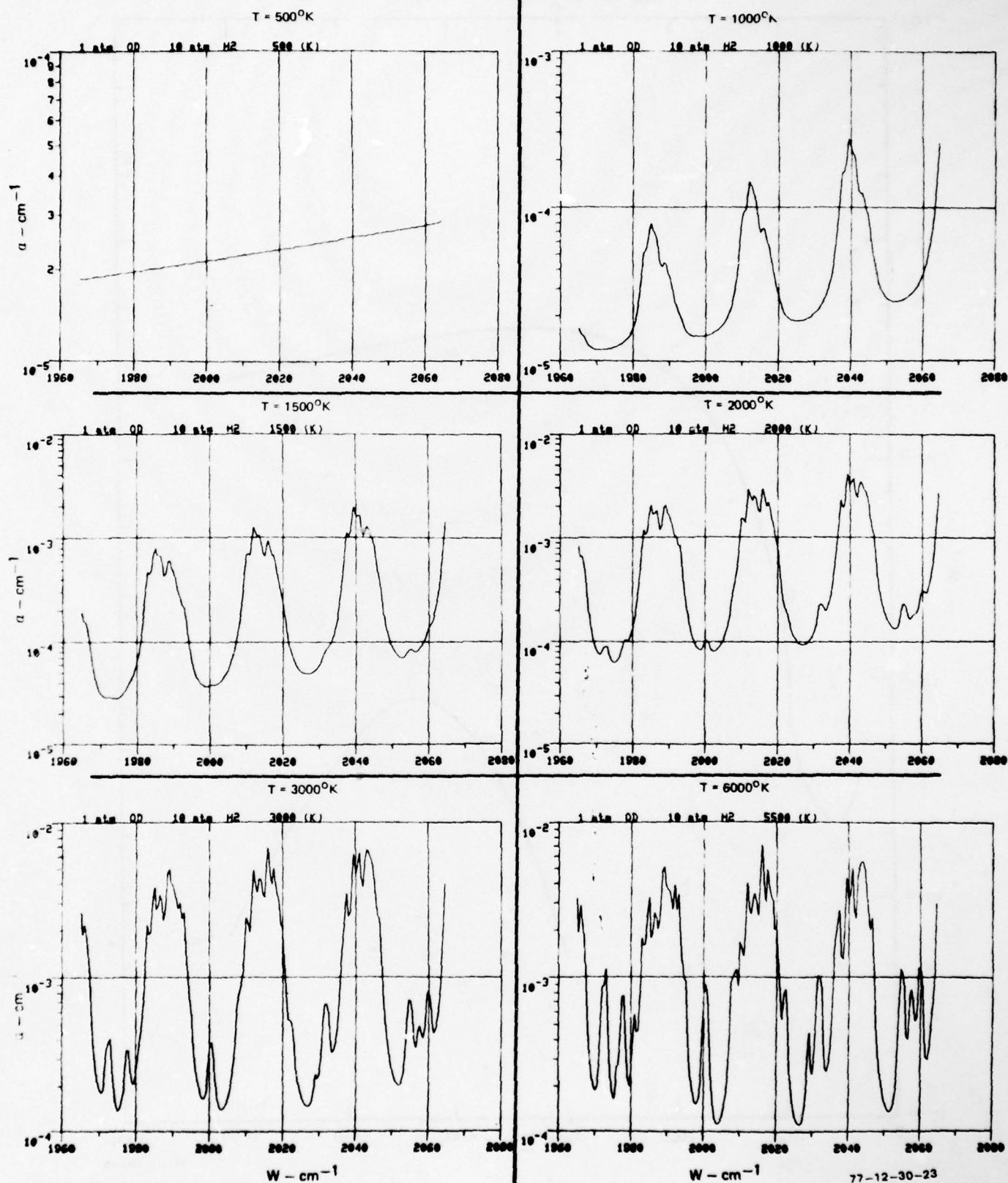
convergent values of Q being obtained over the entire range of interest. Line by line calculation of α for one atmosphere OD in 10 atmospheres D_2 was carried out for the temperature range 300°K to 6000°K. The calculation included P transitions up to $P_9(30)$ for each of the four electronic sublevels, and the results are shown in Fig. 14. At 1000°K the three main peaks shown are each made up of transitions from each the four electronic states mentioned above with the peaks centered on the $P_0(24)$, $P_0(25)$ and $P_0(26)$ transitions. Increase in temperature results in significant contributions from excited vibrational states. The value of α_{OD} with and without equilibrium chemistry considerations included is shown in Fig. 15 for the $P_3(13)$ CO laser line at 2012.73 cm^{-1} . It is seen that although OD is a strong coupler at high temperatures, due in part to the scarcity, relative to H_2O , of vibrational degrees of freedom which raise the value of Q at high temperature, the relatively low value of α_{OD} at even at its maximum value causes this molecule to be of little improvement over H_2O as a CO laser energy absorber. It is recalled that OD is to be considered an alternate and not a supplement to H_2O as a coupling molecule due to hydrogen atom interchange. No significant contribution to the coupling to be expected from D_2O in the D_2O in the D_2 - D_2O -OD system, for an estimation of k indicates this frequency lies too far in the wings of the R branch of the $D_2O \nu_2$ transition to have significant contributions to its absorption coefficient from the latter.

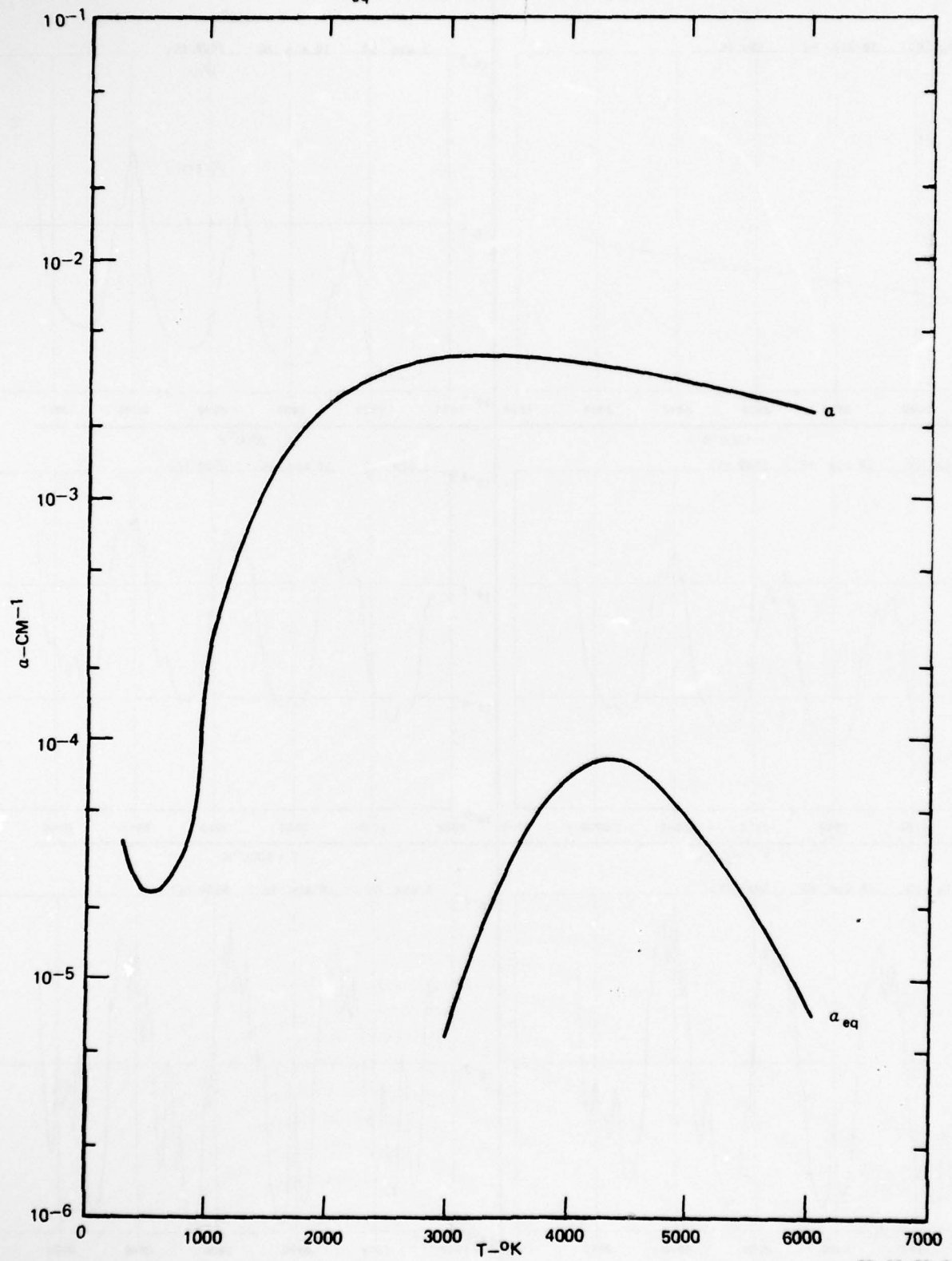
Discussion

In this subsection three candidate molecules have been considered as couplers to CO laser radiation in the 2000 cm^{-1} region. Both line-by-line and, where needed, band model calculations have been employed to estimate absorption coefficients, and equilibrium considerations have been used to determine the temperature dependent density of each. Of the three, CO seems by far the most desirable candidate barring the highly unlikely rapid establishment of equilibrium chemistry conditions at temperatures below 1500°K. This molecule exhibits large absorption and good chemical stability with resultingly good coupling ($\alpha > 0.01 \text{ cm}^{-1}$) properties up to 6000°K and in addition will not exhibit optical saturation in a hydrogen atmosphere at the temperatures of interest. In contrast, H_2O exhibits both a smaller absorption coefficient and poorer chemical stability than CO, and the D_2O - D_2 -OD system, conceived originally to take advantage of the thermal decomposition of D_2O , does not equal CO as a coupler because the OD concentration, even at its largest is still too small to provide significant coupling compared to CO.

ABSORPTION SPECTRA—ONE ATM OD IN 10 ATM H₂

FIG. 14



ABSORPTION PER CM FOR 1 ATM OD IN 10 ATM H₂ VS TEMPERATURE $(\alpha_{eq}$ - INCLUDES CHEMISTRY EFFECTS)

77-12-30-6

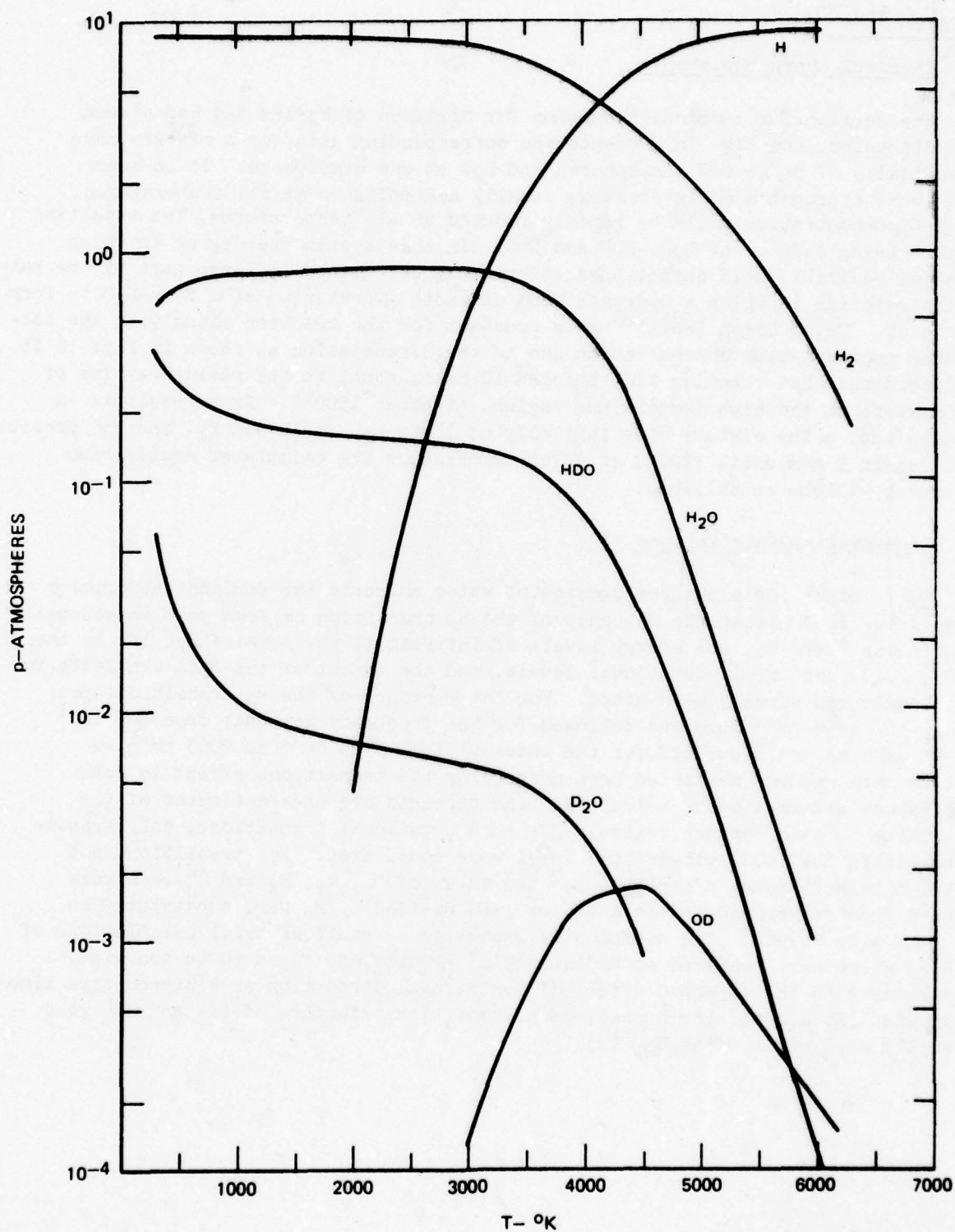
Wavelength Region: 10.6 μm D₂O, H₂O and HDOChemical Characteristics

The equilibrium chemical situation for mixtures of H₂ and H₂O has already been discussed, and Fig. 16 presents the corresponding data for a mixture made up initially of H₂ at ten atmospheres and D₂O at one atmosphere. It is seen that, were hydrogen atom interchange readily accomplished at all temperatures, the D₂O concentration would be rapidly reduced at all temperatures, the resulting mixture being made up of H₂O, HDO and D₂O. In this system the degree to which chemical equilibrium is established is probably determined in large part by the rate of the reaction in which a hydrogen atom extracts a deuterium atom from D₂O to form HD and OD. Using Dixon Lewis'²⁸ rate constant for the reaction along with the calculated hydrogen atom concentration due to the dissociation as shown in Fig. 16 it is determined that reaction time becomes 10 msec, equal to the residence time of the mixture in the high temperature region, at about 1500°C. As a result it is assumed that a the mixture made initially of 1 atm D₂O in 10 atm H₂, the D₂O pressure will remain 1 atm until 1500°C at which temperature the calculated equilibrium pressures will be established.

Line-By-Line-Calculations

H₂O - Since for all three species of water molecule the dominant absorption lines arise from either the P branch of the ν_2 transition or from pure rotational transitions (type b), the energy levels of interest in the case of H₂O lie in the (000), (010) and (020) vibrational levels, and the extent of the data available for this levels has already been noted. For the P branch of the ν_2 transition, precisely the same procedure was followed for the frequency interval from 895 cm^{-1} to 995 cm^{-1} as was described for the interval from 1965 cm^{-1} to 2065 cm^{-1} so that no more need be mentioned here concerning the transitions except to note that Wacker and Pratto's²⁰ calculated line strength are underestimates of the true value in the P branch region. For pure rotational transitions, only transitions within the (000) vibrational level were considered. For transitions not included in McClatchey's compendium,⁷ the value of M_0 , ω_i , E_k and $S_{J,J''}^J$, as calculated from Wacker and Pratto's tables and divided by 2, were substituted in Eq. 3 to give $S(296)$. The division by 2 came as a result of trial calculations of $S_i(296)$ which were compared to McClatchey's⁷ results and found to be too high, consistent with the expected effect of centrifugal distortion on R branch type line strengths. As before, the nuclear spin statistical factors of 1/4 and 3/4 were correctly applied in using Eq. (3).

EQUILIBRIUM CHEMISTRY OF 10 ATM H_2 AND 1 ATM D_2O
VS
TEMPERATURE



77-12-30-4

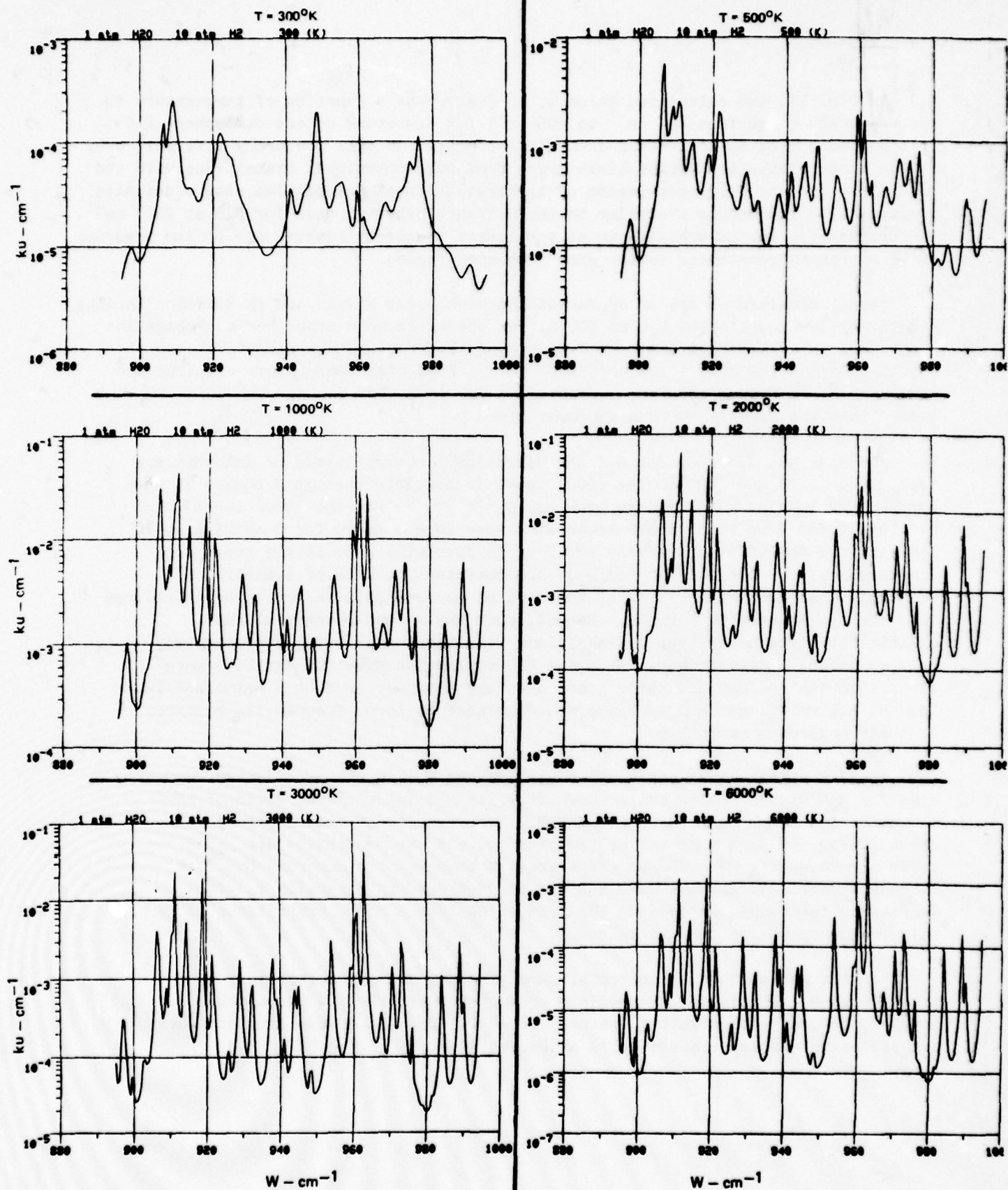
In Fig. 17, the calculated value of α is given as a function of temperature in the frequency range from 895 cm^{-1} to 995 cm^{-1} for a mixture of one atmosphere H_2O in ten atmospheres H_2 neglecting chemistry effects. In this frequency interval, many of the most intense absorption lines arise from pure rotational transitions with the result that in the frequency region of interest the peak intensities show a definite decrease with increasing ω similar to the R branch behavior seen for H_2O at 2000 cm^{-1} . The decrease is not so dramatic as at the larger frequency however due to the presence of ν_2 P branch transitions in the same frequency region.

Laser transitions capable of furnishing high power levels and in addition showing relatively low coupling to H_2O at 300°K , and therefore good atmospheric propagation properties, and high coupling to H_2O at higher temperatures are the P(20) line at 944.15 cm^{-1} and the R(16) line at 972.24 cm^{-1} . Good high temperature coupling and good atmospheric propagation are indicated at 962 cm^{-1} , but the corresponding CO_2 laser line, the R(2) is not a high power line.

HDO - As was the case for H_2O the vibrational energy levels of interest are the (000), (010) and (020). The (000) level is complete through J equals 11 with some energy levels known for J as high as 19.²⁹, 30, 7 For the (010) level all levels for J up to nine are known with some levels known for J as high as 16.⁷ Finally, for the (020) all levels for J up to four with some levels known for J as high as 6.²⁹ Unlike H_2O (or D_2O) HDO possesses no axis of symmetry, a fact which has two results: first there is no nuclear spin factor to be introduced into the line intensity formula. Second, both the ν_2 and rotational band exhibit both type a and type b transitions with the former being approximately half as strong as the former. Thus the HDO absorption spectrum exhibits more lines than that of H_2O and these lines are less intense. Due to D being heavier than H, all rotational and ν_2 lines are displaced to lower frequencies compared to their counterparts in H_2O .

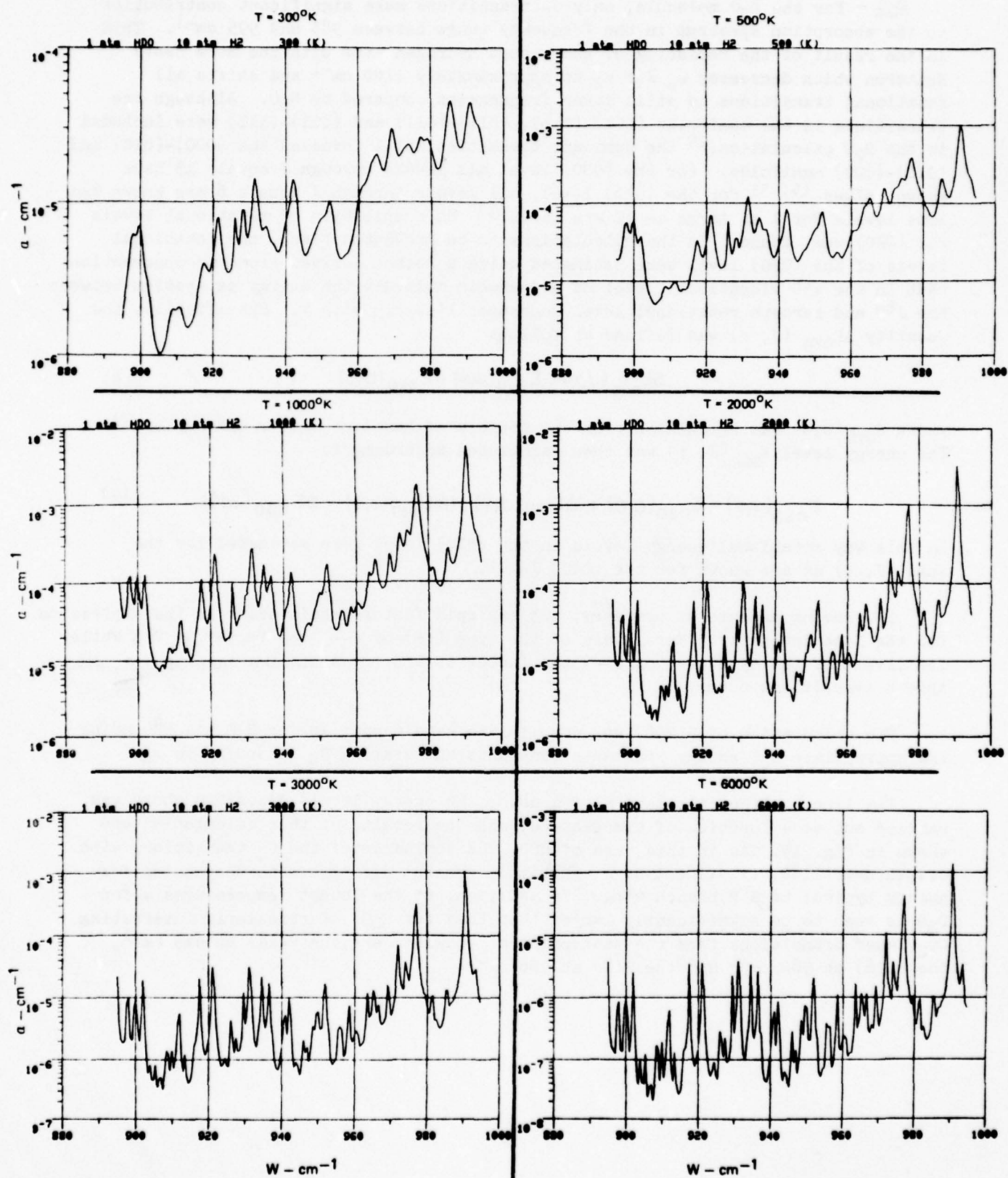
The HDO line by line calculation was carried out in the same manner as was done for H_2O with S_B being scaled down from its H_2O value by the ratio of the ω_0 values of the ν_2 band for H_2O and HDO.⁷ The results of the calculation are shown in Fig. 18 as a function of temperature, and the properties described above are apparent. The HDO spectrum appears to have more numerous but less intense spectral lines than does H_2O and the decrease in intensity is with decreasing frequency, reflecting the greater dominance of ν_2 transitions in this frequency region for the molecule.

For the gas mixture of interest, namely D_2O at one atmosphere in 10 atmospheres H_2 , HDO is an intermediate product between the low temperature coupler, D_2O , and the high temperature one, H_2O . Thus no dovetailing of laser transition to coupler transition is attempted.



ABSORPTION SPECTRA—ONE ATM HDO IN 10 ATM H₂

FIG. 18



D₂O - For the D₂O molecule, only ν_2 transitions make significant contributions to the absorption spectrum in the frequency range between 985 and 995 cm⁻¹. This is the result of the replacing of the second hydrogen atom with the more heavy deuteron which decreases ω_0 for ν_2 to approximately 1180 cm⁻¹ and shifts all rotational transitions to still lower frequencies compared to H₂O. Although the transitions in the manifolds (001)-(011), (011)-(021) and (101)-(111) were included in the D₂O calculation,²⁹ the dominant transition still involved the (000)-(010) and (010)-(020) manifolds. For the (000) level all levels through J equals 15 have known values,^{15, 31} for the (010) level, all levels through J equals 6 are known and some levels for J as large as 12 are known.³² No compilation of rotational levels for (020) was found. In the calculations to be presented first, the rotational levels of the (020) level were estimated using a method derived from the observation that in the ν^{th} vibrational level of a diatomic molecule the energy separation between the J^{th} and zeroeth rotational level decreases linearly with ν . Specifically, the quantity $\Delta E_{\nu 0}(J, \tau)$ was defined as follows

$$\Delta E_{\nu 0}(J, \tau) = E_{\nu 0}(J, \tau) - E_{\nu 0}(0, 0) \quad (18)$$

where $E_{\nu 0}(0, 0)$ was calculated from the formula of Benedict Gailar and Plyler.²⁹ The energy level $E_{020}(J, \tau)$ was then calculated according to

$$E_{020}(J, \tau) = E_{020}(0, 0) + \Delta E_{010}(J, \tau) + (\Delta E_{010}(J, \tau) - \Delta E_{000}(J, \tau)) \quad (19)$$

In this way rotational energy levels in the (020) level were estimated for the same (J, τ) as are known for the (010) level.

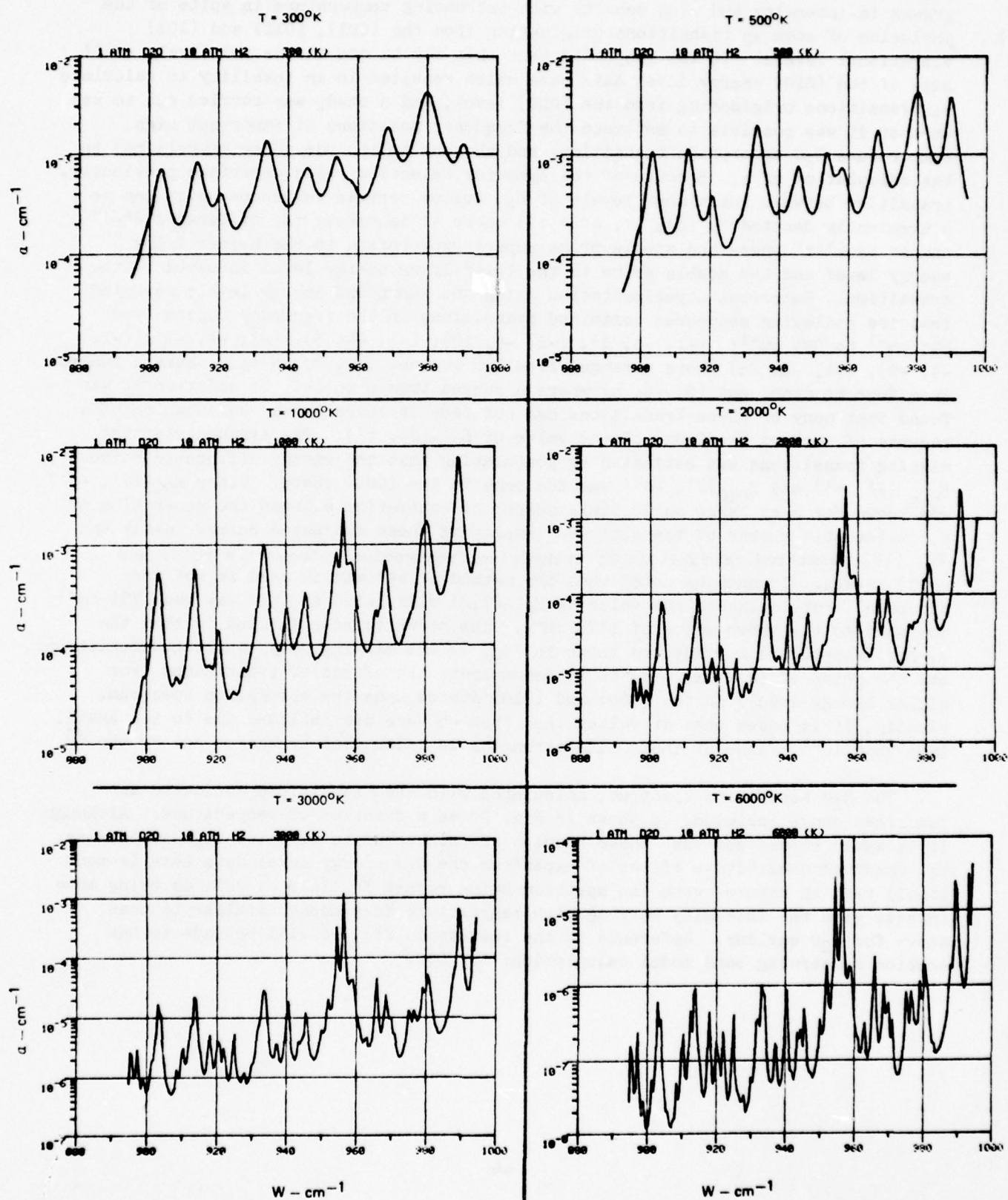
D₂O having an axis of symmetry, nuclear spin factors again occur in the expression for the line intensity. For levels of the type (++) or (--) the factor is 2/3 while for levels of the type (-+) or (+-) the factor is 1/3.¹³ As in the case of H₂O, only type b transitions occur.

The calculation of $S(296)$ was done in the same manner as for H₂O and HDO using the appropriate D₂O energy constants constants and scaling S_B according to ω_0 .

The line by line calculation of α using the energy levels described above was carried out as a function of temperature, and the results of this calculation are shown in Fig. 19. As in this case of HDO, the dominance of the ν_2 transition, with origin near 1180, is evident as α exhibits a general decrease with decreasing frequency typical of a P branch wing. In addition, at the lowest temperatures α for D₂O is seen to be significantly larger than that for H₂O. Particularly interesting CO₂ laser transitions from the standpoint of coupling are the P(18) at 945 cm⁻¹, the R(28) at 980 cm⁻¹ and the R(8) at 968 cm⁻¹.

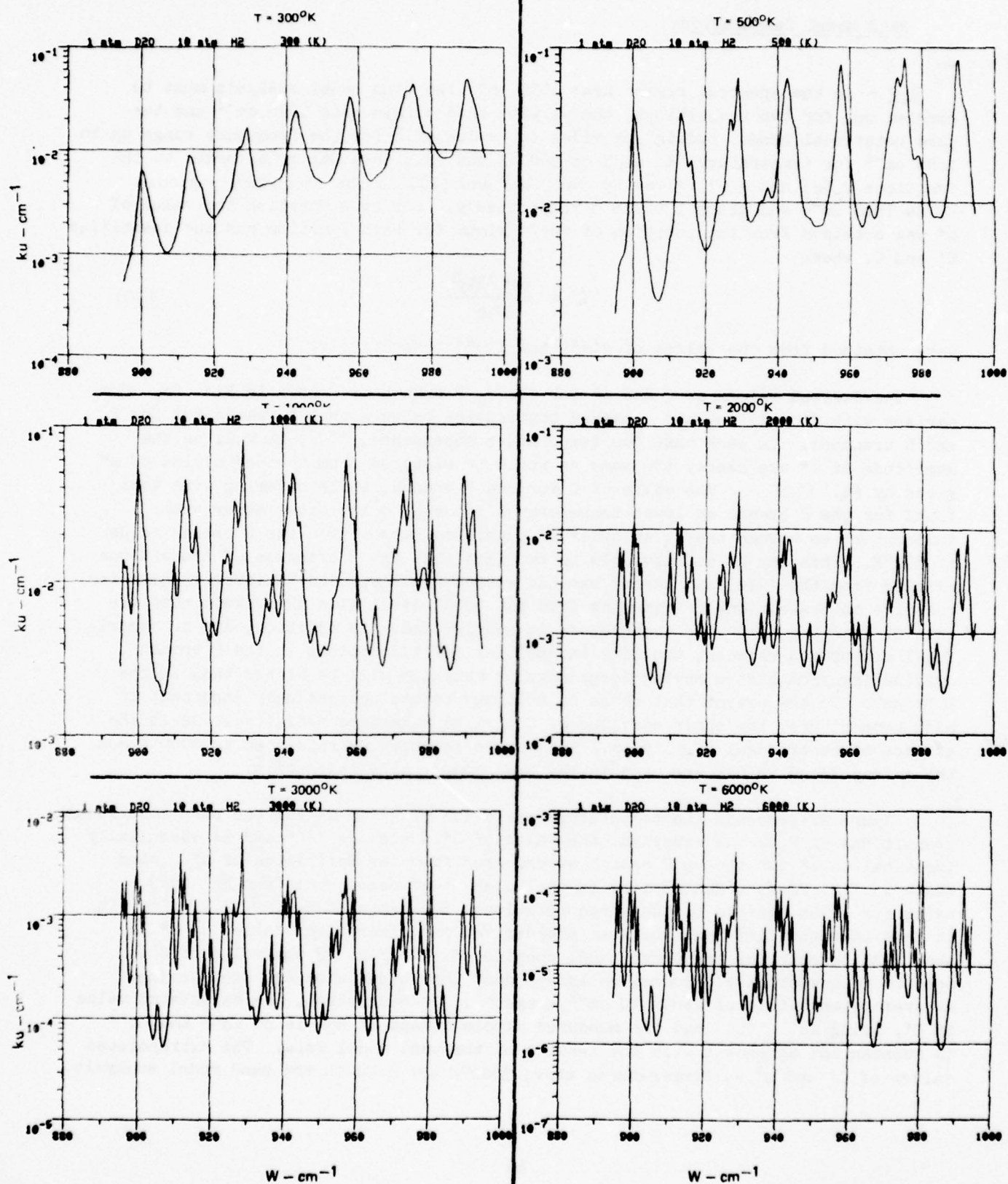
ABSORPTION SPECTRA—ONE ATM D₂O IN 10 ATM H₂

FIG. 19



In contrast to H_2O , the calculated D_2O spectrum exhibits relatively little growth in intensity and line density with increasing temperature in spite of the inclusion of some ν_2 transitions originating from the (001), (011) and (101) vibrational levels. It was suspected that this may be due to the relatively small size of the (010) energy level data base which resulted in an inability to calculate ν_2 transitions originating from the (000) level, and a study was carried out to see whether it was possible to estimate the frequency positions of important high temperature D_2O absorption transitions and thereby to include these transitions in the calculation of α . Because of the symmetry selection rules described previously, transition between rotational levels of D_2O follow certain sequences which can be conveniently denoted by $(\Delta J, \Delta \tau, J'' + \tau'')$ where ΔJ is simply the difference $J' - J''$, and $\Delta \tau$ is $\tau' - \tau''$ where the single prime superscript refers to the higher lying energy level and the double prime to the lower lying energy level involved in the transition. Numerical experimentation using the known D_2O energy levels revealed that the following sequences contained transitions in the frequency region from 895 cm^{-1} to 995 cm^{-1} : $(-1, -6, 8)$, $(-1, -6, 10)$, $(-1, -4, 5)$, $(-1, -4, -7)$, $(-1, -4, -9)$, $(-1, -2, 2n)$ where n ranged from two to ten, $(-1, 0, 2n + 1)$, where n ranged from four to nine, and $(0, -6, n)$ where n ranged from 6 to 14. In addition it was found that many of these transitions had not been included in the calculation of α because of lack of knowledge of the value of $E_{010}(J', \tau')$. The frequency of the missing transitions was estimated by postulating that the energy difference between $E_{010}(J', \tau')$ and $E_{010}(J', -J')$ was the same in the (000) state. Since $E_{010}(J', -J')$ was known for J as large as 12, this method of estimation allowed the generation of a considerable number of transitions. Employing these estimated energy levels and Eq. (19) permitted calculation of transition frequencies between the (010) and (020) levels. It must be noted that the method of estimation used is not very accurate. For instance, the value of $E_{010}(7, 2)$ calculated in this way was 1751 cm^{-1} compared to the known value of 1773 cm^{-1} . The point to keep in mind is that the higher temperature D_2O spectra shown in Fig. 19 are missing many important transitions, and the point of this exercise is to demonstrate the effect of transitions from higher energy levels in the (000) and (010) states upon the absorption spectrum. Finally, it is noted that $\Delta \tau$ values less than -6 were not included due to the small, less than 10^{-4} , value of their line strengths as calculated by Wacker and Pratto.²⁰

The D_2O absorption spectrum, calculated with the transitions estimated as described above included, is shown in Fig. 20 as a function of temperature. Although it is again emphasized that these results are not accurate detailed representations, the observed qualitative effect of expanding the D_2O energy level data base is most likely real in nature, with the spectrum being richer in lines as well as being more intense with the intensity varying with temperature in a manner similar to that shown for H_2O earlier. Reference to the results in Fig. 20 will be made in the section concerning band model calculations for D_2O .

ABSORPTION SPECTRA—ONE ATM D₂O IN 10 ATM H₂(D₂O DATA BASIS AUGMENTED)

Band Model Calculations

H_2O - In the spectral region near 1000 cm^{-1} the band model analysis must be carried out for two transitions, the ν_2 with band origin near 1600 cm^{-1} and the pure rotational band. Ludwig⁴ provides the value of \bar{k} for the frequency range up to 1600 cm^{-1} for temperatures as high as 3000°K and this data was transformed to the functions $f_r(\omega)$ and $g(\omega)$, given by Eqs. (9) and (10) in the frequency regions below 1000 cm^{-1} and above 1000 cm^{-1} respectively. For each function the value of ω^* was obtained from the position of the maximum for each function and the quantities C' and C , where

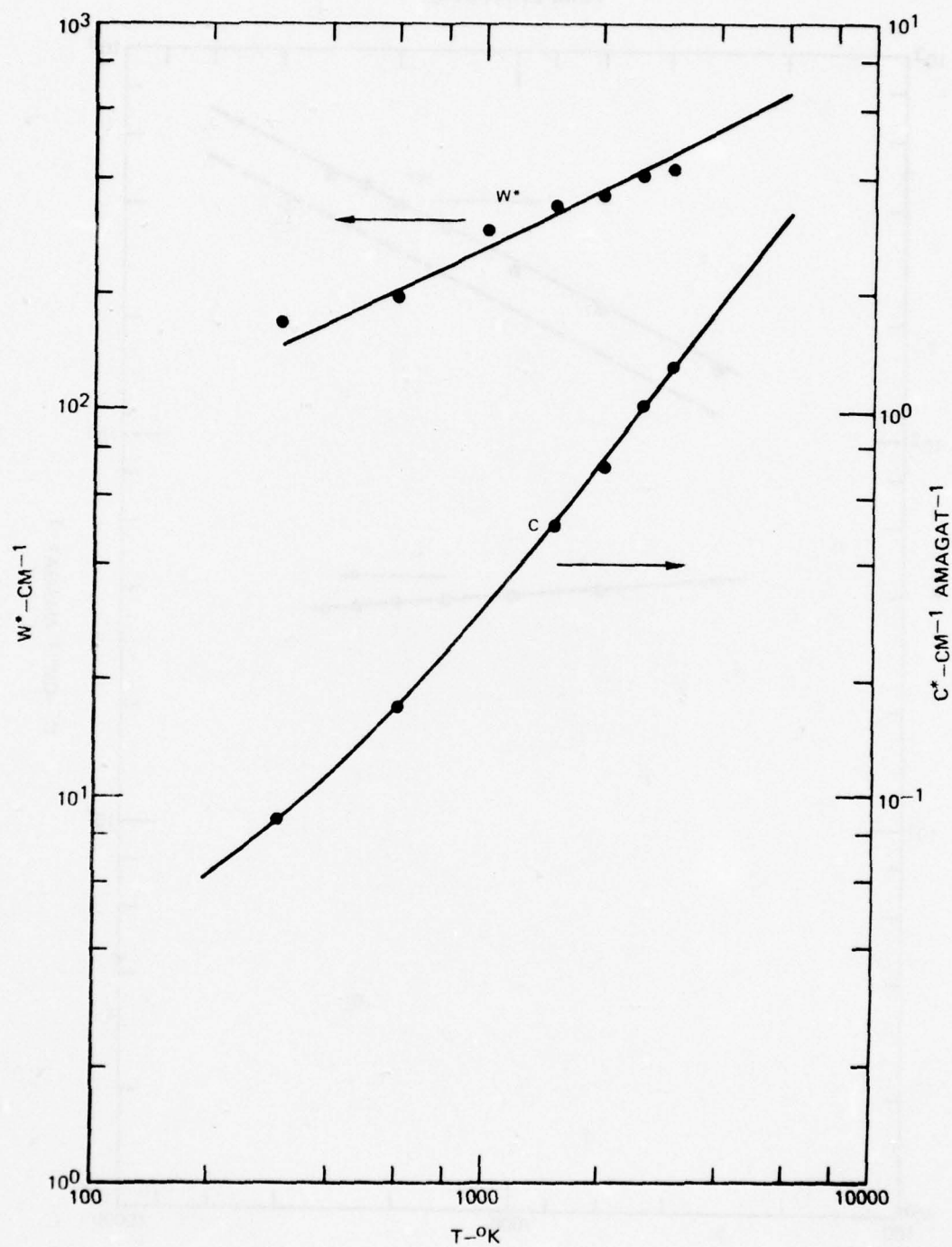
$$C' = \frac{8\pi^3 M_0^2}{3hc} \quad (20)$$

were obtained from the values of $g(\omega^*)$ and $f(\omega^*)$ respectively.

The derived values at C and ω^* for the ν_2 P branch are shown in Fig. 21. Comparison with Fig. 11 reveals a marked consistency between the ω^* values for the P and R branches. In each case the temperature dependence, $T^{1/2}$, as well as the magnitude of ω^* are nearly the same as would be expected from the definition of ω^* given by Eq. (12). The value of C for the P branch, while agreeing with that found for the R branch at lower temperatures is seen to increase faster with temperature to become nearly an order of magnitude larger than the R branch value at 300°K . This may be attributable to the fact that the P branches of transitions arising from the (010) and higher excited states are displaced to lower frequencies relative to transitions originating from the (000) level with the result that the rate of increase of C with temperature is accelerated. In addition, due to centrifugal distortion effects, the line intensities for transitions in the P branch originating from states having large angular momentum will be higher than in the R branch. To the extent that these transitions become increasingly important at high temperature, the observed value of C will be augmented over its value in the absence of centrifugal distortion. Each curve is shown extrapolated to 6000°K and the extrapolated values are used in the band model calculation of \bar{k} .

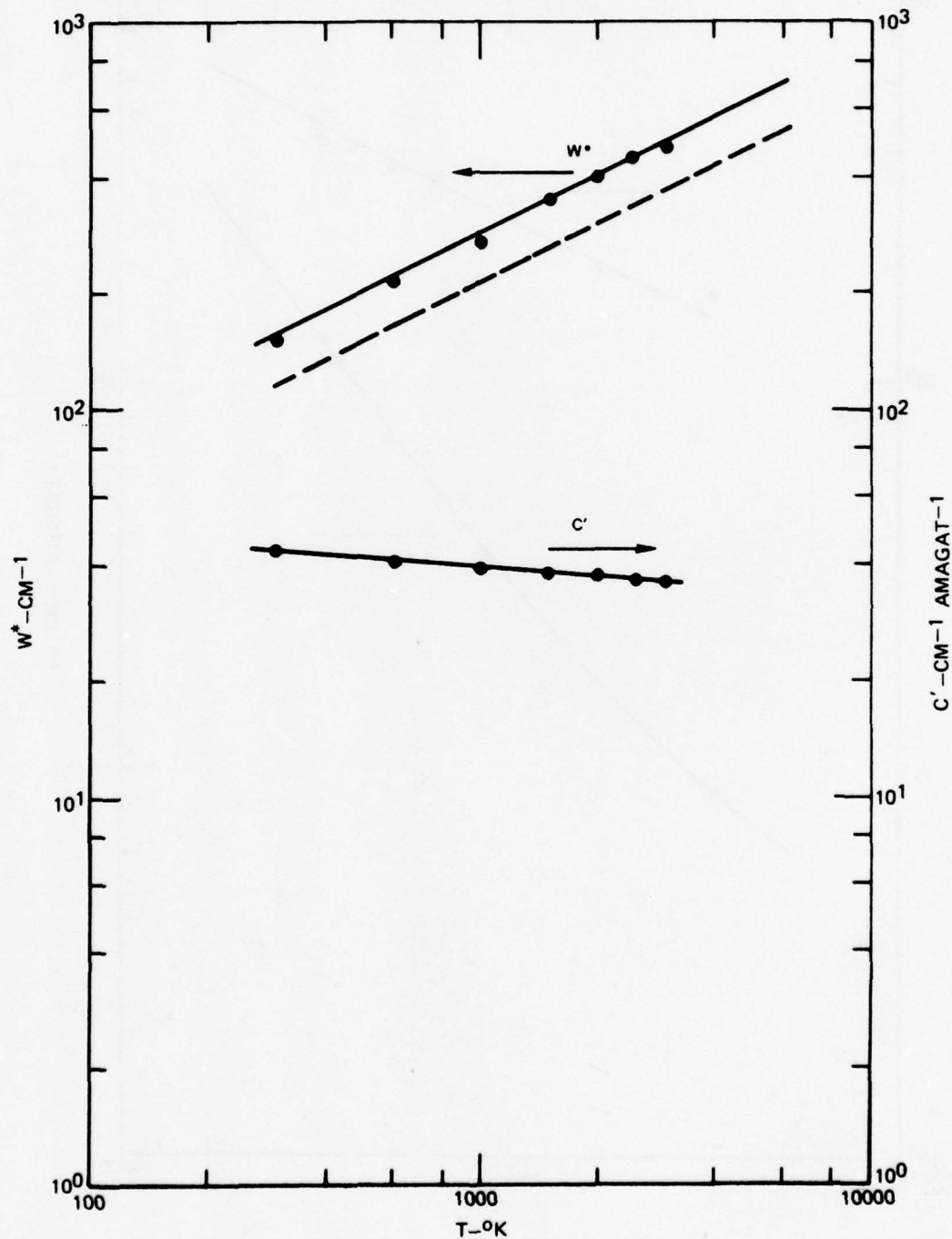
Figure 22 presents the temperature variation of C' and ω^* for the pure rotational transitions of H_2O . As expected, the value of ω^* scales as $T^{1/2}$ and is essentially identical to ω^* for the ν_2 P branch as expected from the definition of ω^* . Also shown in Fig. 22 as a dotted line is the value of ω^* calculated from Eq. (12) using for B the average of the three rotational constants of H_2O ,²⁹ 17.1 cm^{-1} . It is seen that the difference between the derived and theoretical values of ω^* is about +30 percent for the three bands considered. In Fig. 22 the value of C' is seen to be essentially temperature independent consistent with Eq. (20) having an average magnitude of about $40\text{ cm}^{-1}\text{ amagat}^{-1}$. In comparison, the calculated value of C' , using Eq. (20) and the measured dipole moment of H_2O is $38\text{ cm}^{-1}\text{ amagat}^{-1}$ in substantial agreement with the results of the band model data. The extrapolated values of C' and ω^* at temperatures above 3000°K are used in the band model analysis.

H₂O C AND W* PARAMETERS FOR ν_2 P BRANCH
VS
TEMPERATURE



77-12-30-12

H₂O C' AND W* PARAMETERS FOR ROTATIONAL TRANSITIONS
VS
TEMPERATURE



77-12-30-1

The band model analysis for H_2O was completed by calculating $f_r(\omega^*)$ and $f_{rv}(\omega)$ at the desired temperature using the appropriate (ω^*, C') and (ω^*, C) values, adding the two terms and multiplying by the stimulated emission factor $(1 - \exp(-hc\omega/kT))$. The results are given for 950 cm^{-1} in Fig. 23 along with Ludwig's⁴ values and the value of α (945 cm^{-1})/ u . The agreement between the \bar{k} and α/u is quite good until a temperature is reached where absorption by molecules in untabulated very high rotational energy levels becomes dominant in calculating α .

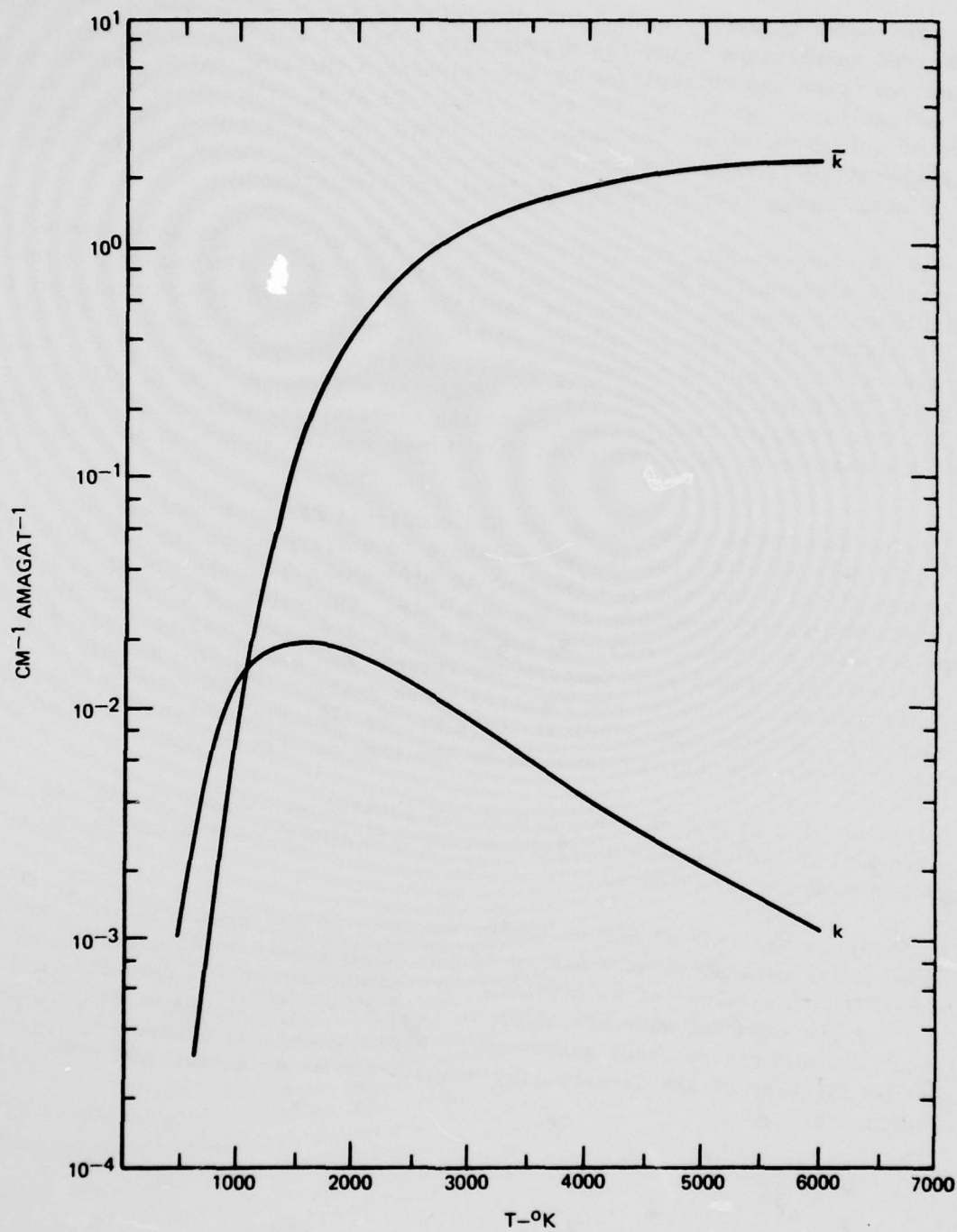
As was the case at 2000 cm^{-1} , the factor $(1 + \bar{k}u/4a)^{1/2}$ is essentially unity in the present study and so $\bar{k}u$ is plotted vs T in Fig. 24 for the cases in which u either includes or does not include the equilibrium chemistry effects relevant to an initial mixture of 10 atm H_2 and one atm H_2O . Taking a ku value of 10^{-2} cm^{-1} as the point at which H_2O is a useful coupler, it is seen that H_2O does not "turn on" until about 1300°K and is "turned off" by chemistry effects at 4800°K . At 2000 cm^{-1} (Fig. 13) it is recalled that the corresponding temperatures were 480°K and 3500°K and that the maximum $\bar{k}u$ value was about four times smaller than that shown in Fig. 24.

HDO - The band model calculation for HDO consisted first of scaling the (C, ω^*) and (C', ω^*) sets obtained for the H_2O molecule to correspond to the HDO molecule. That is each ω^* value was scaled according to $B^{1/2}$ where B is the average of the three rotational energy constants of the molecule. The value of C' was taken to be the same for each molecule. Since S_B scales as ω_0 , C is expected to scale only as $Q_v(T)$ and thus to increase with temperature faster than does H_2O . However, centrifugal distortion effects are expected to be smaller in HDO than in H_2O , thereby causing C to increase not as quickly with T . To take the latter into account, the value of C used for HDO was taken to be the same as that of H_2O .

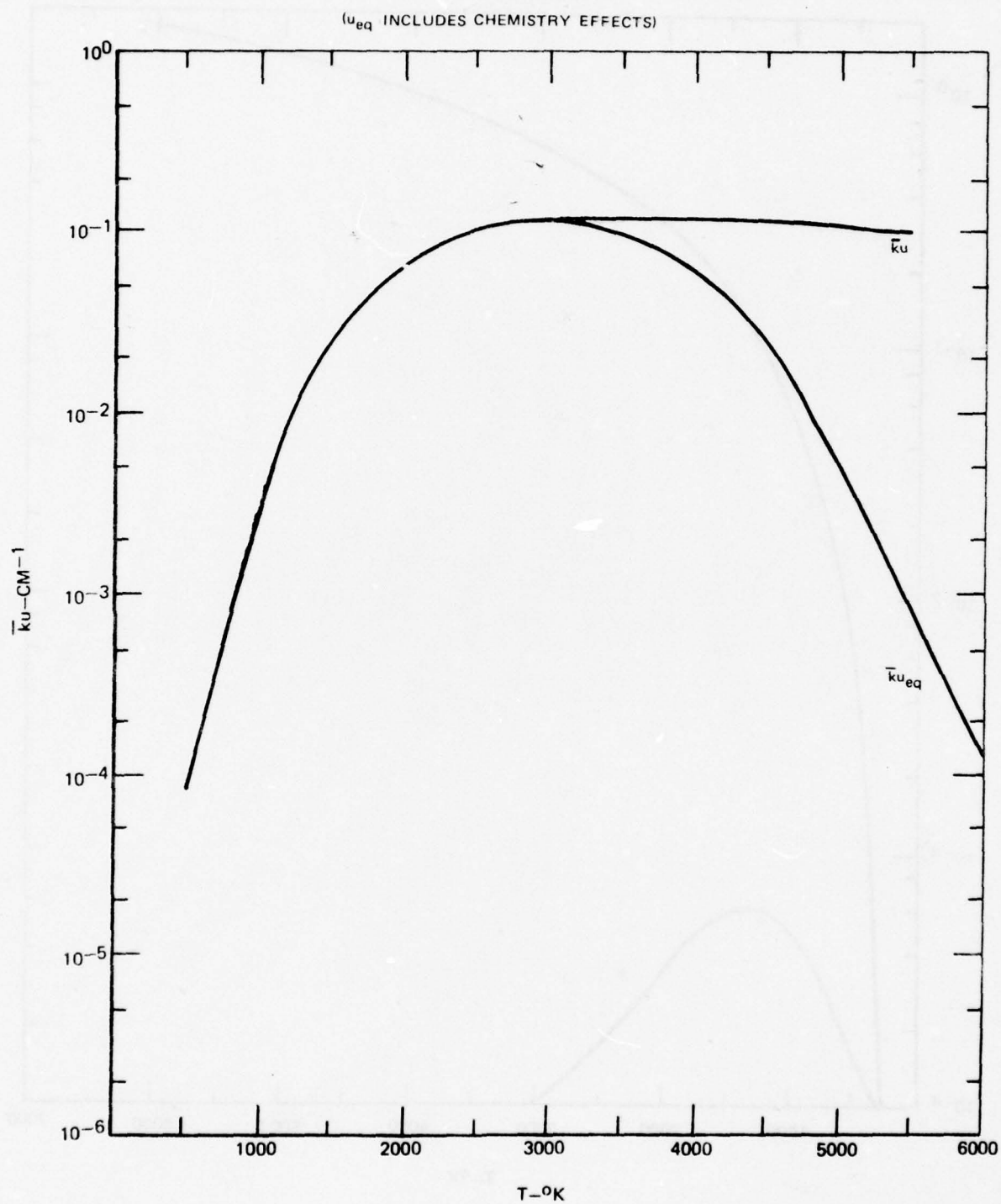
The value of \bar{k} at 950 cm^{-1} and α/u at are plotted vs temperature in Fig. 25. The inadequacy of the line-by-line calculation data was a temperature as low as 500°K for the HDO molecule is evident.

D₂O - As in the case of HDO no change was made in the magnitude of C , and the other band model parameters were scaled to the D_2O molecule as directed by Eqs. (12) and (20). The values of \bar{k} , $\alpha(945)/u$ for the unexpanded D_2O data base and $\alpha(945)/u$ for the expanded base are shown in Fig. 26 as functions of temperature. The additional D_2O absorption lines generated by expanding the data base are seen to enhance the adequacy of the line-by-line calculation as an estimation of the absorption coefficient.

\bar{k} (950 CM^{-1}) AND k (945 CM^{-1}) FOR 1 ATM H_2O IN 10 ATM H_2
VS
TEMPERATURE

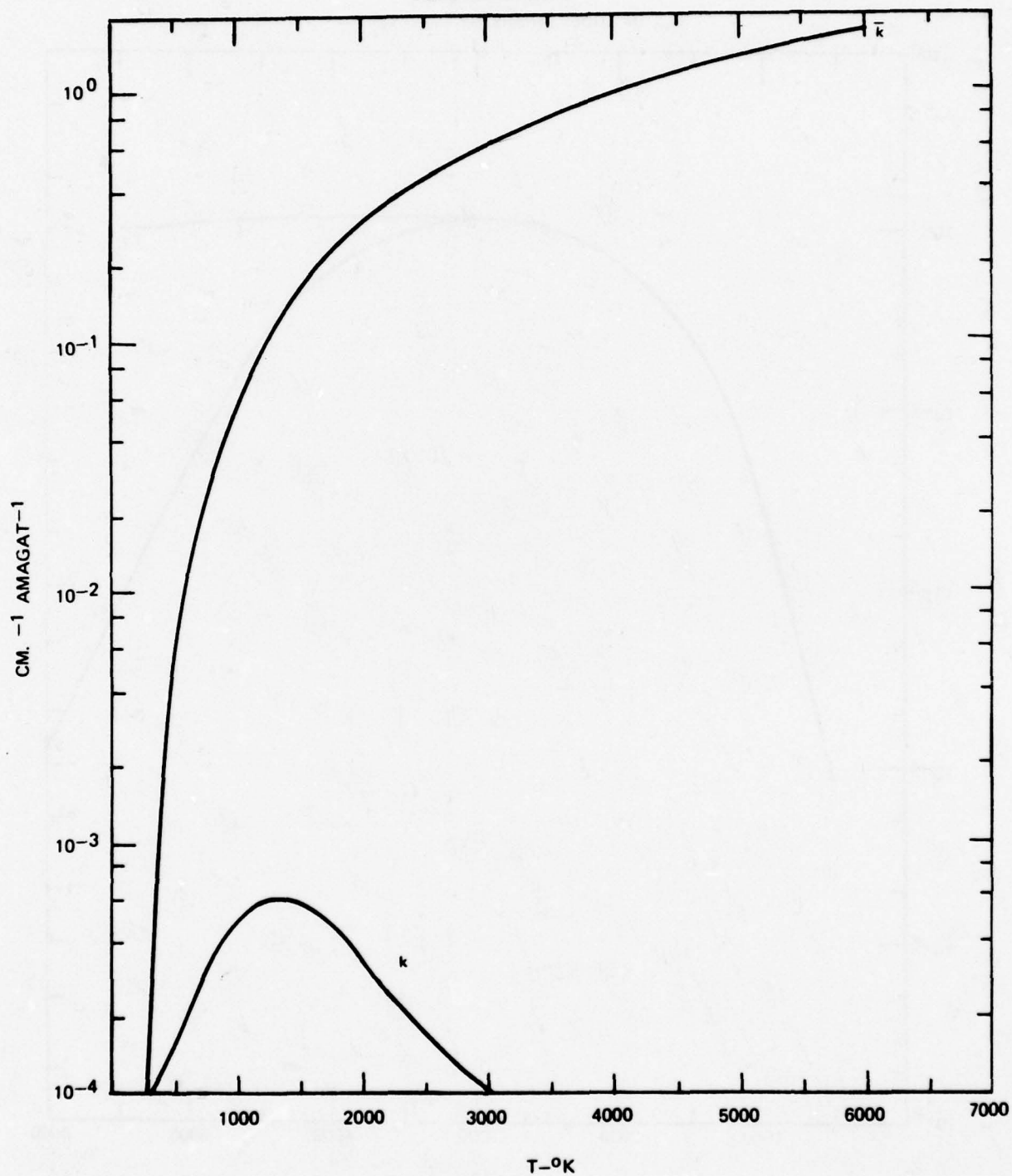


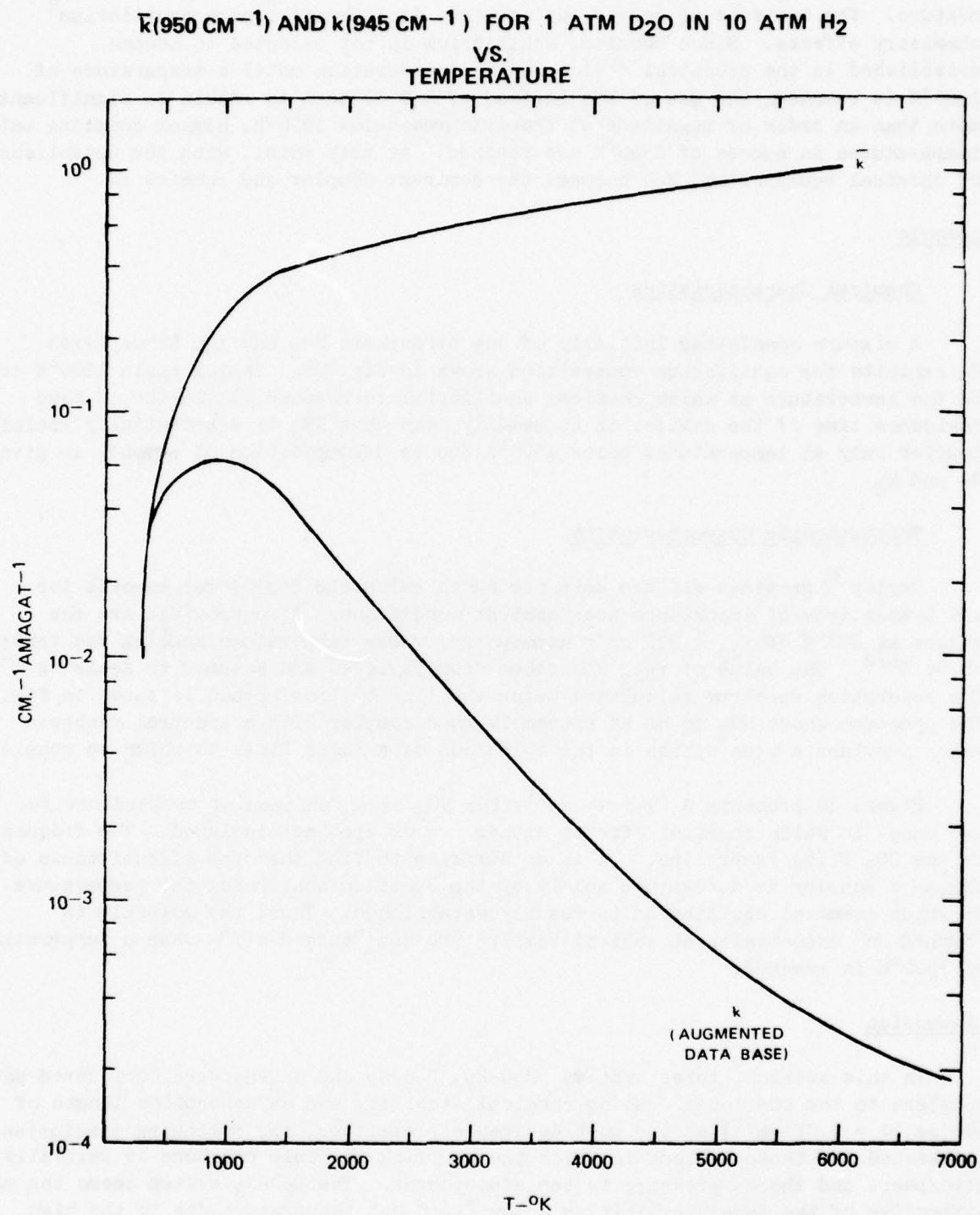
ABSORPTION PER CM ($\bar{k}(950 \text{ CM}^{-1})_u$) FOR 1 ATM H_2O IN 10 ATM H_2
VS
TEMPERATURE



77-12-30-11

$\bar{k}(950\text{ CM}^{-1})$ AND $k(954^{-1})$ FOR 1 ATM HDO IN 10 ATM H_2
VS.
TEMPERATURE





Finally, Fig. 27 presents $\bar{\kappa}_u$ for the one atmosphere D_2O /10 atmosphere H_2 mixture. The two sets of curves, as labeled, include and ignore equilibrium chemistry effects. Since chemical equilibrium is not expected to become established in the practical device under consideration until a temperature of $1500^\circ K$ is reached, the use of D_2O instead of H_2O is seen to result in significantly, more than an order of magnitude at temperatures below $1000^\circ K$, higher coupling until temperatures in excess of $1500^\circ K$ are reached. At this point, with the establishment of chemical equilibrium, H_2O becomes the dominant coupler and remains so.

Ammonia

Chemical Characteristics

A mixture consisting initially of one atmosphere NH_3 and ten atmospheres H_2 exhibits the equilibrium composition shown in Fig. 28. Taking again $1500^\circ K$ to be the temperature at which chemical equilibrium is reached within the 10 msec residence time of the device, it is readily seen that NH_3 is a potentially useful coupler only at temperatures below $1500^\circ K$ due to decomposition of ammonia to give N_2 and H_2 .

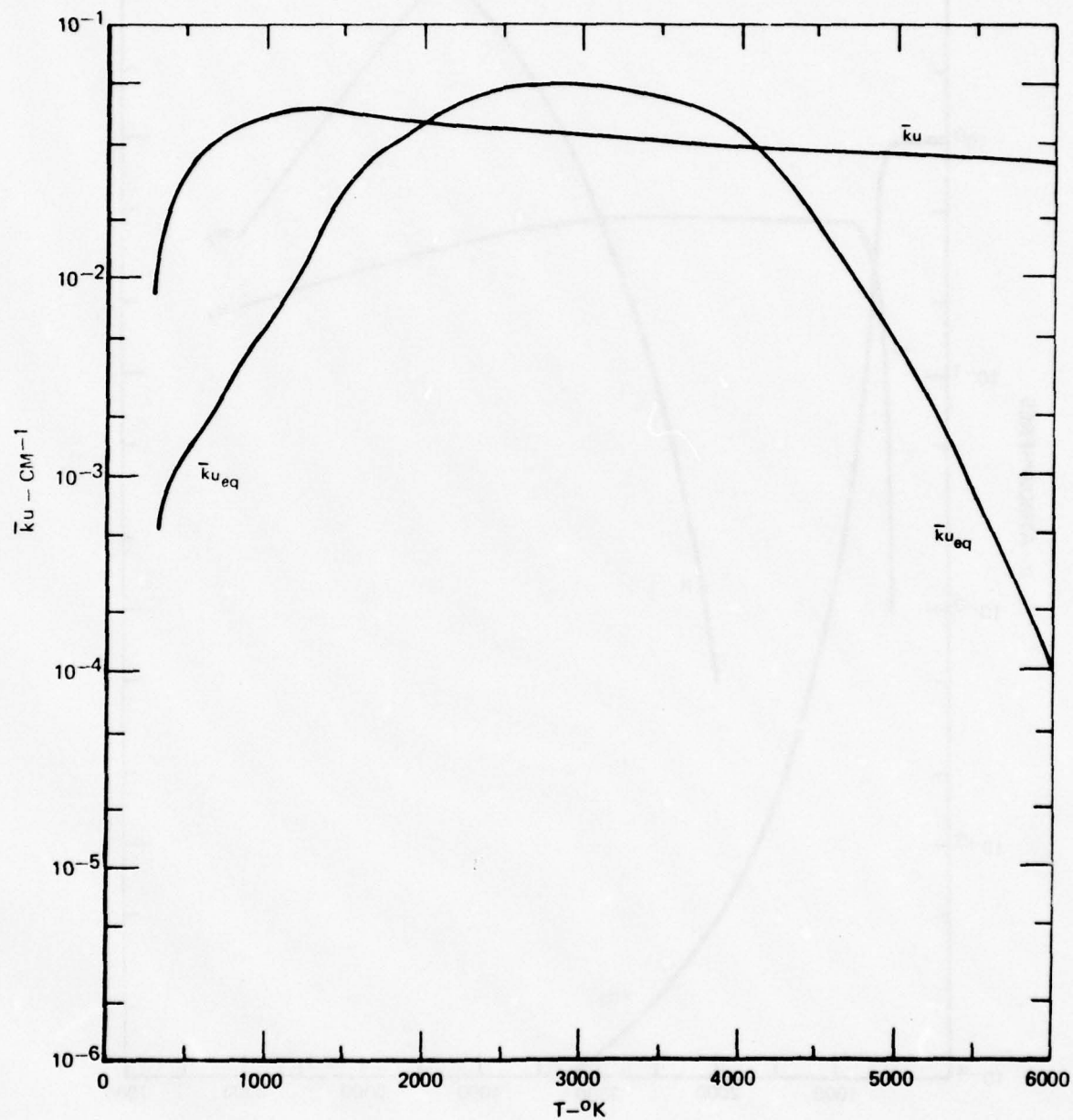
Spectroscopic Characteristics

Taylor³³ provides all the data needed to calculate $S(296)$ for ammonia for all transitions of importance near ambient conditions. Also provided are the values at $300^\circ K$ of γ_{H_2} ($.075 \text{ cm}^{-1}$ atmosphere) whose temperature scaling was taken to be $T^{1/2}$. The value of γ_{NH_3} was taken from Taylor³³ and assumed to scale as T^{-1} . The absorption spectrum calculated using the line by line method is shown in Fig. 29. The spectrum shows NH_3 to be an extremely good coupler with a spectral richness which provides a wide option in the selection of a laser lines to which to couple.

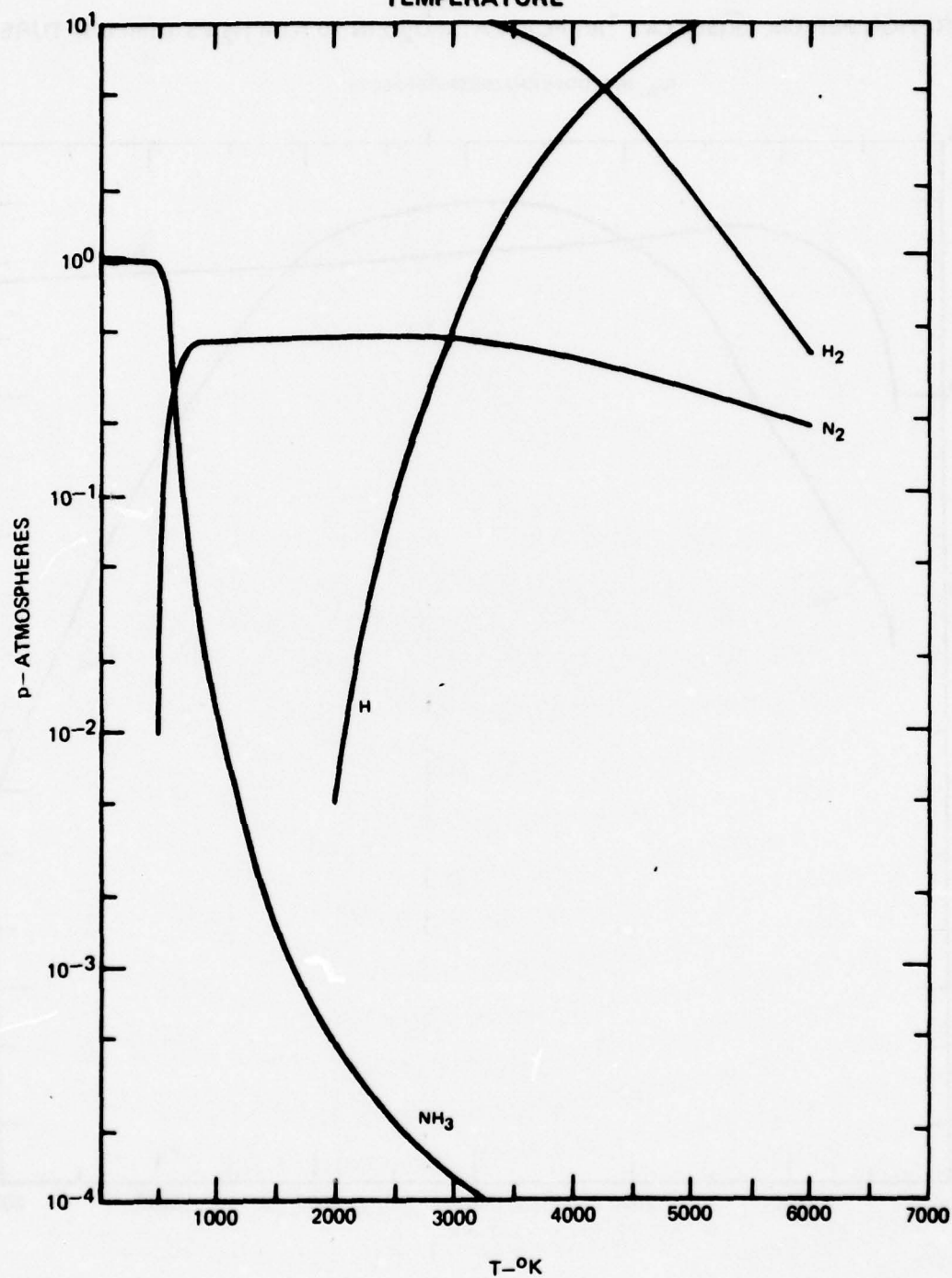
Figure 30 presents α (945.94 cm^{-1}) for NH_3 as a function of temperature for the two cases in which chemical effects either are or are not included. The frequency is the CO_2 P(18) laser line. It is no surprise to find that the effectiveness of NH_3 as a coupler is determined solely by the question concerning the temperature at which chemical equilibrium is readily established. Thus, the molecule is "turned on" essentially at ambient temperature and "turned off" when a temperature of $1500^\circ K$ is reached.

Discussion

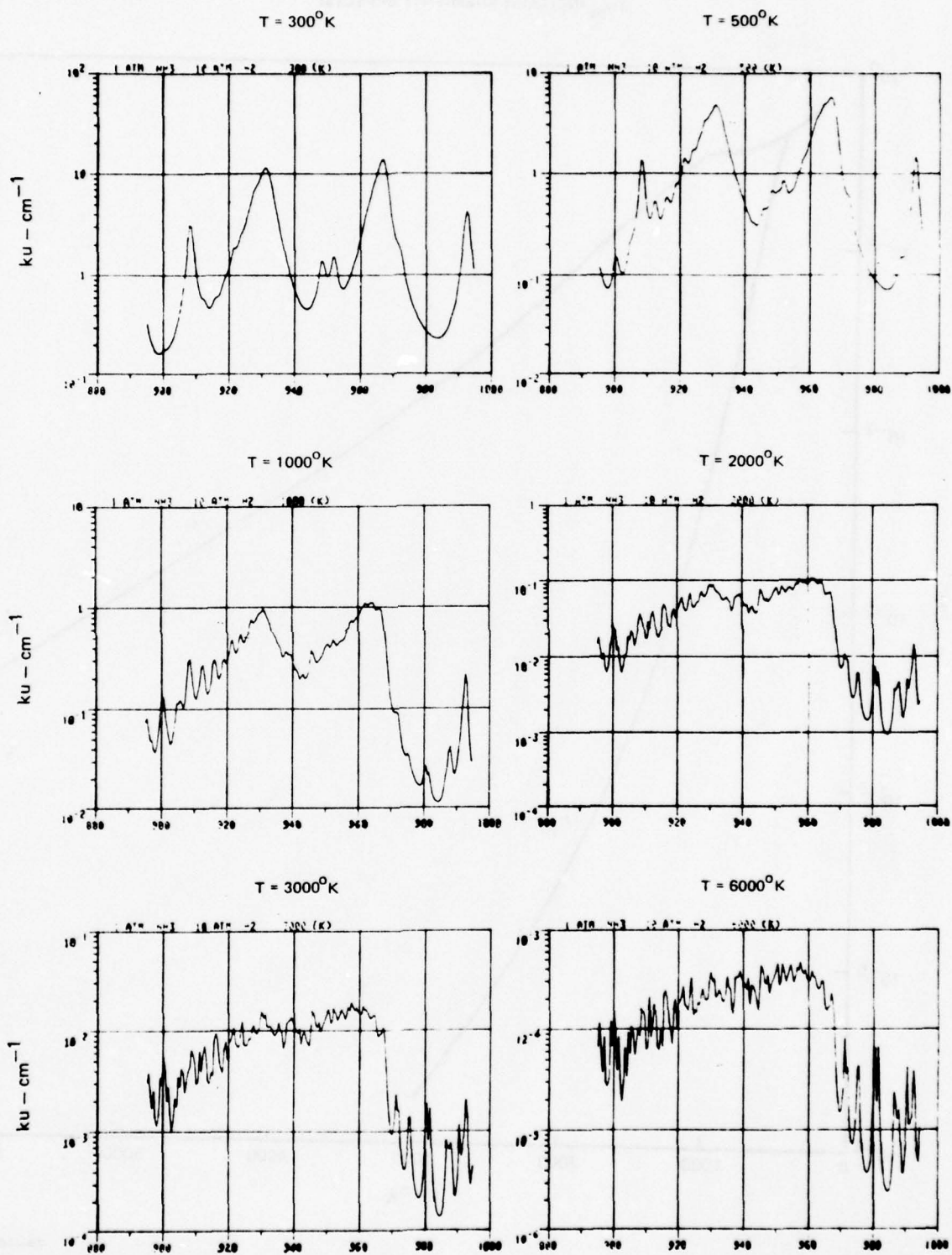
In this section, three systems, H_2O-H_2 , D_2O-H_2 and NH_3-H_2 were considered as couplers to the CO_2 laser. Using chemical stability and an absorption length of 100 cm ($\alpha = 0.01 \text{ cm}^{-1}$) as the most desirable properties, the following conclusion can be reached for these systems in which the coupling molecule pressure is initially one atmosphere and the H_2 pressure is ten atmospheres. The D_2O-H_2 system seems the most attractive of the three, exhibiting a low "turn on" temperature due to the high absorbtivity of D_2O and the fairly good, to $4800^\circ K$, chemical stability of the H_2O

ABSORPTION PER CM ($\bar{k}(950 \text{ CM}^{-1})_u$) FOR 1 ATM D_2O IN 10 ATM H_2 VS TEMPERATURE(U_{eq} INCLUDES CHEMISTRY EFFECTS)

EQUILIBRIUM CHEMISTRY OF 10 ATM H_2 AND 1 ATM NH_3
VS
TEMPERATURE



77-12-30-10

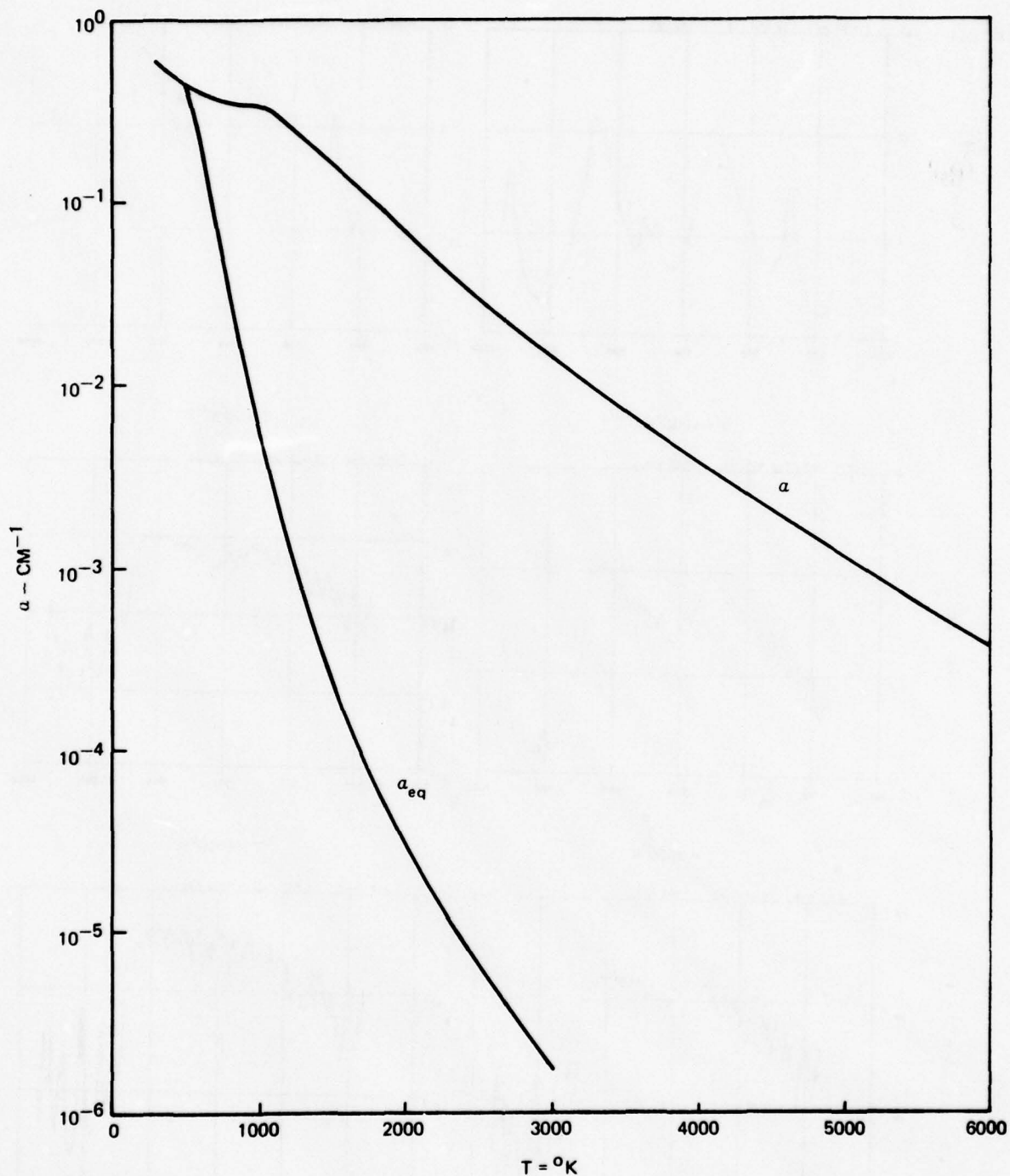
ABSORPTION SPECTRA - ONE ATM NH_3 IN 10 ATM H_2 

79-10-82-1

ABSORPTION PER CM FOR 1 ATM NH_3 IN 10 ATM H_2 VS TEMPERATURE

$$w = 945.94 \text{ cm}^{-1}$$

(a_{eq} INCLUDES CHEMISTRY EFFECTS)



79-10-82-2

molecule which becomes the dominant coupler as a result of hydrogen atom exchange at temperatures above 1500°K. The latter quality is also of course possessed by the $\text{H}_2\text{O}-\text{H}_2$ system which also shows however a higher "turn on" temperature of 1300°K. The NH_3 molecule is "turned on" at all temperatures considered but its poor chemical stability regulates it to use only as a low temperature, less than 1500°K, coupler.

Conclusions

Various candidate molecules have been considered analytically as couplers to CO and CO_2 laser radiation when immersed at a pressure of one atmosphere in ten atmospheres H_2 . Of all the systems considered, the CO molecule as a coupler to CO laser radiation is the best candidate. This molecule exhibits an absorption per unit length of magnitude 10^{-2} cm^{-1} at temperatures as low as 300°K and a chemical stability which permits this magnitude to be maintained to temperatures in excess of 6000°K. In addition the fact that H_2 is a good vibrational deactivator of CO eliminates the problem of optical bleaching of the molecule. The system $\text{D}_2\text{O}-\text{H}_2$ as a coupler to CO_2 laser radiation is second only to the $\text{CO}-\text{H}_2-\text{CO}$ laser system. In this case the high absorptivity of D_2O causes the coupler to attain an absorption coefficient of 10^{-2} cm^{-1} at about 400°K but dissociation of H_2O at high temperature causes the loss per unit length to go below 10^{-2} cm^{-1} at about 4800°K. The $\text{H}_2\text{O}-\text{H}_2$ system was considered for both the CO and CO_2 laser. For the former the $\text{H}_2\text{O}-\text{H}_2$ system was effective from 400°K to 3800°K while for the latter this range ran from 1300°K to 4800°K with a peak absorption coefficient of nearly ten times larger than the former. The concentration of the OD molecule was never high enough even in the $\text{D}_2\text{O}-\text{D}_2$ system to be an effective coupler, and thermal decomposition prevented the NH_3-H_2 system from being useful at temperatures much above 1500°K.

SECTION III

EXPERIMENTAL METHOD

Introduction

The purpose of the experimental segment of this program consisted of measuring the temperature dependent absorption per cm of $\text{H}_2/\text{H}_2\text{O}$, $\text{H}_2/\text{D}_2\text{O}$ and H_2/NH_3 mixtures at $10.6\text{ }\mu\text{m}$ wavelength, approximately ten atmospheres pressures and at temperatures as high as 6000°K . To attain this information, each mixture was placed in a high pressure gas cell in which a hot plasma, sustained by a focused high power CW CO_2 laser beam, provided the region of high temperature. This cell was placed in one arm of a Mach Zehnder interferometer with a CO_2 laser light source, operating at the wavelength of interest, and the interferometer was modified to provide nearly simultaneous determination of the power loss and phase shift of the light traversing the cell due to the presence of the hot gas inside it. Due to the axial symmetry in the properties about the plasma, these data were reduced to provide the radial dependence of both the gas temperature and the absorption per cm and therefore the dependence of the latter on the former.

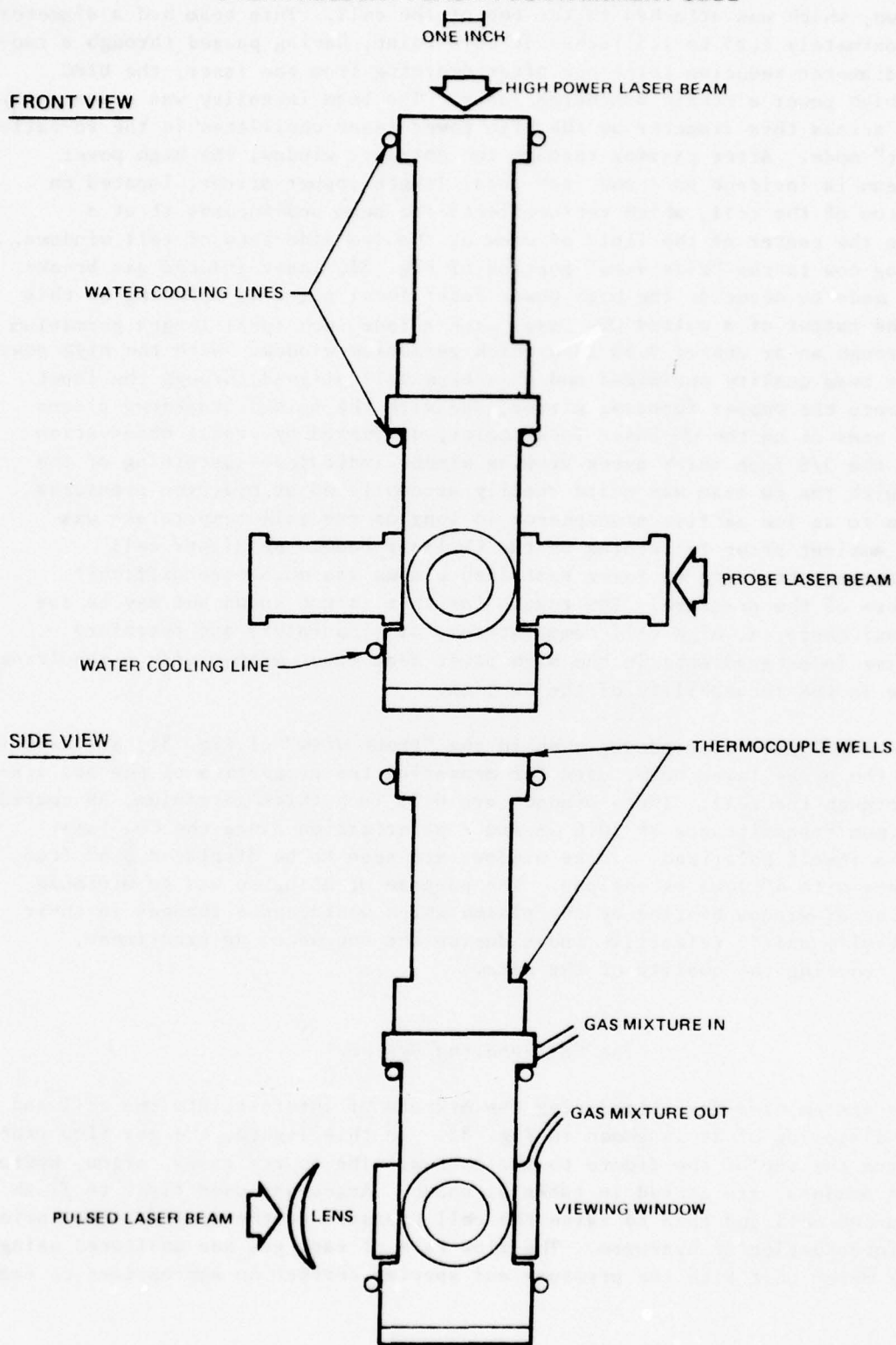
As originally planned, measurements were also to be taken at $5\text{ }\mu\text{m}$ in a similar manner using a CO laser instead of the CO_2 laser as the laser light source. Although time did not permit carrying out these experiments, the CO laser to be used was constructed, and this laser is described in Appendix A.

In this section, we describe in detail the experimental apparatus, the collection of data and its reduction to provide the information of interest.

The High Pressure Cell

The gas cell used in this study is drawn to scale in Fig. 31. The cell was made from brass with copper cooling lines soldered to it. To heat the cell, heating tape was wrapped around it. Between different cell sections and at window-to-cell seals, O-rings made from a low porosity-high thermal stability elastomer were used. It is seen that the cell is somewhat "top heavy" in appearance due to the 7.5 inch long section which rests on the cross which originally constituted the cell. This section was added to the cell after an early experiment in which buoyancy driven convective heat flow from the laser sustained plasma caused the high power laser beam entrance window to crack. No recurrence of this accident happened once the entrance window was moved further from the plasma. The entrance window was zinc selenide, two inches in diameter, 0.35 inches thick and anti-reflectance ("AR") coated for $10.6\text{ }\mu\text{m}$ wavelength. The high power beam was directed through this window by a copper turning mirror in an adjustable mount

HIGH PRESSURE PLASMA CONTAINMENT CELL



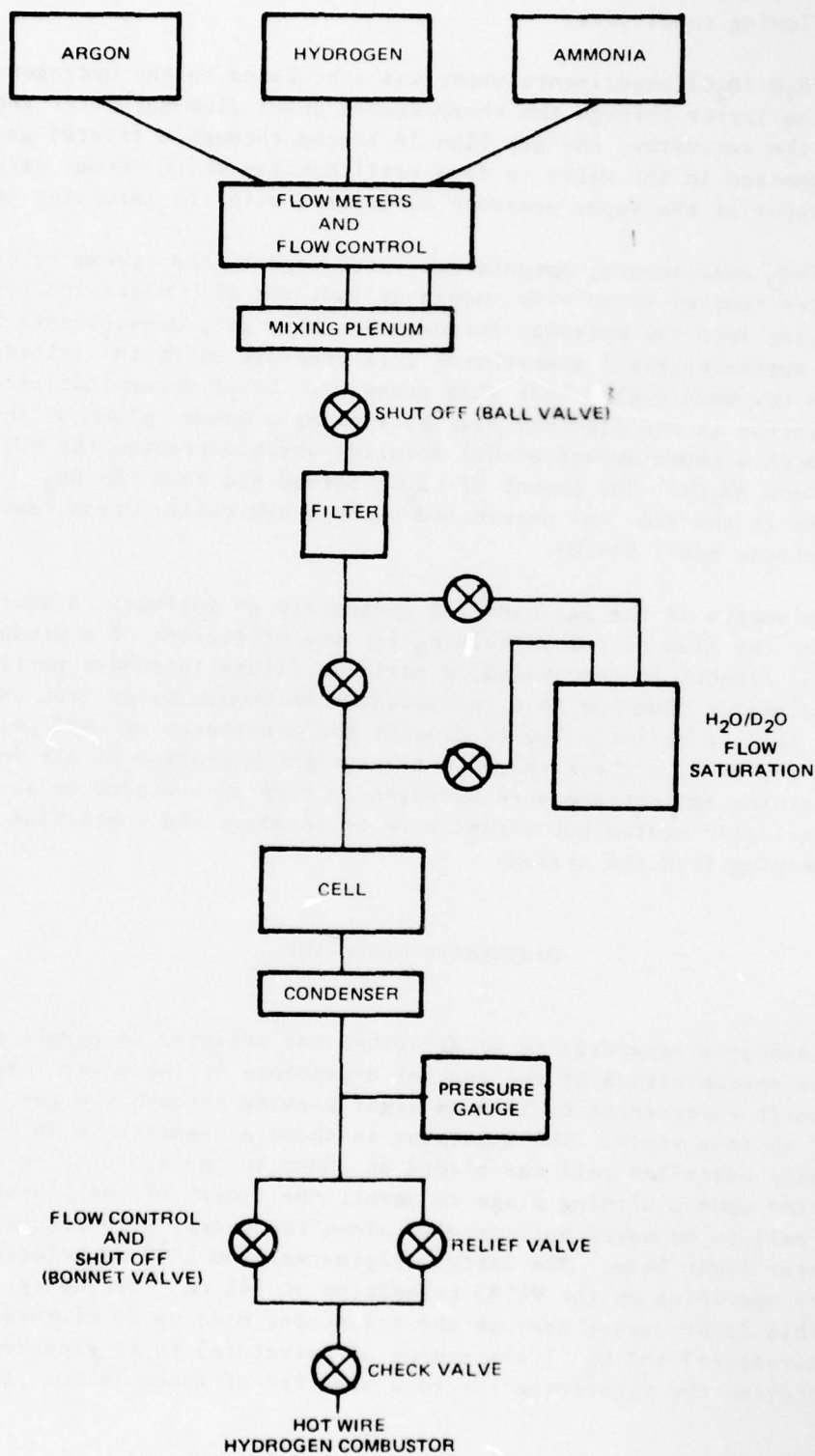
not shown, which was attached to the top of the cell. This beam had a diameter of approximately 1.25 to 1.5 inches at this point, having passed through a two-to-one diameter reducing telescope after emerging from the laser, the UTRC 7.5 kW high power electric discharge laser. The beam intensity was essentially uniform across this diameter as the high power laser oscillates in the so-called "top-hat" mode. After passing through the entrance window, the high power laser beam is incident on a one inch focal length copper mirror, located on the bottom of the cell, which retroreflects the beam and focuses it at a point in the center of the field of view of the two side-sets of cell windows. Referring now to the "side view" portion of Fig. 31, laser induced gas breakdown is made to occur at the high power laser focal point by focusing at this point the output of a pulsed CO_2 laser with a four inch focal length germanium lens through an ar coated 0.35 inch thick germanium window. With the high power CW laser beam quality optimized and this beam well aligned through the input window onto the copper focusing mirror, and with the pulsed breakdown plasma located near or on the CW laser focal point, as judged by visual observation through the 3/8 inch thick pyrex viewing window indicated, sustaining of the plasma with the cw beam was quite readily accomplished at hydrogen pressures from ten to as low as five atmospheres so long as the cell temperature was near to ambient prior to turning on the CW laser beam. At higher cell temperatures, obtaining cw laser sustained plasma was much more difficult regardless of the pressure. The reason for this is not known but may be due to the existence, at high cell temperatures, of temperature and therefore refractive index gradients in the high power beam input window with a resulting decrease in the focusability of the CW beam.

The final pair of windows, seen in the "front view" of Fig. 31, are used for passing the probe laser beam, used for measuring the properties of the gas mixture, through the cell. These windows are 0.35 inch thick germanium, AR coated for maximum transmittance at $10.6 \mu\text{m}$ and s polarization since the CO_2 laser source is itself polarized. These windows are seen to be displaced 5.6" from the plasma with 4" long extensions. The purpose of doing so was to minimize the degree of window heating by the plasma which would cause changes in their absorbitivity and/or refractive index during the course of an experiment, thereby reducing the quality of the data.

The Gas Handling System

The system used for introducing the mixture of interest into the cell and then of disposing of it is shown in Fig. 32. In this figure, the gas flow proceeds from the top of the figure to the bottom. The source gases, argon, hydrogen, and ammonia, are stored in tanks as shown. Argon was used first to flush air from the cell and then to raise the cell pressure to the desired level prior to the introduction of hydrogen. The flow rate of each gas was monitored using the flow meter unit with the pressure and species correction appropriate to each

GAS HANDLING SYSTEM



flow tube used. By monitoring the H_2 flow meter and the pressure gauge and by adjusting the flow meter control valve the desired total pressure and flow rate (10 standard cubic feet per hour) were obtained. All measurements were made under flowing conditions.

For H_2/H_2O (D_2O) experiments water was introduced to the hydrogen flow by forcing the latter through the thermostated brass flow saturator shown in the figure. In the saturator, the gas flow is forced through a fritted gas dispersion tube immersed in the water to form small bubbles which become saturated with water vapor at the vapor pressure associated with the saturator temperature.

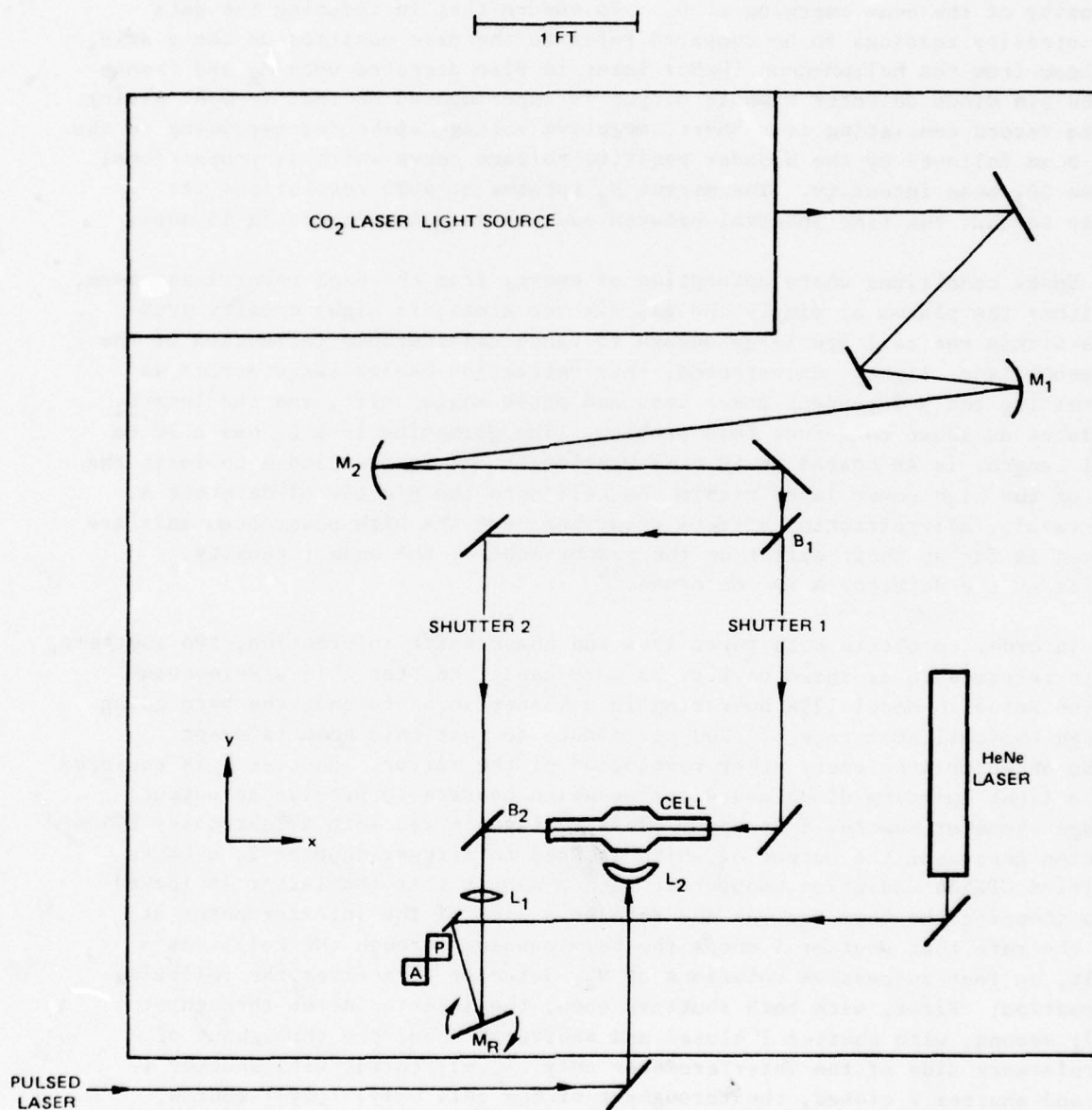
For H_2/NH_3 experiments, ammonia was introduced to the stream by cracking its flow meter control valve wide enough so that the flow meter indicated that NH_3 was flowing into the hydrogen stream. For this gas, measurements were restricted to approximately 5 atmospheres cell pressure since the cylinder delivery pressure was not much higher than this pressure. Exact determination of the NH_3 concentration in the flow was made by flowing a known volume of the mixture through a known amount of HCl solution which extracted the NH_3 from the gas to form NH_4Cl . The amount of NH_4Cl formed and thus the NH_3 concentration in the flow was determined electrochemically (Orion Research ammonia electrode model 95-10).

Other elements in the gas handling system are as follows: a shut off ball valve to stop the flow of combustible H_2 in case of failure of a window or some other sealing element in the system, a particle filter to remove particles larger than $60\text{ }\mu\text{m}$ diameter from the flow, a condenser to remove water from the gas exiting the cell, a relief valve to prevent the occurrence of cell pressures higher than 190 psia, a check valve to prevent the migration of air into the system containing ambient pressure hydrogen in case of a window or seal failure, and an electrically heated hot nickel wire to catalyze the combustion of waste hydrogen emerging from the system.

Diagnostic Apparatus

The diagnostic apparatus to be described was designed to permit the nearly simultaneous determination of the spatial dependence of the power loss and optical phase shift experienced by $10.6\text{ }\mu\text{m}$ light passing through the gas mixtures of interest to this study. The apparatus is shown schematically in Fig. 33. The previously described cell was placed as shown in one arm of a Mach Zehnder interferometer upon a sliding stage to permit the center of the plasma formed within the cell to be moved horizontally along the y axis with respect to the interferometer light beam. The latter originates from a 9W CO_2 electric discharge laser operating on the P(18) transition at 946 cm^{-1} frequency. The beam from this laser passes through the telescope, made up of mirrors M_1 (1.0 m radius of curvature) and M_2 (1.47m radius of curvature) to be expanded in size prior to entering the interferometer to a diameter of about 14 mm. As the laser

DIAGNOSTIC APPARATUS



output was polarized, the interferometer beam splitters B_1 and B_2 were coated for 50 percent transmission at $10.6 \mu\text{m}$ wavelength and S wave polarization. Upon emerging from the interferometer at beamsplitter B_2 the CO_2 laser beam passed through lens L_1 , whose function will be described shortly, and onto the rotating mirror M_R which sweeps the beam across the gold doped germanium detector A, equipped with a mask and a 0.2mm pinhole, whose output is thus the y dependent intensity of the beam emerging at B_2 . To ensure that in reducing the data the intensity readings to be compared refer to the same position on the y axis, the beam from the helium-neon (HeNe) laser is also directed onto M_R and thence to the pin diode detector P whose output is superimposed on that from A, giving a data record consisting of a short, negative voltage spike corresponding to the HeNe beam followed by the broader positive voltage curve which is proportional to the CO_2 beam intensity. The mirror M_R rotates at 4000 revolutions per minute so that the time interval between successive data records is 15 msec.

Under conditions where absorption of energy from the high power laser beam, by either the plasma or simply the gas mixture alone, is high, density gradients within the cell are large enough to cause considerable refraction of the CO_2 probe laser light. Uncorrected, this refraction causes large errors in determining the y dependent power loss and phase angle shift, and the lens L_1 is placed as shown to reduce this problem. The germanium lens L_1 has a 20 cm focal length, is AR coated at $10.6 \mu\text{m}$ wavelength and is positioned to image the axis of the high power laser within the cell onto the pinhole of detector A. As a result, all refraction effects occurring near the high power beam axis are removed as far as their effect on the measurement of the beam intensity profile at the detector A is concerned.³⁴

In order to obtain both power loss and phase shift information, two shutters, herein referred to as shown on Fig. 33 were used. Shutter 1 is a Princeton Applied Research Model 125A operating in a manner so as to chop the beam going through the cell at a rate of 2000 per minute so that this beam is swept across detector A on every other revolution of the mirror. Shutter 1 is equipped with a light emitting diode and detector which operate to provide an output voltage whenever shutter 1 is open. This voltage is fed into a Tektronics FG504 function generator the output of which is used to trigger shutter 2, a Laser Precision CTX534 Radiation Chopper in such a manner that the latter is locked on to chopping the beam through the reference side of the interferometer at half the rate that shutter 1 chops the beam passing through the cell. As a result, on four successive rotations of M_R , detector A receives the following information; First, with both shutters open, the interferometer throughput $I_i(y)$; second, with shutter 1 closed and shutter 2 open, the throughput of the reference side of the interferometer only, $I_r(y)$; third, with shutter 1 open and shutter 2 closed, the throughput of the cell only, $I_c(y)$; fourth, with both shutters closed no laser intensity is seen by the detector, but any detectable spontaneous emission occurring in the cell as a result of the presence of plasma is recorded by the detector, $I_n(y)$.

Assuming that no spontaneous emission is detected so that $I_n(y)$ is zero, the absorption $\Delta P(y)$ and phase angle change $\Delta \phi(y)$ were calculated from intensity profiles measured with plasma present combined with those obtained prior to the establishment of plasma, denoted by the superscript zero:

$$\Delta P(y) = \ln(I_r(y)/I_c(y)) + \ln(I_c^0(y)/I_r^0(y)) \quad (21)$$

$$\Delta \phi(y) = \cos^{-1} \left(\frac{I_i(y) - I_r(y) - I_c(y)}{2(I_r(y)I_c(y))^{1/2}} \right) - \cos^{-1} \left(\frac{I_i^0(y) - I_r^0(y) - I_c^0(y)}{2(I_r^0(y)I_c^0(y))^{1/2}} \right) \quad (22)$$

If spontaneous emission is detected, the quantities $I_i(y)$, $I_r(y)$ and $I_c(y)$ were corrected for this simply by subtracting $I_n(y)$ from each. It is thus seen that the quantities $\Delta P(y)$ and $\Delta \phi(y)$ were obtained from information collected in two 45 msec intervals, respectively located after and prior to the establishment of the laser sustained plasma.

Detector Signal Conditioning and Storage

As can be seen from the foregoing discussion, complete data sets consisting of $I_i(y)$, $I_r(y)$, $I_c(y)$ and $I_n(y)$ were collected at the rate of about 17 sec^{-1} for a total of nearly 100 sets for a six second long data collecting interval, and it was necessary to find a means of storing this mass of data until it was convenient to analyze it. This was done by storing the data signal on magnetic tape.

The output of detectors A and P were fed into the positive and negative input channels respectively of a Tektronix 1A7A differential amplifier, and the gain of the latter was adjusted to obtain an amplifier output signal of 0.10 to 0.15 volt at the maximum value of $I_i(y)$. Larger output signals from this amplifier resulted in a saturated signal being recorded on the tape due to saturation of the amplifier of the tape recorder which had a gain of about ten. The output of the 1A7A was fed into a Tektronix Type O operational amplifier with unity gain which provided the impedance matching necessary to obtain successful recording of the signal on the magnetic tape by the Sony AV-3650 videocorder used. If for the interferometer, the angle ϕ is defined according to Eq. 23,

$$I_i = I_r + I_c + 2(I_r I_c)^{1/2} \cos \phi \quad (23)$$

then the largest signal recorded is $I_i(y)$ corresponding to ϕ equaling zero. The magnitude of this signal was on the order of one volt.

Data Processing

Data Selection

Experimentally it was found that subsequent to a significant change in the rate of energy deposition into the cell contents, either by simply turning on the high power laser or by establishing a CW laser sustained plasma in the cell, there was always a period of no more than 5 seconds during which the quantity $I_i(y)$ exhibited marked temporal variation prior to settling into a quasi steady state in which its temporal variation was much smaller. This induction time is consistent in magnitude with the calculated time, τ , needed to obtain a steady state temperature distribution by thermal conduction inside a radius of magnitude a in a gas of density, ρ , specific heat C_p , and thermal conductivity K as given by

$$\tau = \frac{\rho C_p a^2}{4K} \quad (24)$$

For hydrogen at eleven atmospheres and a radius, 1.6 cm, consistent with the high power laser beam-to-cell wall distance, a value of 5 seconds is calculated for τ . Typically, then, an experimental run that lasted 15 seconds provided 10 seconds of data during which a quasi steady state situation persisted inside the cell. During this period, $I_i(y)$ did not remain constant but typically showed periods 180-235 msec long of rapid variation followed by periods of similar duration during which it remained nearly constant. The reason for this behavior is not known but may be due to instabilities in the buoyancy driven vertical gas flow field about the high power laser axis. The tape record for the quasi steady state time interval was scanned, advancing the tape manually with the recorder at stop action playback, and data was selected for reduction under the criterion that the data selected occurred between successive identical $I_i(y)$ profiles.

Transfer of Data to Computer

Each data record, consisting of the He-Ne and CO₂ probe laser intensity profiles was 200μsec long for the beam dimension, mirror M_R rotation rate and M_R -to-A distances used in these experiments. From each data record, detailed and accurate intensity information had to be obtained for use in Eqs. (21) and (22). To do this, each selected 200μsec long voltage trace stored on the magnetic tape was digitized and stored as a 512 element array on an IBM Diskette 1 type "floppy disk." With the tape recorder in the stop action-playback mode a portion of the tape containing the 200μsec interval of interest was repeatedly scanned and fed into a Tektronix 7A22 differential amplifier in a Tektronix 7704A oscilloscope system equipped with a P7001 processor. The desired 200μsec interval was selected using the oscilloscope's 7B71 Delaying Time Base, and this

interval was sampled twenty times to average out noise not present on the tape record and then stored on the "floppy disk." The computer system used is a Digital RX01 equipped to interface with the P7001 processor, and the computer program STOR2 used is listed in Appendix B. Details of the language and computer subroutines used in this and the other computer codes listed in the appendices are found in Ref. 35.

Final Adjustments on Computer-Stored Data

Prior to their use in Eqs. (21) and (22), the data records, now consisting of 512 element numerical arrays, denoted herein simply by the alphabetic character associated with the physical quantity, are finally adjusted to ensure first that the given address in each array refers to the same value of y , second that the base line of each array is correctly zeroed and third that a tape recorder imposed noise signal approximately 7 mv in magnitude and 66 μ sec in period is subtracted from each array. When appropriate, the spontaneous emission from the cell as stored in I_n was subtracted from the intensity record. This exercise is carried out using the computer program RED5, described in Appendix C.

B. Calculation of Absorption

With the data corrected for zero level, periodic noise and array address and spontaneous emission as described above, a power loss array was calculated using a computer program corresponding to Eq. (21), and this program, DAL1, is described in Appendix D.

Calculation of Phase Angle Shift

To calculate the phase angle shift array $\Delta\phi$ experienced by the probe laser beam passing through the cell with plasma present, three distinct calculations were made, starting first with the calculation of the phase angle array ϕ from Eq. (23), and the computer program, P, associated with this calculation, is given in Appendix E. The quantity ϕ was then calculated using the computer program, DRED4, listed in Appendix F. Operationally this program first computes the arrays X and $\cos X$ and then compares each element in $\cos\phi$ with each in $\cos X$, to select the element in the latter closest in value to the former and finally to assign the corresponding element in X to ϕ .

As indicated by Eq. 22, to calculate $\Delta\phi$ the preceding operations were carried out on data sets taken prior to and during the presence of the laser supported plasma, with $\Delta\phi$ being the resultant difference between the calculated values. However, the only values of ϕ directly calculable lie between $-\pi$ and 0 and there

is therefore a second array, $-\phi$, corresponding to the same values of $\cos\phi$. There is therefore the ambiguity as to which of the four quantities $\phi-\phi^*$, $\phi+\phi^*$, $-\phi-\phi^*$, or $-\phi+\phi^*$ accurately describes $\Delta\phi$.

The above ambiguity is resolved by considering the physical situation giving rise to $\Delta\phi$. The phase shift is given in terms of the change in the index of refraction, n , along the path $(-X_0, X_0)$ traversed by the beam

$$\Delta\phi(y) = \frac{2\pi}{\lambda} \int_{-X_0}^{X_0} (n(x,y) - n^0(x,y)) dx \quad (25)$$

where λ is the radiation wavelength, $10.6\mu\text{m}$. The index of refraction is related to the gas pressure, p , and temperature T as well as the polarizability of the gas α according to (36)

$$n = \frac{2\pi p \alpha}{kT} \quad (26)$$

It is seen that $\Delta\phi(y)$ is negative and if as in the present experiments, the temperature distribution has cylindrical symmetry with a maximum on the axis, which is the high power laser beam axis, then $\Delta\phi(y)$ passes through a minimum at y equals zero. With this knowledge, $\Delta\phi$ is obtained first by examining the four quantities described above and deciding which is most likely to describe $\Delta\phi$ based on its shape and the position of its minimum compared to the position of the plasma center as determined from the position of maximum detected plasma spontaneous radiation. This procedure was carried out in the computer program CHOOS2 described in Appendix G.

Obtaining Absorption Coefficient and Temperature

Given a sample with axial symmetry in the property ϵ about the z axis on any xy plane, the observed quantity E measured along the X direction at a distance y from the zx plane is given by

$$E(y) = 2 \int_0^{(r_0^2 - y^2)^{1/2}} \epsilon(r) dx \quad (27)$$

where r_0 is the radial boundary past which the property $\epsilon(r)$ vanishes. With $E(y)$ measured and known, $\epsilon(r)$ is obtained from the Abel transform³⁷

$$\epsilon(r) = -\frac{1}{\pi} \int_r^{r_0} \frac{dE(y)}{dy} (y^2 - r^2)^{-1/2} dy \quad (28)$$

When the quantity $E(y)$ is the absorption Δp , $\epsilon(r)$ is the difference between the product of the absorption coefficient $k(r)$ and the absorber density $u(r)$ from its value prior to establishing the plasma. Similarly, when $E(y)$ is the phase angle shift, $\epsilon(r)$ is the refractive index differential $n(r) - n^0(r)$

In the present work, this technique, commonly referred to as Abel inversion, was accomplished by first fitting $E(y)$ to the form

$$E(y) = \sum_{n=0}^N a_n y^{2n} \quad (29)$$

for which case

$$\epsilon(r) = \sum_{n=1}^N 2na_n F_n(r) \quad (30)$$

where

$$F_n(r, r_0) = \int_r^{r_0} \frac{y^{(2n-1)}}{(y^2 - r^2)^{1/2}} dy$$

and

$$F_n(y, r) = \sum_{m=0}^{n-1} \frac{(-1)^m 2^{2m} m! (n-1)! (y^2 - r^2)^{\frac{2m+1}{2}} y^{2(n-m-1)}}{(2m+1)! (n-m-1)!} \quad (31)$$

That Eq. (31) is true is seen by observing that

$$\frac{dF_n(y, r_0)}{dy} = \frac{y^{2n-1}}{(y^2 - r^2)^{1/2}} \quad (32)$$

The task of fitting $\Delta P(y)$ and $\Delta \Phi(y)$ to y is accomplished by use of the computer program MASAG5 which is listed in Appendix H. In this program, the portion of the array to be fitted to a polynomial is selected, and random noise in this portion is averaged over. The subroutine assigns values of y to the locations of the array to be fitted, and the z axis is in practice always assigned to whatever address is observed to occur at the plasma center as observed from the spontaneous emission from a plasma established in H_2 . In assigning y values to array locations, use is made of a factor which is the number of centimeters per unit change in array address number and is based on the rotation rate of the mirror, the mirror-to-detector distance and the known $200 \mu\text{sec}$ temporal width of the arrays used in this work. The size of this factor is $.00535 \text{ cm}$ per array address change. It is thus seen that the 200μ pinhole causes the recorded data to be effectively an average over nearly four array addresses. In selecting the expression $E(y)$ to fit the data, the polynomial order, is increased until the resulting graph of $E(y)$ is judged by visual inspection to be a good representation of the data.

The value of r_0 is the value of y for which the polynomial fit first crosses zero. In the case of $\Delta \Phi$, the procedure as described thus far does not permit accurate determination of the magnitude of the minimum in $\Delta \Phi$. That is, the minimum calculated may differ from the actual value by an increment equal to an integral factor of 2π . For experiments in which the high power laser beam was simply focused into the gas mixture with relatively small interaction with it, the temporal variation in I_1 was slow enough to permit accurate estimation of $\Delta \Phi$, and it was found that in these cases the magnitude of $\Delta \Phi$ was such that r_0 was equal to or slightly less than the distance of the z axis to the cell wall, 1.6 cm . When the high power beam-mixture interaction was intense as in the pressure of plasma, the variation in I_1 was too fast to follow from the recorded data and so the increments of -2π were added to the value of the minimum in $\Delta \Phi$ until the calculated value of r_0 fell close to 1.6 cm .

With the data fitted to the polynomials, the task remained to carry out the Abel inversion, and this was done for both $\Delta P(y)$ and $\Delta \Phi(y)$ by the computer program ABEL8 listed in Appendix I.

Obtaining $k(r)u(r)$ from $\Delta P(y)$ was carried out in a quite straightforward manner, but the method of obtaining $T(r)$ from $\Delta \Phi(y)$ merits more discussion at this point. Combining Eqs. (25) and (26) and substituting the density ρ for p/kT inversion results in calculation of the temperature itself but rather the product of the density and the species averaged polarizability $\bar{\alpha}$ of the medium at radius r :

$$\rho(r)\bar{\alpha}(r) = \frac{\lambda}{4\pi^2} \epsilon \phi(r) + \rho^0 \bar{\alpha}^0 \quad (33)$$

where $\epsilon_\phi(r)$ is the value of $\epsilon(r)$ with $E(y)$ being $\phi(y)$. Using the temperature dependent chemical equilibrium calculation shown in Fig. 7 and a similar one for ten atmospheres pure H_2 , along with literature values of the zero frequency polarizability of H_2 , H and O_2 ³⁸, O ³⁹ and H_2O ⁴⁰, the species averaged polarizability was calculated for ten atmospheres H_2 and compared to that for ten atmospheres H_2 and $0.5 H_2O$. The latter was found to exceed the former by 8 percent due to the large H_2O polarizability, but this difference vanished at around 3000°K due to the dissociation of H_2O . Due to the small size of this difference, the polarizability of a mixture originally pure H_2 was used in the temperature calculation. The density ρ^0 in Eq. (37) was obtained from readings of cell pressure, P_0 , and temperature, T_0 , using the pressure gage in Fig. 32 and a chromel-alumel thermocouple in the lower thermocouple well in Fig. 31. In practice, the cell pressure, P' , during the experimental run was found to differ from P_0 by as much as 15 percent due to the heat addition from the high power laser beam. Accordingly, this pressure was used in obtaining the temperature at r from $p(r)\bar{\alpha}(r)$ and a calculated plot of $\rho(T)\bar{\alpha}(T)$ vs. T .

As a result of this inversion, both the temperature and the absorption per cm were known as a function of radial position relative to the high power laser beam axis, thereby revealing the dependence of the latter upon the former.

SECTION IV

EXPERIMENTAL RESULTS

Refraction Effects

In an experiment in which a laser beam is used to obtain spatially detailed information near a hot dense plasma which gives rise to steep temperature and refractive index gradients, the question arises as to what extent the latter cause significant refraction of the diagnostic laser beam and thereby affect the quality of the data. As mentioned earlier, the 20 cm focal length lens was placed at the exit of the interferometer to correct such refraction effects, and this section describes the success obtained.

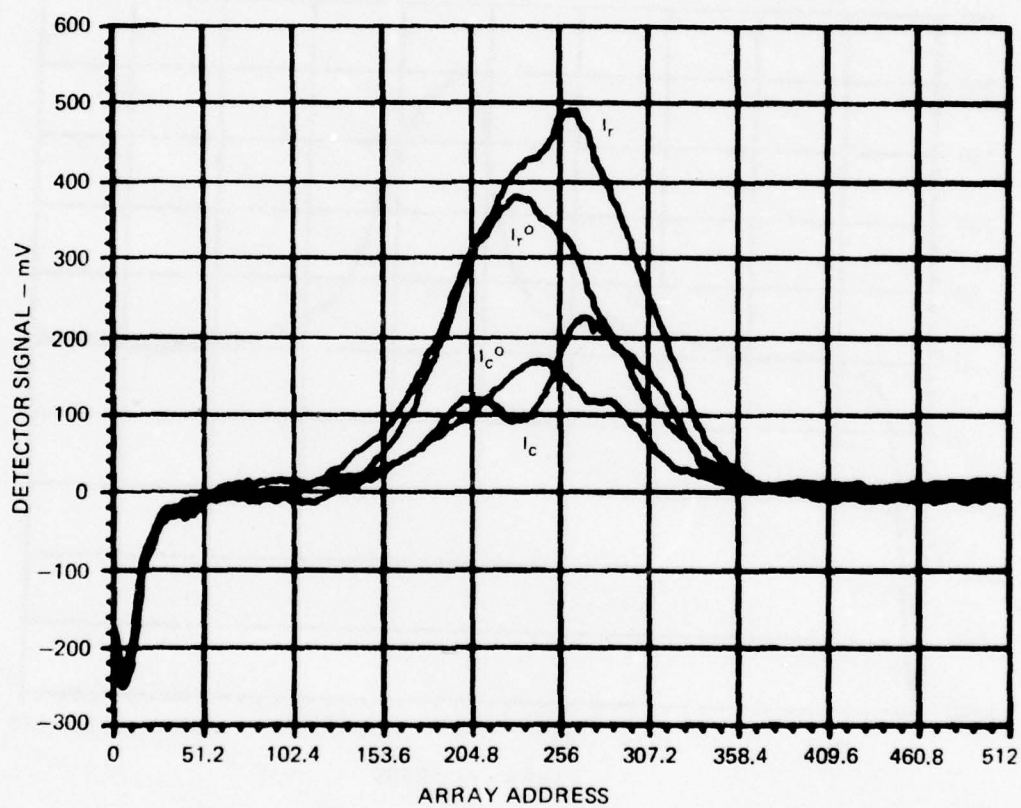
With the cell filled with H_2 at 150 psig, a laser sustained plasma was established and data taken as described in the previous sections. Figure 34 shows the arrays I_r , I_c , I_r° and I_c° the former pair exhibiting substantial distortion due to spontaneous emission from the plasma, and Fig. 35 shows the array I_n containing the detected spontaneous emission. The arrays I_r and I_c were processed through RED5 which subtracted out I_n to eliminate the effect of the emission on the latter, and the same four arrays are re-plotted in Fig. 36. The attenuation of I_r by the plasma is seen to occur at nearly the same location as the onset of the radiation intensity. The exact separation between the two onsets is about 0.05 cm, with essentially no distortion in I_r occurring at points further away from this point which is 0.4 cm from the plasma core. When this data was fully reduced, the onset of absorption was calculated to occur at a radius of about 0.4 cm, where the temperature was calculated to be 8200°K, in substantial agreement with the results given for the onset of inverse bremsstrahlung absorption in hydrogen in Ref. 41. Of more importance however, the fact that no distortion of I_r occurs at greater radial positions and lower temperatures, as expected for pure H_2 , infers that refraction, even in the presence of plasma, has no significant effect on the data in the temperature region of interest to this study.

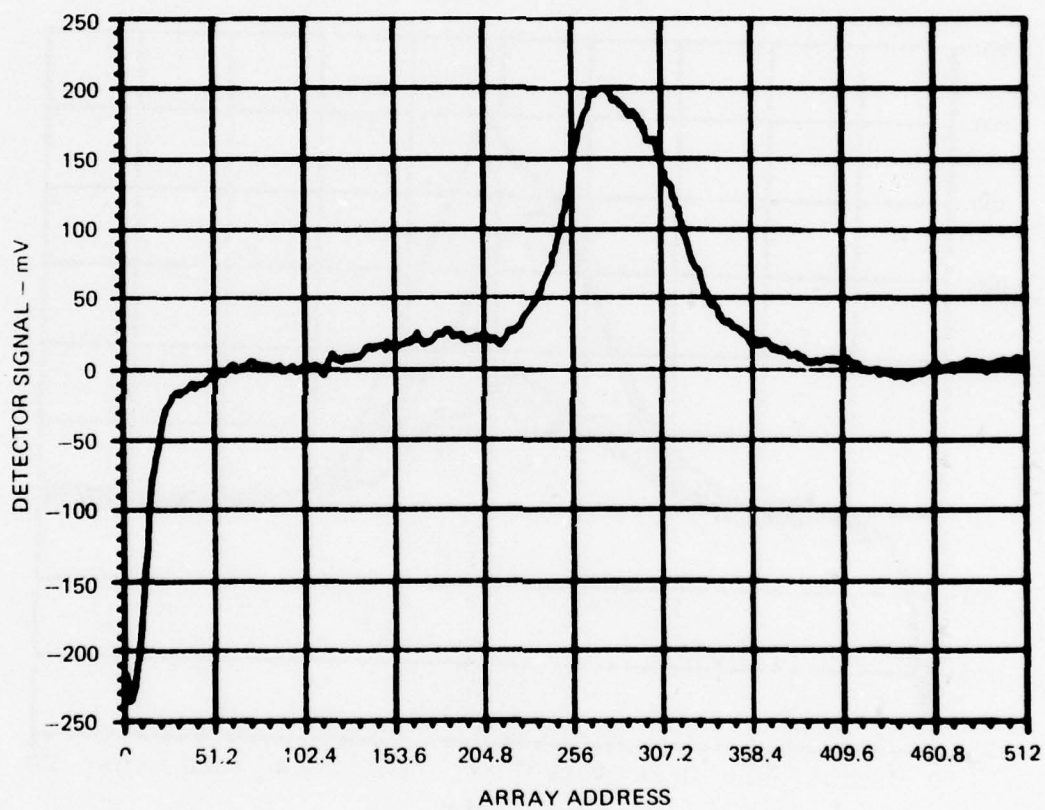
The Laser Sustained Flame

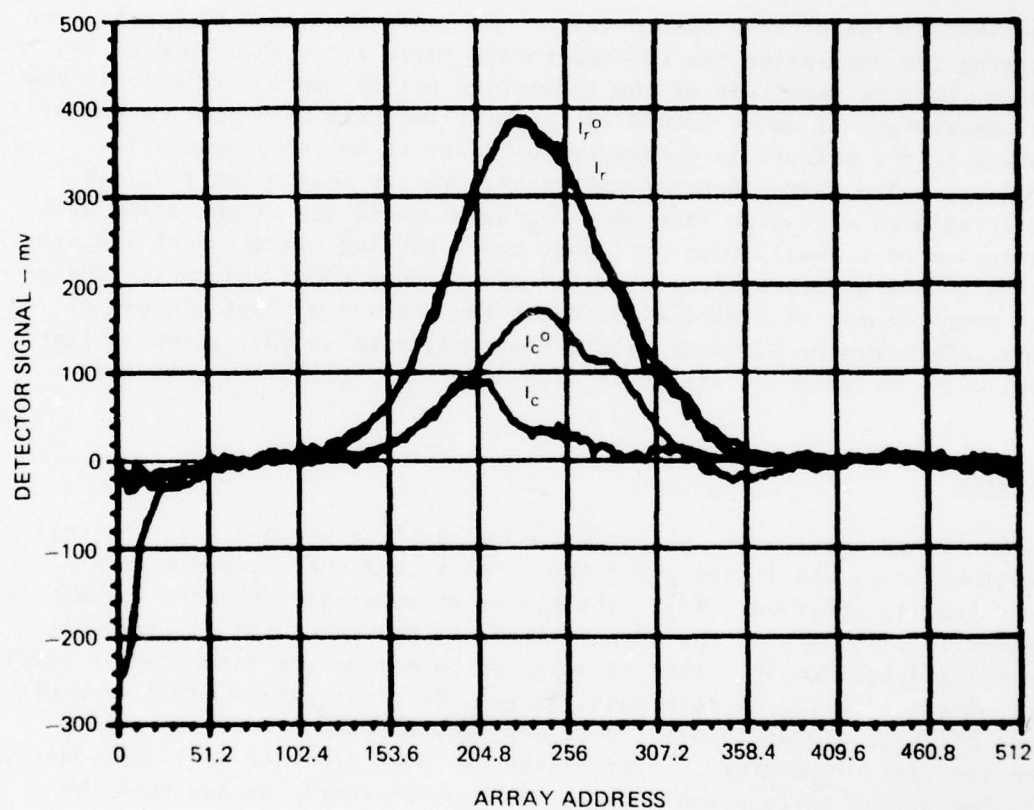
Introduction

In all three of the gas mixtures reported on here, an interesting phenomenon was observed which has important implications for the laser energized rocket thruster as well as providing a second source of experimental data for the present study. In all of the H_2/NH_3 experimental runs and in many of the H_2/H_2O and H_2/D_2O runs, a tenuous visible glow appeared at the focal spot of

MEASURED PROFILES I_r^0 AND I_c^0 ALONG WITH I_r AND I_c
IN THE PRESENCE OF LASER SUSTAINED PLASMA IN 11 ATM H_2



MEASURED SPONTANEOUS EMISSION PROFILE I_n 

PROFILES OF I_r^0 , I_c^0 , I_r AND I_c AFTER BEING PROCESSED THROUGH "RED5"

the high power laser beam in the absence of plasma. This glow was not observed in pure H_2 and its color was characteristic of the mixture in each case, having in each case a shape reminiscent of the flame from a match or stove burner, hence the application of the term "flame" to the phenomenon. Each flame was blunt at its base which was several millimeters in diameter and located at the high power beam focal spot. In length, each flame extended several cm above its base. The term flame does not infer the presence of combustion in the cell but rather the presence of a very hot region, as high as $3000^\circ K$ - $4000^\circ K$, heated by the absorption of energy from the focused high power laser beam by the mixture under study.

Importance

The implication of this phenomenon to the laser energized rocket is seen by examining the absorption per cm/temperature curve for H_2/H_2O in Fig. 24. It is seen that the magnitude of the absorption per cm remains relatively low until a temperature of about $1500^\circ K$ is reached, implying that some method of pre-heating of the mixture is necessary to render it suitably opaque for practical use. The flame phenomenon however, implies that a $300^\circ K$ H_2/H_2O mixture irradiated with high intensity CO_2 laser radiation is unstable, with the absorption of a small amount of laser power causing elevation of temperature which causes an increase in k_u which causes more power absorption and so on until temperatures of practical interest are reached without the use of auxiliary preheaters or low temperature absorbers such as NH_3 , which in fact was originally included in this study because of its possible use in this way.

Water Flames

As mentioned previously, plasma was most easily sustained when the cell was relatively cool and it was under these conditions that H_2/H_2O flames were most readily observed. This fact may be attributable at least in part to the greater focusability of the high power laser beam when the cell is cool, as hypothesized previously. Another explanation may be the formation of small droplets of water in the mixture when, as was often the case when water partial pressures of about 0.3 atmospheres were desired, the saturator temperature exceeded the cell temperature. Evaporation of these droplets or larger ones on the focusing mirror surface would cause the H_2O concentration and thus the absorption per cm in the beam to increase substantially and create a flame. However, temperature elevation characteristic of a flame was obtained in an experiment in which the cell temperature exceeded that of the saturator, inferring that extreme conditions such as the presence of droplets may not be necessary to flame formation. Experiments with H_2/H_2O and Ar/H_2O mixtures showed that the color of the flame is determined by the majority host gas, for the color in H_2/H_2O was orange with, for very strong flames, a white center while the color in Ar/H_2O was grayish blue.

Ammonia Flame

The H_2/NH_3 flame, like that for $\text{H}_2/\text{H}_2\text{O}$ and $\text{H}_2/\text{D}_2\text{O}$ was orange in color but, for the NH_3 concentration tested, redder and not as bright.

Example of Data Reduction

Reduction of Data

With the cell filled with hydrogen to a pressure P_0 of 147 psig (11.0 atmospheres) H_2 along with 0.3 atm H_2O , the recorded detector output appeared as shown in Fig. 37, and the presence of plasma in the cell had the effect shown in Fig. 38. Although the detected spontaneous emission in this experiment was not large enough to permit determination of the position of the high power laser beam axis, this property can be obtained from the calculated values of $\Delta\phi$ and ΔP shown in Fig. 39 and is seen to be at array address 170.

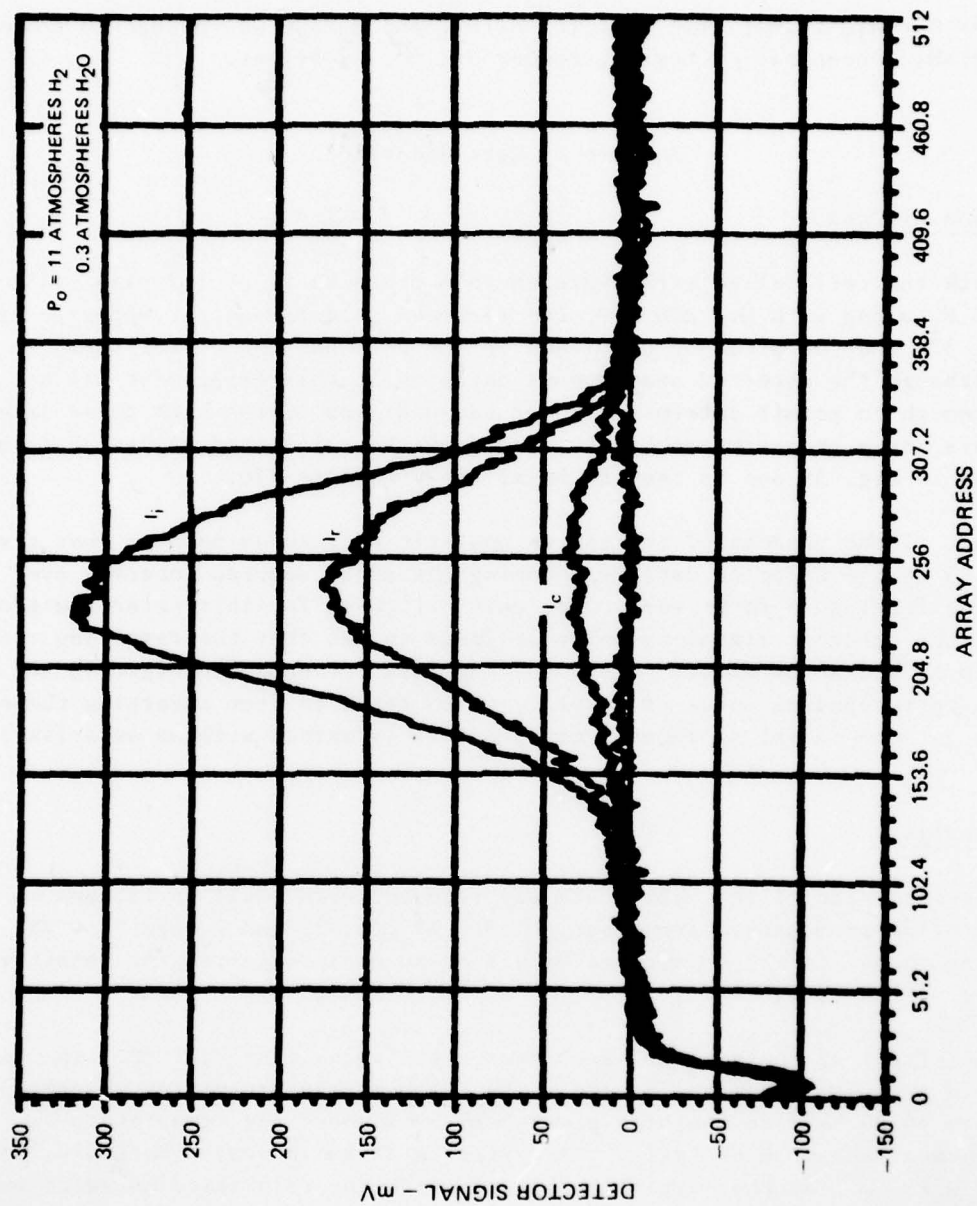
Part of the process of fitting an analytic expression such as that given in Eq. 33 to the $\Delta\phi$ or ΔP data is choosing the array address interval over which the fitting is to be made. The main criterion for this selection process is that the detector signal-to-noise be large enough that the resulting random noise in $\Delta\phi$ and ΔP be small. The resulting fits are shown in Figs. 40 and 41, and the corresponding curve of k_u vs T , which resulted from inverting these fits to get the radial dependence of k_u and T , is marked with an asterisk in Fig. 42.

Error Analysis

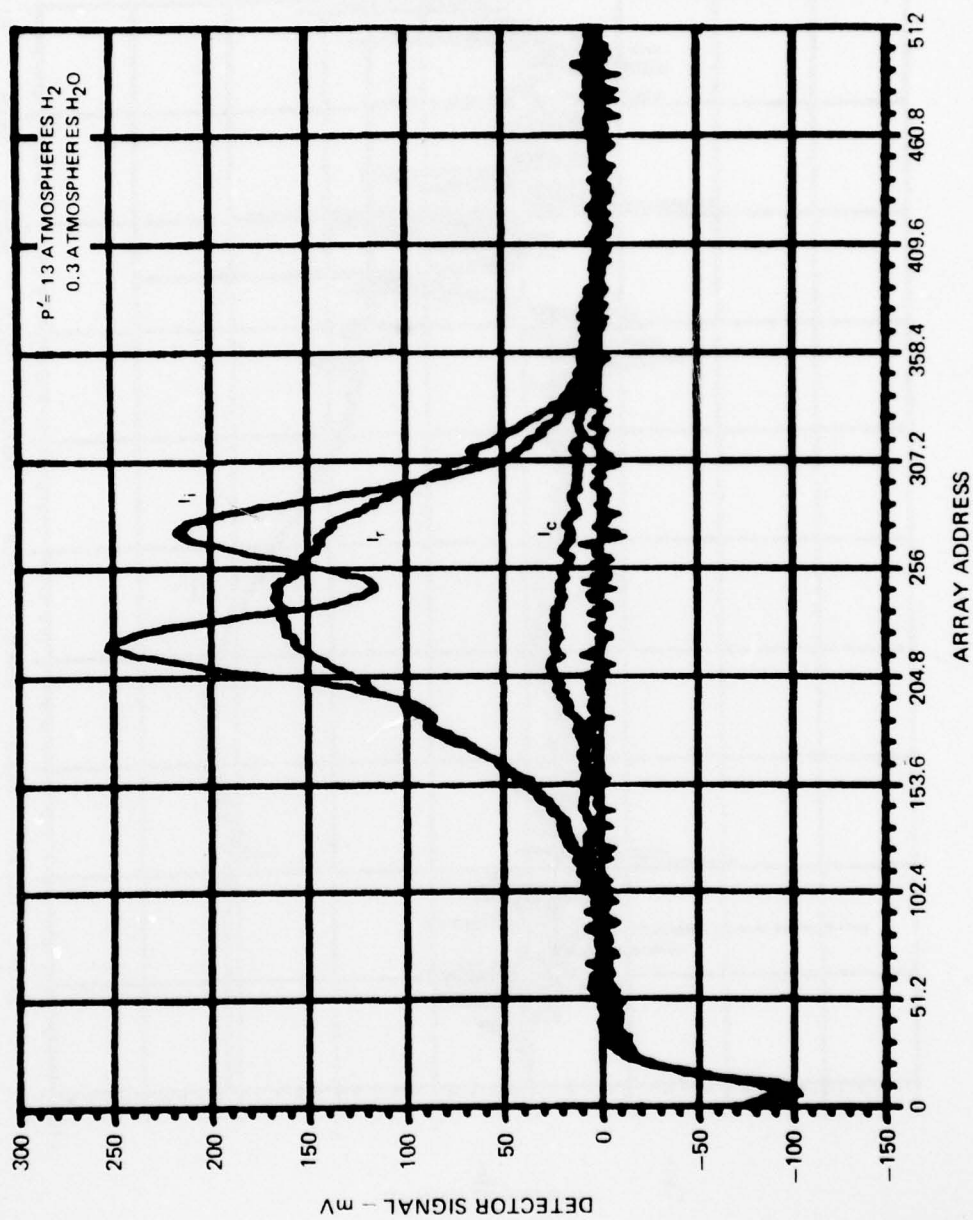
The inversion of the above data was repeated with small variations in each of the following measured input variables: ΔP , $\Delta\phi$, T_0 and P_0 and P' . The resulting change in the calculated values of k_u or T reflected the sensitivity of these on the variables.

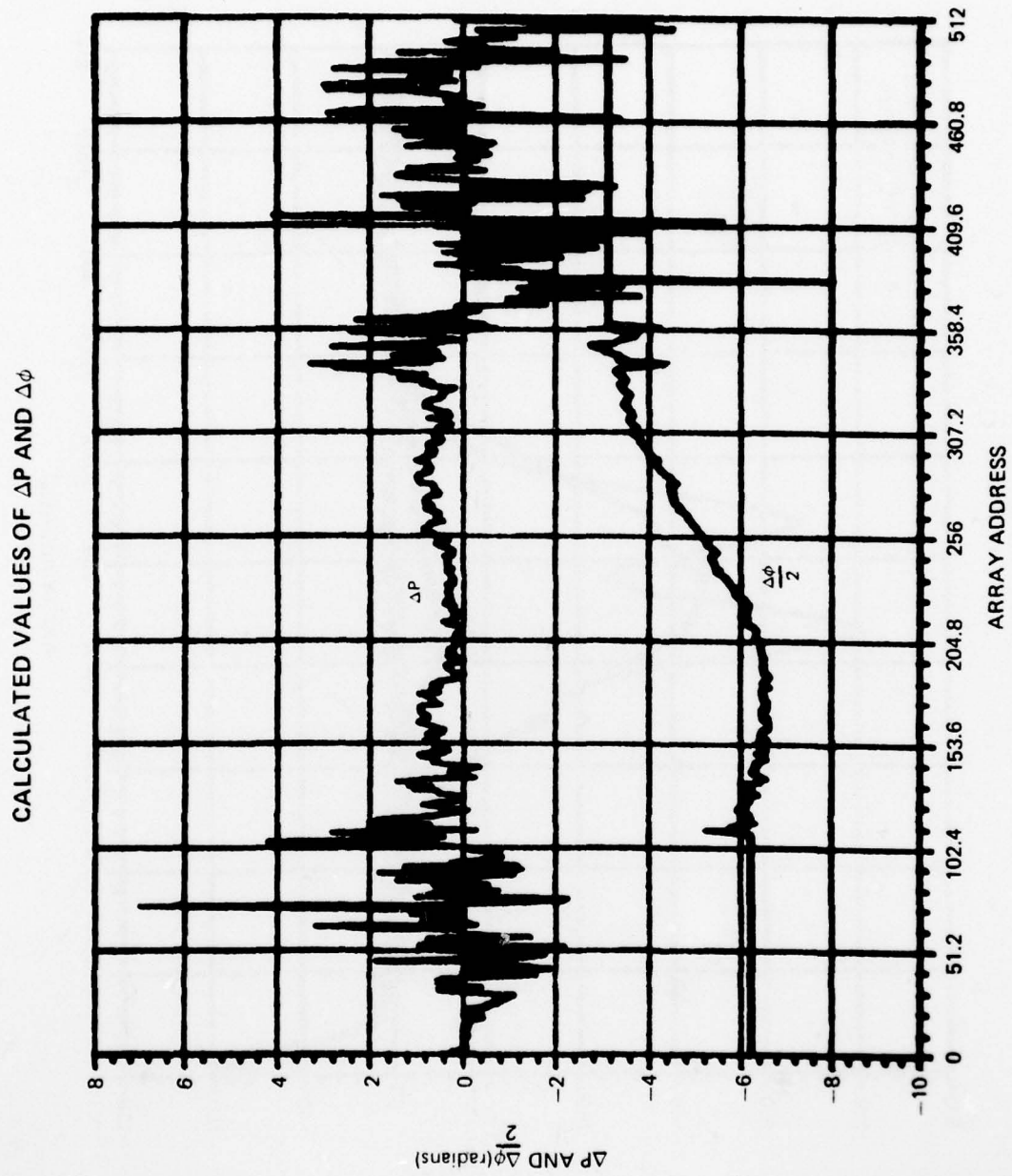
The effect of changing ΔP is to change the value of r_0 for ΔP . The applied change in ΔP was ± 0.1 which changed r_0 by ± 15 mm. The resulting change in k_u was $\pm 0.05 \text{ cm}^{-1}$ on the high power beam axis where the temperature was highest. Far from the axis, the variation in k_u increased markedly, being about $\pm 0.15 \text{ cm}^{-1}$ at the largest radii for which the calculated k_u value exceed zero. Therefore, the effect on the k_u vs T curve in Fig. 42 of increasing ΔP by 0.1 is to decrease significantly the severity of downward trend in k_u with decreasing temperature at the lowest temperatures while having much less effect at higher temperatures. Similarly decreasing ΔP , increases this downward trend.

BEAM PROFILES IN ABSENCE OF PLASMA



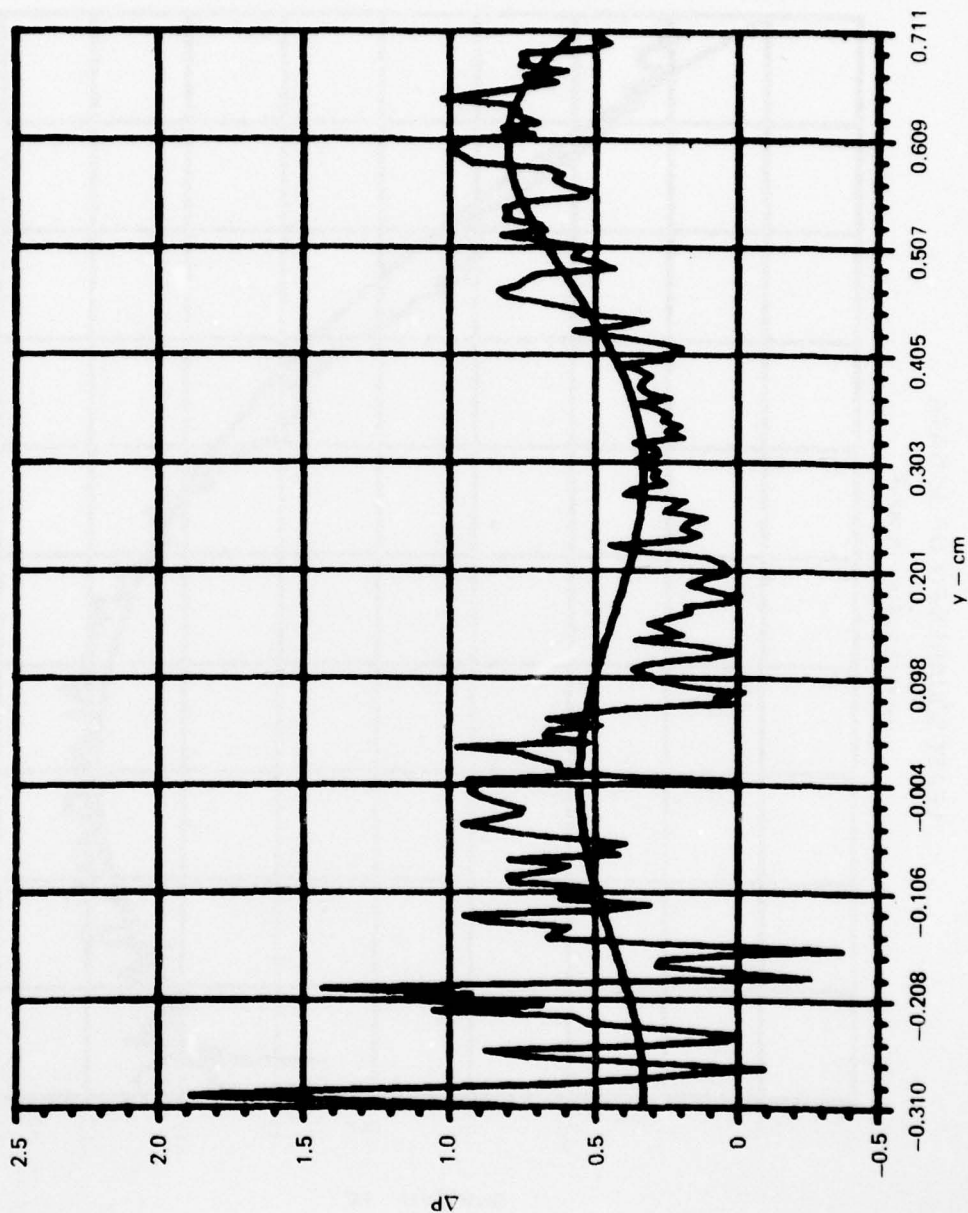
BEAM PROFILES IN PRESENCE OF PLASMA





LEAST SQUARES FIT OF ΔP DATA

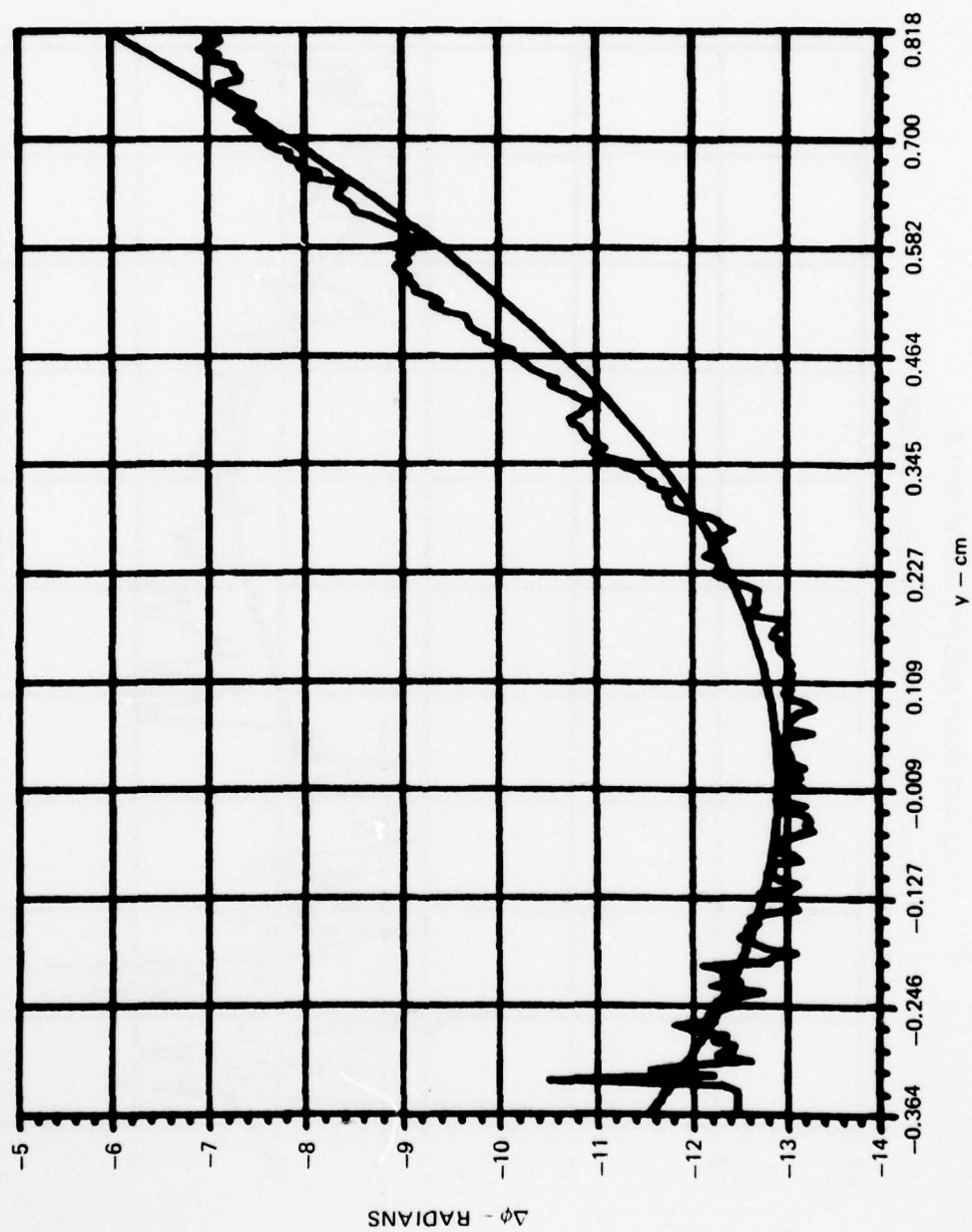
$$\Delta P(y) = 0.551 - 5.7529y^2 + 45.06y^4 - 97.23y^6 + 60.64y^8$$



79-06-12-9

LEAST SQUARES FIT OF $\Delta\phi$ DATA

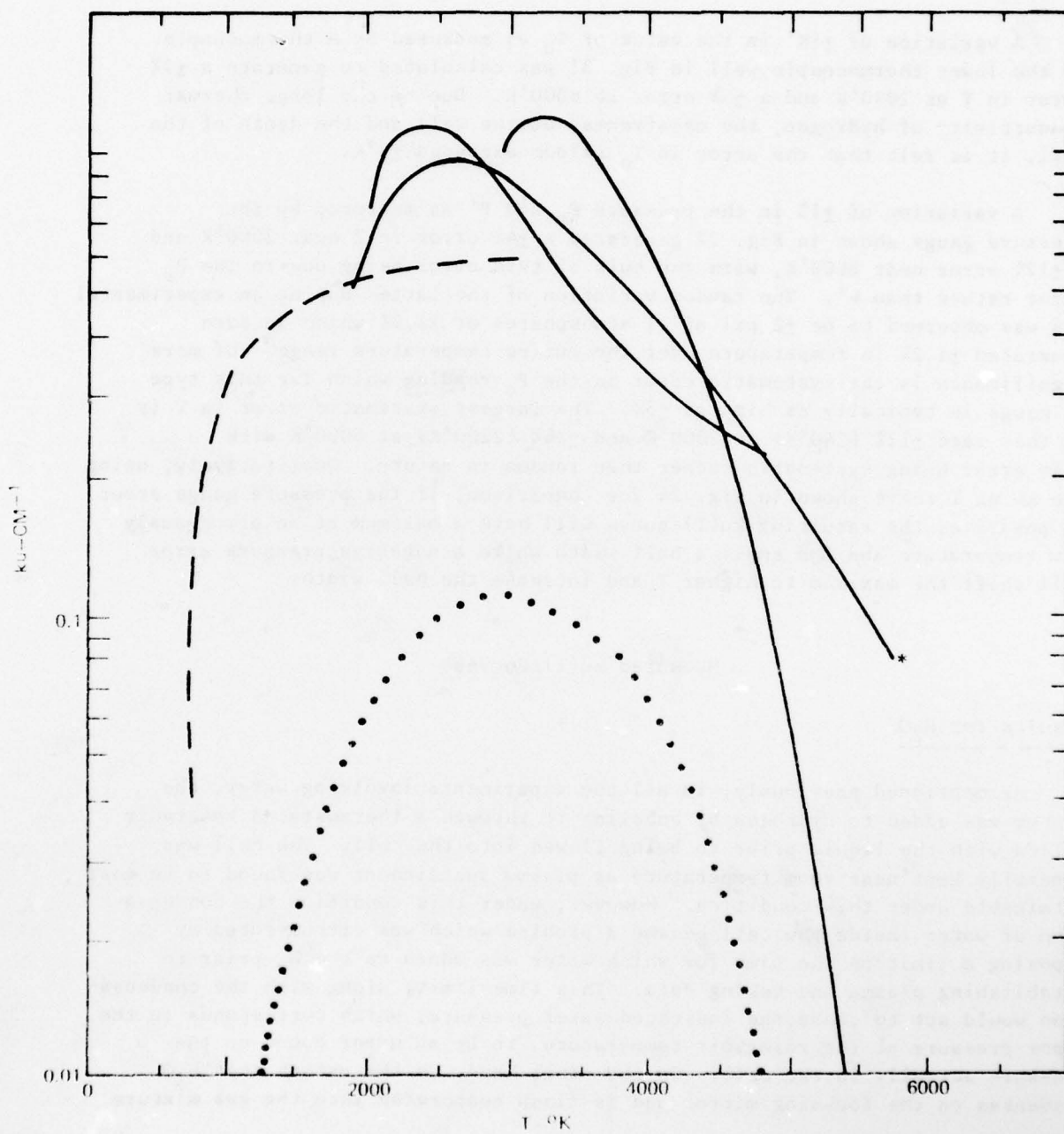
$$\Delta\phi(y) = -12.916 + 10.382 y^2$$



79-06-12-8

MEASURED k_u VS TEMPERATURE (T) H_2O (0.3 ATM) IN H_2 (13 ATM)

- PLASMA DATA
- - - FLAME DATA
- • • CALCULATED FOR
 $H_2: H_2O = 10:1$



Similarly, the effect of shifting $\Delta\phi$ is to change r_0 for $\Delta\phi$. At large radii and the low end of the temperature range, near 2000°K, it was found that a $\pm 1\%$ change in $\Delta\phi$ resulted in a $\pm 3\%$ change in T while at the smaller radii and larger temperatures the error increased to $\pm 7\%$. From Fig. 41, it is seen that the error in $\Delta\phi$ is likely to be typically $\pm 3\%$ generating a temperature error of 180°K near 2000°K and about 1200°K near 6000°K.

A variation of $\pm 1\text{K}^\circ$ in the value of T_0 as measured by a thermocouple in the lower thermocouple well in Fig. 31 was calculated to generate a $\pm 1\%$ error in T at 2000°K and a $\pm 5\%$ error at 6000°K. Due to the large thermal conductivity of hydrogen, the massiveness of the cell and the depth of the well, it is felt that the error in T_0 seldom exceeded $\pm 1^\circ\text{K}$.

A variation of $\pm 1\%$ in the pressure P_0 and P' as measured by the pressure gauge shown in Fig. 32 generated a $\pm 4\%$ error in T near 2000°K and a $\pm 12\%$ error near 6000°K, with the bulk of this error being due to the P_0 error rather than P' . The random variation of the latter during an experimental run was observed to be ± 2 psi at 11 atmospheres or $\pm 1.2\%$ which in turn generated $\pm 1.2\%$ in temperature over the entire temperature range. Of more significance is the systematic error in the P_0 reading which for this type of gauge is typically as high as $\pm 3\%$. The largest systematic error in T is in this case $\pm 12\%$ (240°K) at 2000°K and $\pm 36\%$ (2200°K) at 6000°K with this error being systematic rather than random in nature. Qualitatively, using the ku vs T curve shown in Fig. 24 for comparison, if the pressure gauge error is positive, the resulting $ku(T)$ curve will have a maximum at an erroneously low temperature and too small a half width while a negative pressure error will shift the maximum to higher T and increase the half width.

Measured $ku(T)$ Curves

Results for H_2O

As mentioned previously, in all the experiments involving water, the latter was added to hydrogen by bubbling it through a thermostated reservoir filled with the liquid prior to being flowed into the cell. The cell was generally kept near room temperature as plasma sustainment was found to be most attainable under this condition. However, under this condition the condensation of water inside the cell became a problem which was circumvented by imposing a limit on the time for which water was added to the H_2 prior to establishing plasma and taking data. This time limit, along with the condensation would act to cause the indicated water pressure, which corresponds to the vapor pressure at the reservoir temperature, to be an upper bound on the pressure actually in the cell. On the other hand, to the extent that H_2O condenses on the focusing mirror and is flash evaporated into the gas mixture

when the high power laser is turned on, the indicated H_2O pressure would be lower than that actually in the cell. Thus, the actual water pressure in the experiments reported on in this and the following D_2O section is characterized as being only an estimate.

The measured value of k_u as a function of temperature is presented for the H_2/H_2O system in Fig. 42. In this figure, there are five separate curves. The three solid curves are experimental results from data obtained in the presence of the laser sustained plasma, the one marked with an asterisk having been obtained as described in the preceding subsection. The dashed curve is also an experimental result obtained in the presence of the laser sustained H_2/H_2O flame. The dotted curve is the analytical result shown in Fig. 24.

Comparing the two sets of experimental results, denoted "plasma data" and "flame data", it is seen that they are quite consistent in magnitude while being complementary with respect to temperature, combining as they do to cover the temperature range from $700^\circ K$ to $5500^\circ K$.

Optical Saturation Effects

The similarity in magnitude between the flame and plasma data at $3000^\circ K$ is interesting when one notes that in the former case, this temperature is highest in the cell and occurs at the highest incident high power laser intensity, one to ten MW/cm^2 , whereas this same temperature range in the case of the plasma data lies outside the core of the laser sustained plasma where the incident high power laser intensity is on the order of $0.01 MW/cm^2$. It is recalled that the high power laser operates at essentially the same wavelength as the diagnostic laser so that the measured value of k_u is apparently not greatly affected by optical saturation effects at intensities as high as 1 to $10 MW/cm^2$.

With respect to optical saturation, two subject areas have been considered during the course of this study: first, collisional effects wherein the depopulation of an absorbing energy level by photon absorption exceeds the depopulation by intermolecular collisions, second, diffusion effects wherein the collisional effect is masked by flux of ground state molecules into the region irradiated by the laser. The former of these was treated in some detail in Section II for a 10:1 H_2/CO mixture at ten atmospheres pressure irradiated by CO laser radiation. In that study, the CO laser saturation intensity, I_s , at which the CO absorption coefficient decreased by 50% due to optical saturation was calculated to increase from $5.6 MW/cm^2$ at $2000^\circ K$ to $12 MW/cm^2$ at $3000^\circ K$. Although these values are consistent with the incident laser intensities used in the flames experiments, it must be remembered that collisional deactivation for diatomic molecules such as CO occurs at a much lower rate than for polyatomic molecules such as H_2O , and the I_s values calculated for CO are probably low compared to the actual value for H_2O so that the observed gap between the flame and plasma data for H_2/H_2O is probably not ascribable to optical saturation involving collisional phenomena.

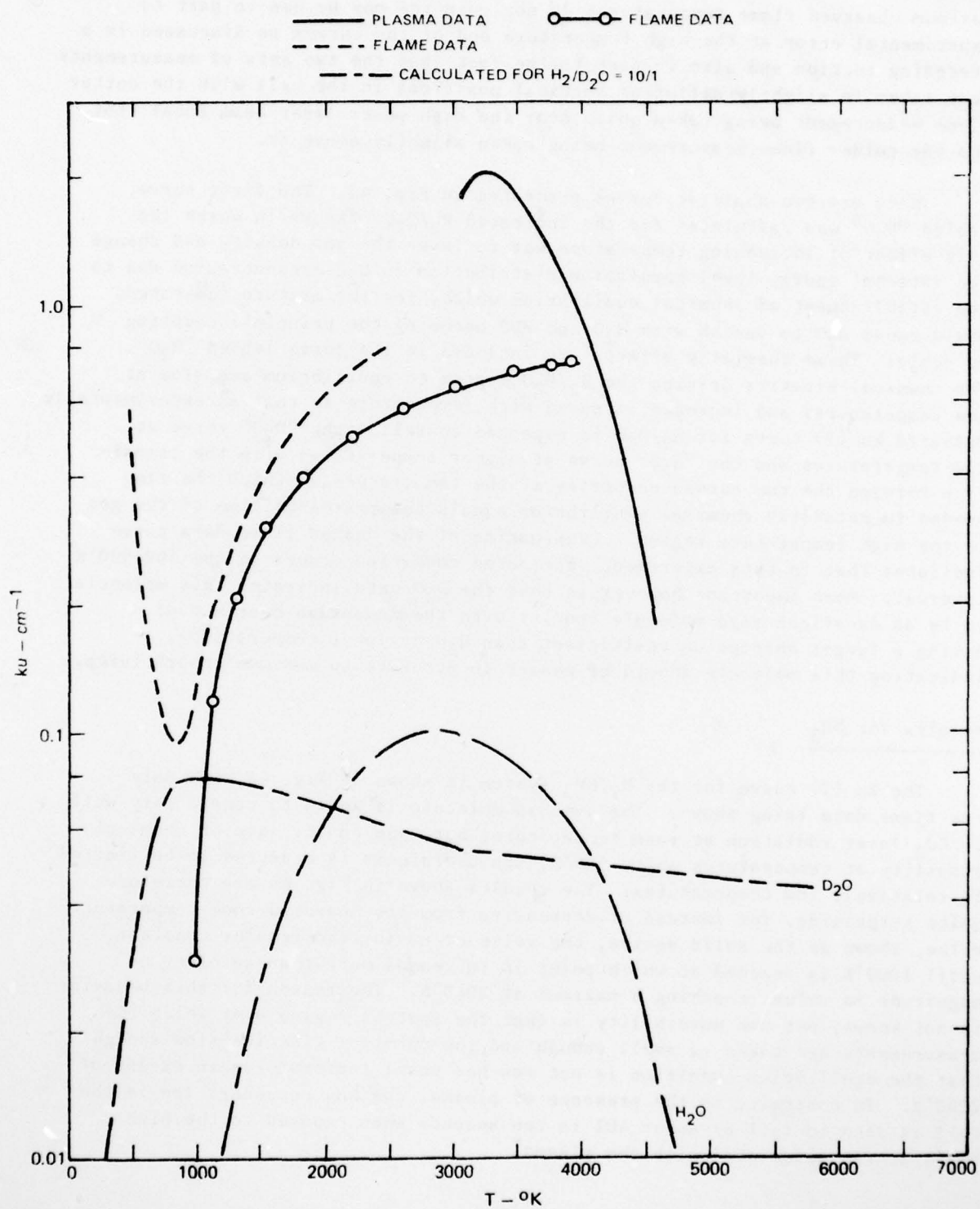
The second phenomenon mentioned was cited in Ref. 42 for cancelling optical saturation involving collisions by renewing, through diffusion into the laser beam, the supply of ground state molecules at a faster rate than through collisional deactivation of excited molecules. The beam diameter at which the rate of collisional deactivation equals that of diffusion is given by the square root of the ratio of twice the diffusion coefficient to the collisional deactivation rate and this diameter was calculated for H_2/H_2O to range from $9.76\mu m$ to $3.95\mu m$ over the temperature range between $300^\circ K$ and $6000^\circ K$ at 10 atm pressure. Since the smallest high power beam diameter in the flame experiments was roughly $80\mu m$, it is seen that diffusion effects cannot influence the value of I_s in these experiments.

Significance of Results

The most noteworthy feature of the results shown in Fig. 42 is their magnitude compared to the calculated value. It is seen that the former are consistently about an order of magnitude greater than the latter throughout the temperature range shown. At the same time, it is seen that a curve rough drawn through the entire experimental data set is nearly parallel to the calculated curve. These facts indicate that although the magnitude of the experimental results is significantly higher than calculated, their temperature dependence is consistent with that predicted by analysis. Part of the difference between the analytical and experimental results may stem from the fact that the former are derived from measurements averaged over 25 cm^{-1} intervals so that significant excursions from them are expected for measurements made over narrower intervals as in the present case. The expected degree of variation over a 25 cm^{-1} wide interval may be seen in Fig. 8. The important point to be noted is that the measured value of k_u is so large as to make H_2O a very attractive molecular seed for a laser energized rocket thruster.

Results for D_2O

The measured value of $k_u(T)$ is shown for H_2/D_2O mixtures in Fig. 43. As was the case in Fig. 42 several experimental runs are shown. The solid and dashed curves resulted from plasma and flame data respectively taken at a D_2O pressure of approximately 0.3 atm in 13 atm H_2 . The solid line-and-circles curve resulted from a flame measurement in which the cell temperature exceeded the saturator temperature so that more confidence can be placed on the D_2O pressure given than in the other H_2/D_2O experiments. As in the case of the H_2/H_2O experiments, the flame and plasma data at the same water partial pressure are seen to be consistent with one another and to provide data from about 500 to $4500^\circ K$. In addition, the flame data taken at the lower D_2O partial pressure is quite similar in shape to the other flame curve, but the two curves do not exhibit magnitudes which scale as the D_2O partial pressure, indicating that the 0.3 atm D_2O partial pressure given is probably an upper

MEASURED k_u VS TEMPERATURE (T) D_2O (0.3 atm) IN H_2 (13 atm) D_2O (0.10 atm) IN H_2 (11.4 atm)

79-06-12-13

bound to the value actually present in those experiments. The fact that the maximum observed flame temperatures do not coincide may be due in part to experimental error at the high temperature end of the curves as discussed in a preceding section and also in part to the fact that the two sets of measurements were taken in slightly different vertical positions in the cell with the hotter flame measurement being taken quite near the high power laser beam focal spot and the colder flame measurement being taken slightly above it.

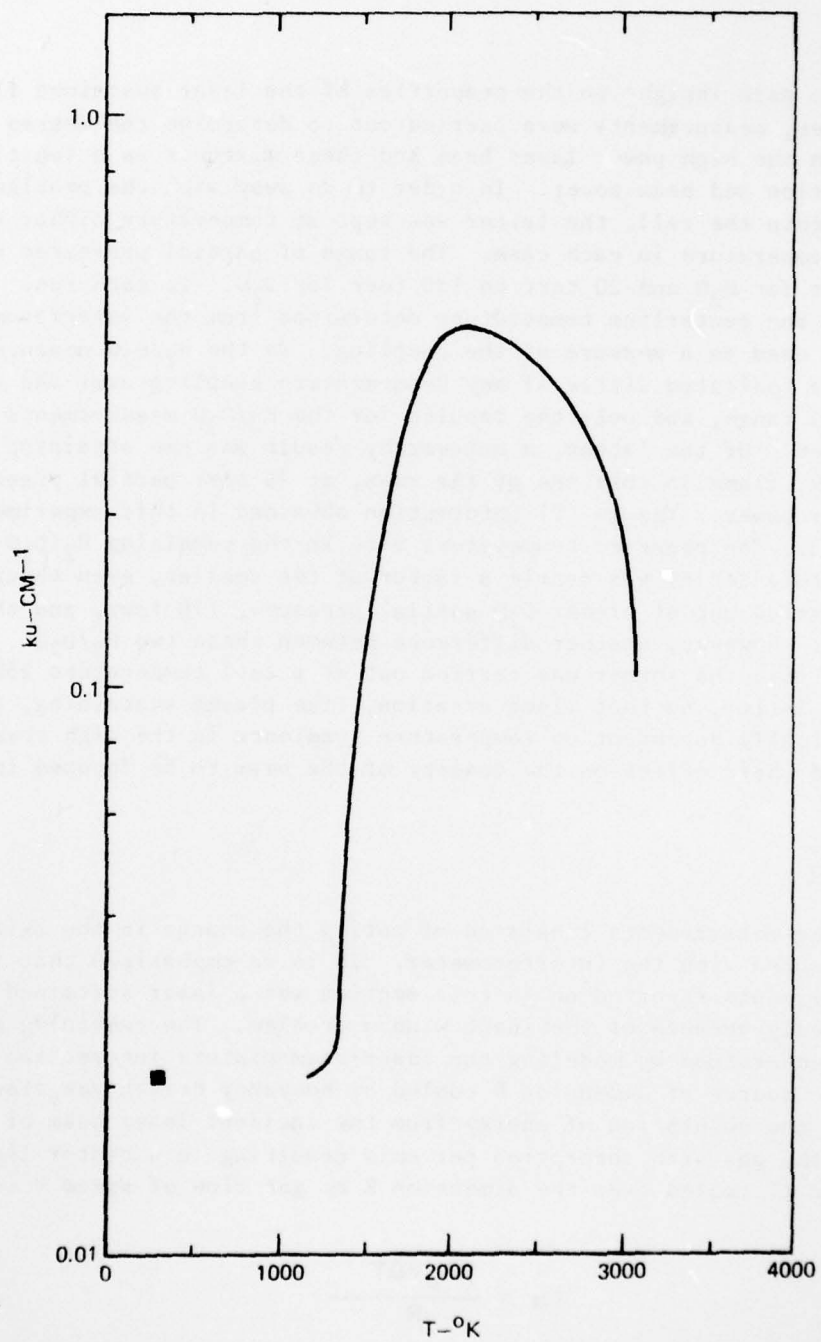
There are two analytic curves presented in Fig. 43. The first curve, labeled " D_2O " was calculated for the indicated H_2/D_2O mixture in which the only effect of increasing temperature was to lower the gas density and change the internal energy level population distribution in D_2O concentration due to the establishment of chemical equilibrium which, for the mixture indicated, would cause D_2O to vanish with H_2O and HDO becoming the principle coupling molecule. These chemistry effects are included in the curve labeled " H_2O ". The chemical kinetics driving the H_2/D_2O system to equilibrium are slow at low temperatures and increase in speed with temperature so that an experimentally measured $ku(T)$ curve for H_2/D_2O is expected to follow the " D_2O " curve at low temperatures and the " H_2O " curve at higher temperatures with the transition between the two curves occurring at the temperature at which the time needed to establish chemical equilibrium equals the residence time of the gas in the high temperature region. Examination of the dashed flame data curve indicates that in this experiment, the noted condition occurs in the 500-900°K interval. Most important however is that the D_2O data indicates this molecule to be an excellent seed molecule coupler with the advantage over H_2O of having a larger absorption coefficient than H_2O at lower temperatures, indicating this molecule should be easier to activate to maximum absorbtivity.

Results for NH_3

The $ku(T)$ curve for the H_2/NH_3 system is shown in Fig. 44 with only the flame data being shown. The ammonia molecule is known to couple very well to CO_2 laser radiation at room temperature, but, due to its lack of chemical stability at temperatures above 500°K, its usefulness is expected to be limited to relatively low temperatures. The results shown in Fig. 44 are therefore quite surprising, for instead of decreasing from its measured room temperature value, shown as the solid square, the value of ku instead remains constant until 1000°K is reached at which point it increases more than an order of magnitude in value, reaching a maximum at 2000°K. The reason for this behavior is not known, but one possibility is that the spatial region over which the measurements are taken is small enough and the chemical kinetics slow enough that the equilibrium condition is not reached until temperatures in excess of 2000°K. In contrast, in the presence of plasma, the NH_3 concentration in the cell is seen to fall by about 40% in ten seconds when exposed to the high temperatures associated with the plasma.

MEASURED k_u VS TEMPERATURE (T) $\text{NH}_3(0.086 \text{ ATM})$ IN 5.7 ATM H_2

FLAME DATA ONLY



AD-A080 037

UNITED TECHNOLOGIES RESEARCH CENTER EAST HARTFORD CONN
BEAMED ENERGY COUPLING STUDIES.(U)

F/G 21/8

JAN 80 M C FOWLER, L A NEWMAN, D C SMITH

F04611-77-C-0039

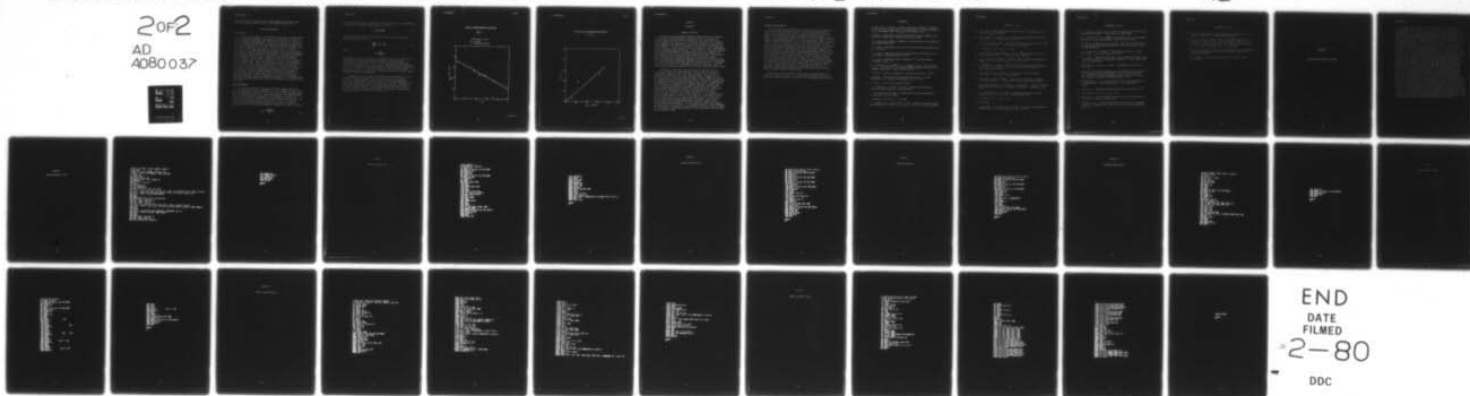
UNCLASSIFIED

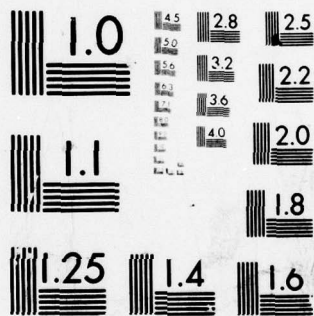
UTRC/R79-922895-25

AFRPL-TR-79-51

NL

2 of 2
AD
A080 037





MICROCOPY RESOLUTION TEST CHART
NATIONAL BUREAU OF STANDARDS-1963-A

The persistence of a large ku value at high temperatures makes NH_3 a more attractive coupling candidate molecule than was heretofore expected.

Coupling Measurements

Introduction

In order to gain insight to the properties of the laser sustained flame in H_2 /water mixtures, measurements were carried out to determine the degree of coupling between the high power laser beam and these mixtures as a function of water concentration and beam power. In order to do away with the problem of condensation within the cell, the latter was kept at temperature higher than the saturator temperature in each case. The range of partial pressures was 20 torr to 180 torr for H_2O and 20 torr to 130 torr for D_2O . In each run, the increase in the centerline temperature determined from the interferometric measurement was used as a measure of the coupling. In the H_2/H_2O measurements the measurements indicated little if any beam-mixture coupling over the entire partial pressure range, and only the results for the H_2/D_2O measurements will be presented. Of the latter, a noteworthy result was the attaining of a very hot, $3900^\circ K$, flame in only one of the runs, at 76 torr partial pressure and 7.1 kW laser power. The $ku(T)$ information obtained in this experiment is shown in Fig. 43. The observed temperature rise in the remaining H_2/D_2O experiments in this series was nearly a factor of ten smaller, even though one of these was carried out at higher D_2O partial pressure, 130 torr, and the same beam power. However, another difference between these two H_2/D_2O experiments was that the former was carried out at a cell temperature $25K^\circ$ cooler than the latter, so that flame creation, like plasma sustaining, is apparently critically dependent on temperature gradients in the high power beam input window and their effect on the quality of the beam to be focused into the gas mixture.

The Measurements

The coupling measurements consisted of noting the change in the axial temperature measured with the interferometer. It is re-emphasized that in only one of the experiments reported on in this section was a laser sustained flame attained presumably because of the input window problem. The remaining measurements are best understood by modeling the laser-beam-mixture interaction region as a heat source of dimension R cooled by buoyancy driven gas flow. The balance between the absorption of energy from the incident laser beam of intensity I by the gas with absorption per cm α resulting in a center line temperature rise ΔT cooled over the dimension R by gas flow of speed V is given by

$$I\alpha = \frac{\rho C_p V \Delta T}{R} \quad (34)$$

If I is given by the ratio of beam power p to its area A , and α is approximated for D_2O in the temperature range from 300 to 1000°K by

$$\alpha = \alpha_0 + \Delta T \partial_\alpha \quad (35)$$

Then the quantity $\alpha_0 P / \Delta T$ is a linear function of P the incident beam power and can be written in the form

$$\frac{\alpha_0 P}{\Delta T} = a^{-1} - P \partial_\alpha \quad (36)$$

where

$$a \equiv \frac{R}{AV_\rho C_p}$$

The absorption per cm of the mixture was measured under pre-run conditions to be 0.026 cm^{-1} at 130 torr D_2O pressure and 368°K, and this value was combined with the experimental values of P and ΔT to calculate $\alpha_0 P / \Delta T$ as a function of P as shown in Fig. 45. The results denoted by the solid points are seen to be consistent with this simple model, giving values of 1.37 cm deg/W and $5.3 \times 10^{-5} \text{ cm}^{-1} \text{ deg}^{-1}$, for a and ∂_α respectively. The lone flame results, denoted by the cross, is seen to fall far from the others due to the much larger ΔT value attained in this experiment.

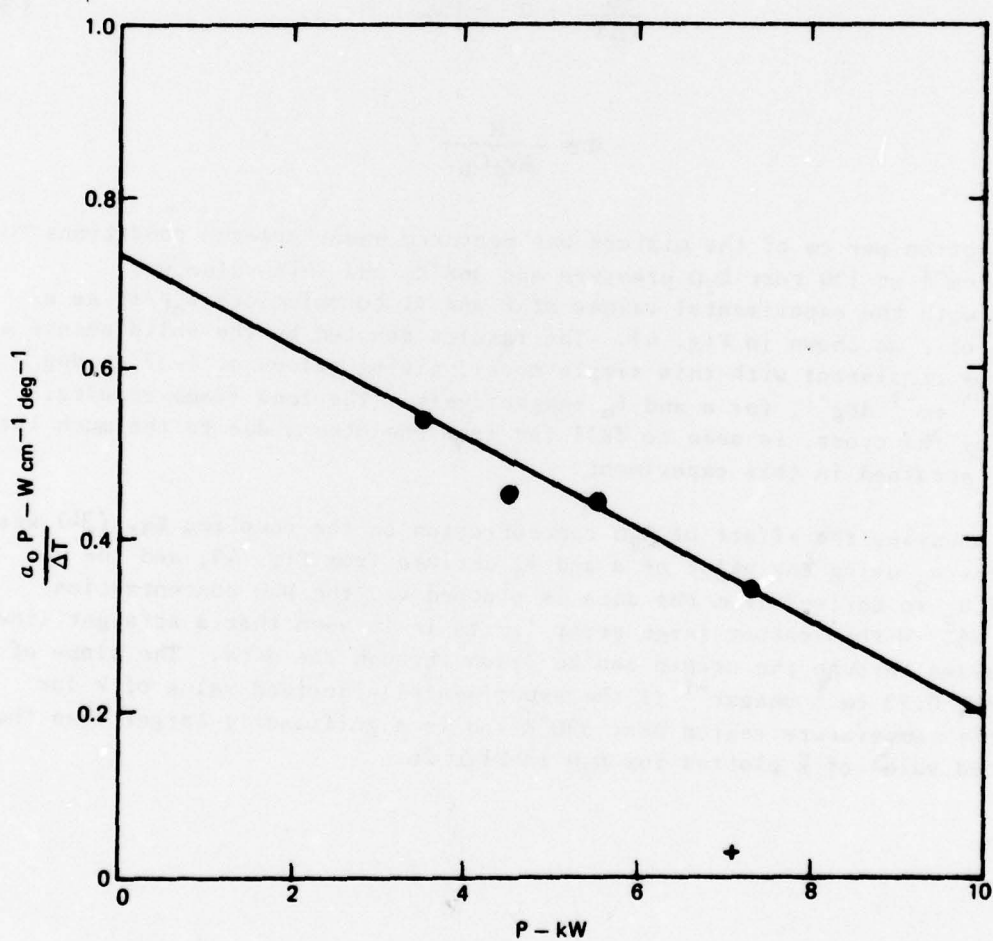
In studying the effect of D_2O concentration on the coupling Eq. (34) was solved for α_0 using the value of a and ∂_α derived from Fig. 45, and the value of α_0 so derived from the data is plotted vs. the D_2O concentration in Fig. 46. Within rather large error limits it is seen that a straight line which passes through the origin can be drawn through the data. The slope of this line, $0.23 \text{ cm}^{-1} \text{ amagat}^{-1}$ is the experimentally derived value of k for D_2O in the temperature region near 330°K and is significantly larger than the calculated value of \bar{k} plotted for D_2O in Fig. 26.

EFFECT OF BEAM POWER ON COUPLING

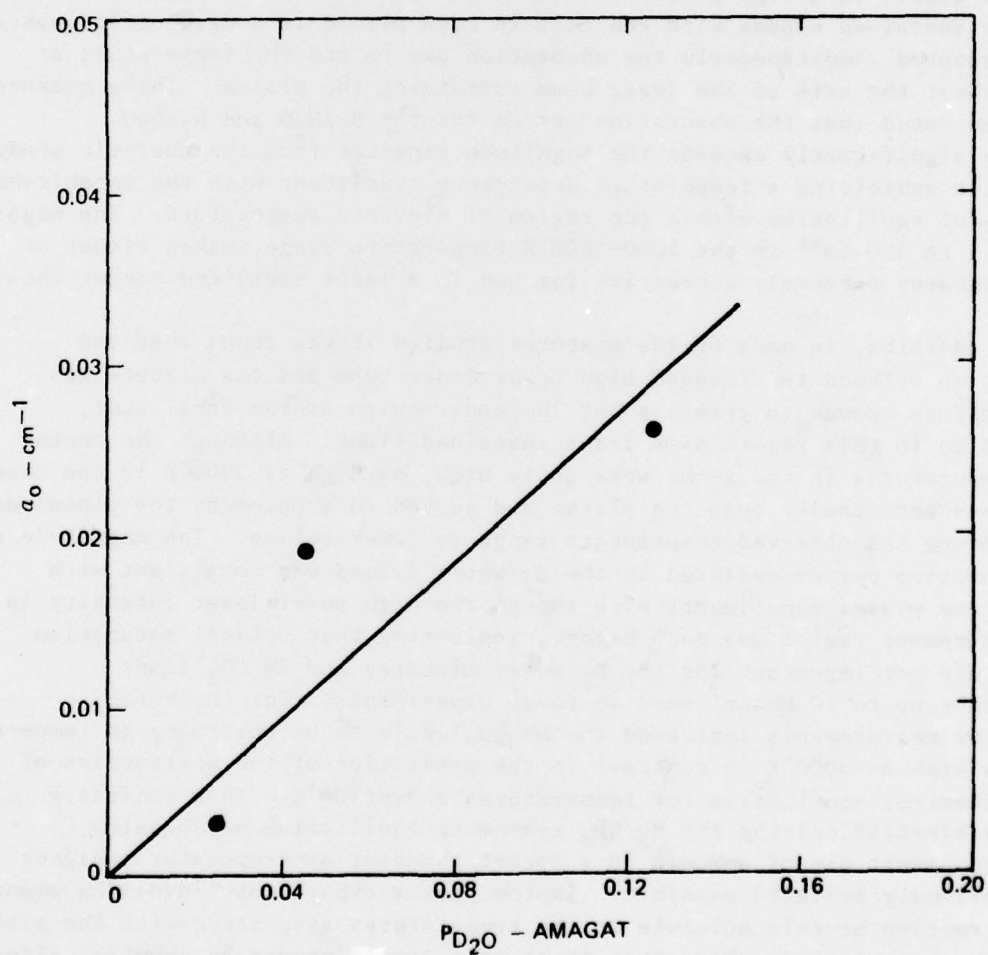
$$\frac{a_0 P}{\Delta T} \text{ vs } P$$

130 TORR D₂O IN 11 ATM H₂

- NO FLAME
- + LASER SUSTAINED FLAME



79-06-12-15

EFFECT OF D₂O PRESSURE ON COUPLING α_0 VS P_{D_2O} 

79-06-12-14

SECTION V

DISCUSSION

Summary of Results

An analytical and experimental program has been carried out to evaluate the usefulness of binary mixtures of hydrogen with H_2O , D_2O and NH_3 for coupling energy transported from a distant source by a laser beam to heat a rocket working fluid. Specifically, the desired information was the temperature dependence of the absorption per cm of these mixtures for temperatures as high as $6000^\circ K$. To obtain this information, the gas mixture under investigation was placed in a high pressure cell in the presence of a hot, $10000-15000^\circ K$, CW laser sustained plasma with the cell in turn placed in a diagnostic apparatus which measured simultaneously the absorption per cm and the temperature at points about the axis of the laser beam sustaining the plasma. These measurements indicated that the absorption per cm for the H_2/H_2O and H_2/D_2O mixtures significantly exceeds the magnitude expected from the analytic study while also exhibiting a temperature dependence consistent with the establishment of chemical equilibrium within the region of elevated temperature. The magnitude, 0.1 to 1.0 cm^{-1} in the $1000-5000^\circ K$ temperature range, makes either of these mixtures extremely attractive for use in a laser energized rocket thruster.

In addition, in each of the mixtures studied it was found that the interaction between the focused high power laser beam and the mixture was often intense enough to create a hot luminous region at the focal spot, referred to in this report as a laser sustained flame. Although the center line temperatures in the flame were quite high, as high as $3900^\circ K$ in one case, the flames were cooler than the plasma and served to supplement the plasma data by extending the observed temperature range to lower values. The magnitude of the absorption per cm measured in the H_2 /water flames was consistent with that in the plasma experiments even though the high power laser intensity in the measurement region was much higher, indicating that optical saturation effects are not important for the H_2 /water mixtures and CW CO_2 laser intensities up to 10 MW/cm^2 used in these experiments. For the H_2/NH_3 flame, the measurements indicated the NH_3 molecule to be absorbing at temperatures as high as $3000^\circ K$ in contrast to the prediction of the destruction of NH_3 at chemical equilibrium for temperatures above $500^\circ K$. This indicates that the kinetics driving the H_2/NH_3 system to equilibrium may be slow enough to permit use of ammonia in a rocket thruster at temperatures higher than previously believed possible. In the plasma experiments involving ammonia, the destruction of this molecule at the temperatures associated with the plasma was very apparent, indicating that there is a limit imposed by chemical effects on the usefulness of NH_3 .

Unknown Flame Properties

One of the more interesting results of this study is the observation of the ability of the high power laser beam to raise the temperature of the mixture under study to a level useful in a laser energized rocket thruster. Very little is known about the ease with which such flames are made. It is known that for a focal spot diameter of about 0.01 cm, flames can be created in H_2/H_2O , H_2/D_2O and H_2/NH_3 mixtures with 7 kW of laser power. However, there is evidence, described in Section IV, that if the laser beam quality is decreased, e.g., by distortion on passing through the cell window, and the focal spot diameter becomes larger, creation of the flame is more difficult. This problem was also encountered in sustaining plasma with laser radiation, and one is therefore led to the conclusion that just as the laser power needed to create and sustain plasma in gases exhibits a beam diameter dependence,⁴³ so will the power needed to create and sustain a flame. Put another way, it is not clear that just because 7 kW focused into a spot 10^{-3} cm² in area will create a flame, 7 MW focused into a spot 1 cm² in area will do the same even though the intensity is the same in both cases. Other questions of interest concern the beam diameter at which the time needed for NH_3 destruction is exceeded by the diffusion lifetime of NH_3 inside the beam, and the possibility that the beam power needed to create a flame in H_2/H_2O might be lowered by the addition of a NH_3 "Priming charge" to bring the H_2O absorption per cm high enough to permit ignition of the H_2O flame.

In any event, the discovery of the H_2O laser sustained flame was an unexpected result of this Air Force sponsored research program and one which might prove extremely valuable in the area of laser energized rocket thrusters.

REFERENCES

1. S. Gordon and B. J. McBride: "Computer Program for Calculation of Complex Chemical Equilibrium Compositions, Rocket Performance, Incident and Reflected Shocks, and Chapman-Jouguet Detonations" NASA SP-273 (1971).
2. W. Malkmus: "Intensities of Pure Rotational Band Systems of Symmetric Top Molecules" J. Quant. Spect. and Rad. Trans. 5, 621 (1965).
3. C. B. Ludwig and W. Malkmus: "Handbook of Infrared Radiation from Combustion Gases" NASA SP-3080 (1973).
4. C. B. Ludwig: "Measurements of the Curves of Growth of Hot Water Vapor" App. Opt. 1057 (1971).
5. S. S. Penner: "Quantitative Molecular Spectroscopy and Gas Emissivities" (Addison-Wesley, Reading MA 1959) p. 275 ff.
6. C. R. Noller: "Chemistry of Organic Compounds" (W. B. Saunders Company, Philadelphia, 1957) p. 83.
7. R. A. McClatchey, W. S. Benedict, S. A. Clough, D. E. Burch, R. F. Calfee, K. Fox, L. S. Rothman and J. S. Garing: "AFCRL Atmospheric Absorption Line Parameters Compilation". AFCRL-TR-73-0096 (1973).
8. N. Davidson: "Statistical Mechanics". (McGraw Hill NY 1962) p. 116-123.
9. G. Herzberg: "Molecular Spectra and Molecular Structure". (D. Van Nostrand Co. Inc., Princeton, 1950) 2nd ed., Vol. I, p. 522.
10. R. A. Toth: J. Mol. Spectry, 40, 605 (1971).
11. G. E. Caledonia, P. K. Wu and A. N. Pirri: "Radiant Energy Absorption Studies for Laser Propulsion". NASA CR-134809.
12. R. C. Millikan and D. R. White: "Systematics of Vibrational Relaxation". J. Chem. Phys., 39, 3209 (1963).
13. G. Herzberg: Op. Cit. Vol. II, pp. 42-60.
14. W. S. Benedict, H. H. Claassen and J. H. Shaw: "Absorption Spectrum of Water Vapor Between 4.5 and 13 μ ". J. Res. Nat'l. Bur. Std. (U.S.), 49, 91 (1952).

REFERENCES (Cont'd)

15. N. Ginsburg: "Additional Rotational Energy Levels of H_2O and D_2O molecules. Phys. Rev., 74A, 1052 (1948).
16. J. H. Taylor, W. S. Benedict and J. Strong: "Infrared Spectra of H_2O and CO_2 at 500° ". J. Chem. Phys., 20, 1884 (1952).
17. P. E. Fraley and K. N. Rao: "High Resolution Infrared Spectra of Water Vapor: ν_1 and ν_2 Bands of H_2O ". J. Mol. Spectry, 29, 348 (1969).
18. G. Herzberg: Op. Cit., Vol. II, p. 506.
19. W. S. Benedict, N. Gailor and E. K. Plyler: "Rotation Vibration Spectra of Deuterated Water Vapor". J. Chem. Phys., 24, 1139 (1965).
20. P. F. Wacker and M. R. Pratto: "Microwave Spectral Table-Line Strengths of Asymmetric Rotors". NBS Monograph 70, Vol. II, (1964).
21. R. Herman and R. F. Wallis: "Influence of Vibration-Rotation Interaction on Line Intensities in Vibration-Rotation Bands of Diatomic Molecules". J. Chem. Phys. 23, 637 (1955).
22. W. S. Benedict and L. D. Kaplan: "Calculation of Line Width in H_2O-N_2 Collisions". J. Chem. Phys., 30, 388 (1959).
23. W. S. Benedict and L. D. Kaplan: "Calculation of Line Widths in H_2O-H_2O and H_2O-O_2 Collisions". J. Quant. Spect. and Rad. Trans., 4, 453 (1964).
24. F. A. Blum, K. W. Nill, P. L. Kelley, A. P. Calawa and T. C. Harman: "Tunable Infrared Laser Spectroscopy of Atmospheric Water Vapor". Science 177, 694 (1972).
25. R. A. McClatchey and J. E. A. Selby: "Atmospheric Attenuation of Laser Radiation From 0.76 to $31.25 \mu m$ ". AFCRL-TR-74-0003 (1974).
26. G. Herzberg: Op. Cit. Vol. I, p. 560.
27. Ibid, p. 208.
28. G. Dixon Lewis, M. M. Sutton, and A. Williams. The Kinetics of Hydrogen Atom Recombination". Discussions Faraday Soc. 33, 205 (1962).

REFERENCES (Cont'd)

29. W. S. Benedict, N. Gailor and E. K. Plyler: "Rotation Vibration Spectra of Deuterated Water Vapor". J. Chem. Phys., 24, 1139 (1956).
30. D. W. Posner and M. W. P. Strandberg: "Centrifugal Distortion in Asymmetric Top Molecules III H_2O , D_2O and HDO ". Phys. Rev., 95, 374 (1959).
31. N. Fuson, H. M. Randall and D. M. Dennison: "The Far Infrared Absorption Spectrum and The Rotational Structure of the Heavy Water Molecule." Phys. Rev. 56, 989 (1939).
32. F. P. Dickey and J. M. Hoffman: "Vibration-Rotation Band ν_2 of Heavy Water Vapor." J. Chem. Phys., 23, 1718 (1955).
33. F. W. Taylor: "Spectral Data for the ν_2 Bands of Ammonia With Applications to Radiative Transfer in the Atmosphere of Jupiter." J. Quant. Spect. Rad. Trans., 13, 1181 (1973).
34. Huddleston, R. H., and S. L. Leonard: Plasma Diagnostic Techniques. p. 431 ff.
35. Tektronix. TEK SPS Basic Software System Vol. CP85871 Instruction Manual. 1976, TEK SPS Basic Graphic Package Vol. CP91271 Instruction Manual. 1976, TEK SPS Basic DPO Driver Package Vol. CP71171 Instruction Manual. 1976, The ABC's of TEK Basic Instruction Manual. 1974.
36. Hirschfelder, J. O., C. F. Curtis, and R. B. Bird: Molecular Theory of Gases and Liquids. (John Wiley and Sons, Inc., New York, 1954). p. 882.
37. Griem, H. R.: Plasma Spectroscopy (McGraw-Hill, New York 1964) p. 176.
38. Hirschfelder, J. O., et al. op cit, p. 950.
39. Nesbet, R. K.: Atomic Polarizabilities for Ground and Excited States of C, N, and O. Phys. Rev. A. 16, 1 (1971).
40. Stillinger, F. H.: Theory and Molecular Models for Water in Non-Simple Liquids. I. Prigogine and S. A. Rice eds. (John Wiley & Sons, New York, 1975) p. 1.

REFERENCES (Cont'd)

41. Krascella, N. L.: Theoretical Investigation of the Spectral Opacities of Hydrogen and Nuclear Fuel. AFSCR RTD-TDR-63-110 (1963).
42. Smith, D. C., and J. H. McCoy: Effects of Diffusion on the Saturation Intensity in a CO₂ Laser, Appl. Phys. Letters 15 282 (1969). C. P. Christensen, C. Freed, and H. A. Haus, Gain Saturation and Diffusion in CO₂ Lasers, IEEE J. Quantum Electron. QE5, 276 (1969).
43. Smith, D. C., and M. C. Fowler: Ignition and Maintenance of a cw Plasma in Atmospheric Pressure Air with CO₂ Laser Radiation. Appl. Phys. Letters 22 500 (1973).
44. M. L. Bhaumik: Carbon Monoxide Laser Studies Final Report: Part I. NCL-31R (1971).

APPENDIX A

CARBON MONOXIDE LASER LIGHT SOURCE

The carbon monoxide laser, which was to be used as the diagnostic light source at frequencies near 2000 cm^{-1} , was built largely based on the work described in Ref. 44. The laser cavity itself was approximately 2.2 meters in length, with a 10 m radius of curvature gold-coated copper high reflectivity mirror, and a flat germanium 95 percent reflectance mirror output coupler. The active medium was an electric discharge, powered by current regulated power supplies, in a gas mixture of approximately 16 torr pressure containing helium, carbon monoxide, nitrogen, and oxygen in the ratio of 1500 : 40 : 40 : 1. The helium was passed through a coil of copper tubing immersed in liquid nitrogen to freeze out any water in the helium prior to entering the discharge region. The discharge tube had two identical sections made from pyrex and joined in the middle by a short pyrex cross which held the gas outlet as well as the common cathode to each section's discharge. The inside diameter of the discharge tubes was $3/4$ in. The active medium was sealed at each end with water cooled calcium fluoride windows mounted at Brewster's Angle, and the region between each window and cavity mirror was continually flushed with dry nitrogen to drive out water vapor which, if left in the cavity, absorbed cavity radiation, thereby becoming thermally and optically inhomogeneous and causing the laser output to be both temporally unstable and diminished with respect to both output and beam quality. The laser could be operated both at ambient temperature, with water cooling, and cryogenic temperature with liquid nitrogen cooling. The cooling jackets for each discharge section were approximately 75 cm long with a metal bellows blown into the middle of the outer wall of the jacket. The purpose of the bellows was to relieve stress caused by the difference of length which was assumed by the inner wall of the cooling jacket at liquid nitrogen temperature compared to the outer wall which, of course, assumed some temperature between liquid nitrogen and ambient. Experience showed that cracking of the jackets routinely occurred in the absence of the bellows. The inter-wall distance in the jackets was 1.6 cm. It was found that such a large distance was necessary to have the discharge tube completely immersed in the liquid nitrogen while leaving enough free space at the top of the jacket to allow nitrogen vapor to collect and exhaust without causing wave formation in the liquid nitrogen which resulted, at smaller inter-wall spacings, in blowing liquid nitrogen out of the exhaust port. With water cooling, the multiline output of the laser was as high as 20 watts, with 13 watts being obtained routinely over hour-long periods. With liquid nitrogen, 70 watts of multiline output power were obtained.

APPENDIX B

COMPUTER PROGRAM "STOR2"

```

2 REM N IS ARRAY TRACE NUMBER--NUMERIC
3 LET N=0
4 REM R$ IS RUN NUMBER--SPELLED OUT
5 PRINT "INPUT RUN NUMBER; THEN 'RETURN'"
6 INPUT R$
10 LOAD "DPO"
20 ATTACH #2 AS DPO
25 WHEN #2 HAS "CB1" GOSUB 40
26 RETURN
40 PUT "PI" INTO #2
42 PAGE
43 LET N$=STR(N)
44 LET RN$=R$&N$
46 OPEN #1 AS DX1:RN$ FOR WRITE
50 PRINT "INPUT WAVEFORM TO VERTICAL PLUG-IN, WAVEFORMS MUST SPAN 10 DIVS
60 PRINT "UNGROUND PROBE AND ADJUST KNOBS FOR PROPER SENSITIVITY"
70 PRINT "PRESS 'RETURN' WHEN READY"
80 WAIT
85 PAGE
90 WAVEFORM WA IS A(511),HA,HA$,UA$
100 PUT "STO" INTO #2,"A"
110 PUT "MEM" INTO #2
120 PUT "ZHO" INTO #2,"A"
130 PRINT "TO ACQUIRE GROUND-REFERENCE LEVEL, GROUND PLUG-IN"
140 PRINT "PRESS 'PROG CALL' BUTTON 14 ON DPO-PRESS 'RETURN' WHEN READY"
150 WAIT
155 PAGE
170 PRINT "TO ACQUIRE AVE WAVEFORM, UNGROUND PLUG-IN"
180 PRINT "PRESS 'RETURN' WHEN READY"
190 WAIT
195 PAGE
196 PUT "STO" INTO #2,"A"
197 PUT "MEM" INTO #2
200 GET WA FROM #2,"AVE20,A"

```

210 GRAPH WA
211 WRITE #1, WA
212 CLOSE #1
213 LET N=N+1
230 RETURN

READY
*

APPENDIX C

COMPUTER PROGRAM "RED5"


```

8 DIM MB(511)
9 DIM MAX(511),WZ(511)
10 INPUT Z$
20 OPEN #1 AS DX1:Z$ FOR READ
30 READ #1,WZ
40 CLOSE #1
50 INPUT A$
60 OPEN #1 AS DX1:A$ FOR READ
70 READ #1,WA
71 CLOSE #1
80 PAGE
90 GRAPH WZ(0:100)
100 WAIT
110 PAGE
120 GRAPH MAX(0:100)
130 WAIT
140 PAGE
150 INPUT A,B,C,D,E
160 FOR I=A TO B STEP C
170 MB(I)=MAX I+D)*E
180 NEXT I
185 GOTO 3000
190 PAGE
200 GRAPH MB,WZ
201 WAIT
202 PAGE
210 INPUT J
220 IF J=0 THEN GOSUB 1000
229 GOSUB 2000
230 OPEN #1 AS DX1:B$ FOR WRITE
240 WRITE #1,MB
250 CLOSE #1
300 END
1000 INPUT DE

```

```

1010 MB=MB+DE
1015 PAGE
1020 GOTO 200
1030 RETURN
2000 MB=MB-MZ
2010 GRAPH MB
2020 INPUT B$
2030 RETURN
3000 GRAPH MB(360:509)
3010 WAIT
3020 PAGE
3030 INPUT IB,UB
3040 FOR I=0 TO 511
3050 MB(I)=MB(I)-UB*COB(243.14159*((IB-I)/167.5))
3060 NEXT I
3070 GOTO 190

READY
*
```

APPENDIX D

COMPUTER PROGRAM "DAL1"

```

10 DIM A(511),B(511),C(511),D(511)
20 INPUT A$,B$,C$,D$
30 OPEN #1 AS DX1:A$ FOR READ
40 READ #1,A
50 CLOSE #1
60 OPEN #1 AS DX1:B$ FOR READ
70 READ #1,B
80 CLOSE #1
90 OPEN #1 AS DX1:C$ FOR READ
100 READ #1,C
110 CLOSE #1
120 OPEN #1 AS DX1:D$ FOR READ
130 READ #1,D
140 CLOSE #1
149 PAGE
150 GRAPH A,B,C,D
151 WAIT
160 E=LOG(A/B)*LOG(C/D)
170 PAGE
179 DELETE A,B,C,D
180 GRAPH E
190 INPUT N
200 IF N=0 THEN GOTO 300
210 INPUT R$
220 OPEN #1 AS DX1:R$ FOR WRITE
230 WRITE #1,E
240 CLOSE #1
250 GOTO 400
300 DELETE 150
310 GOTO 30
400 END

```

READY
*

APPENDIX E

COMPUTER PROGRAM "P"

```

10 DIM A(511),B(511),C(511),D(511)
20 INPUT A$,B$,C$,D$
30 OPEN #1 AS DX1:A$ FOR READ
40 READ #1,A
50 CLOSE #1
60 OPEN #1 AS DX1:B$ FOR READ
70 READ #1,B
80 CLOSE #1
90 OPEN #1 AS DX1:C$ FOR READ
100 READ #1,C
110 CLOSE #1
120 PAGE
130 GRAPH A,B,C
139 WAIT
140  $D = (A - B - C) / (2 * \text{SQR}(B * C))$ 
150 PAGE
160 GRAPH D
161 WAIT
162 PAGE
170 INPUT M
180 IF M=0 THEN GOTO 300
190 OPEN #1 AS DX1:D$ FOR WRITE
200 WRITE #1,D
210 CLOSE #1
300 END

```

READY
*

APPENDIX F

COMPUTER PROGRAM "DRED4"

```

10 DIM A(500),B(500),WA(511),AX(511)
15 PI=3.14159
16 X=-PI
20 FOR I=0 TO 500
30 A(I)=X
40 B(I)=COS(X)
45 X=X+PI/500
50 NEXT I
60 INPUT R$
65 WA=0
66 AX=0
70 OPEN #1 AS DX1:R$ FOR READ
80 READ #1,WA
89 PAGE
90 CLOSE #1
91 GRAPH WA
92 WAIT
100 INPUT MN,MX
120 FOR I=MN TO MX
121 IF ABS(WA(I))>1 THEN GOTO 127
122 IF WA(I)>0 THEN GOTO 125
123 AX(I)=-PI
124 GOTO 170
125 AX(I)=0
126 GOTO 170
127 FOR J=0 TO 500
130 IF ABS(WA(I)-B(J))<5E-03 THEN GOTO 150
140 NEXT J
150 AX(I)=AX(J)
170 NEXT I
178 PAGE
179 PRINT R$
180 GRAPH WA,AX
181 WAIT

```



```
190 INPUT S$  
200 OPEN #1 AS DX1:S$ FOR WRITE  
210 WRITE #1,AX  
220 CLOSE #1  
230 END
```

```
READY  
*
```

APPENDIX C

COMPUTER PROGRAM "CH00S2"

```

9 DIM S(511),R(511)
10 INPUT S$,R$
15 OPEN #1 AS DX1:S$ FOR READ
20 READ #1,S
30 CLOSE #1
35 WAIT
40 OPEN #1 AS DX1:R$ FOR READ
50 READ #1,R
60 CLOSE #1
61 PAGE
62 GRAPH S,R
63 WAIT
70 PAGE
80 PRINT "                ",S$
90 GRAPH S
100 WAIT
110 PAGE
120 PRINT "                ",R$
130 GRAPH R
140 WAIT
141 PAGE
150 D=S-R
160 PRINT "                ",S$,"-",R$
170 GRAPH D
180 WAIT
181 PAGE
190 D=R-S
200 PRINT "                ",R$,"-",S$
210 GRAPH D
220 WAIT
221 PAGE
230 D=S+R
240 PRINT "                ",S$,"+",R$
250 GRAPH D

```

```

260 WAIT
261 PAGE
270 D=-D
280 PRINT "      -",S$,"-",R$
290 GRAPH D
300 WAIT
310 PAGE
320 INPUT M
330 IF M=0 THEN GOTO 500
340 INPUT T$
350 OPEN #1 AS DX1:T$ FOR WRITE
360 WRITE #1,D
370 CLOSE #1
380 END

```

```

READY
*
```


APPENDIX H

COMPUTER PROGRAM "MASAG5"

```

1 REM DATA SMOOTHING ROUTINE "MASAG"
9 DIM WAX(511),WBX(511),WC(511),WDX(511),AX(9,10)
10 INPUT R$,S$
20 GOSUB 2000
21 GRAPH WB
22 WAIT
24 GRAPH WA
25 INPUT MN,MX
30 GRAPH WAX(MN:MX)
40 INPUT SA
50 IF SA=1 THEN 110
51 WC=0
52 WD=0
60 INPUT JA
70 GOSUB 3000
80 DISPLAY 1,WC(MN:MX)
90 INPUT SA
100 GOTO 50
110 WA=0
111 WB=0
113 GOSUB 4000
2000 OPEN #1 AS DX1:R$ FOR READ
2001 EOF #1 GOTO 2020
2002 READ #1,WA
2003 CLOSE #1
2025 GOSUB 5000
2030 RETURN
3000 FOR J=MN TO MX STEP JA+1
3001 WC(J)=0
3002 WDX(J)=0
3004 CH=0
3005 FOR I=J TO J+JA
3006 CH=CH+WAX(I)
3008 NEXT I

```

```

3009 WC(J+JA/2)=CW/(JA+1)
3010 WD(J+JA/2)=WB(J+JA/2)
3020 NEXT J
3030 RETURN
4000 REM
4020 II=0
4030 FOR I=MN TO MX
4040 IF WC(I)=0 THEN 4080
4050 WA(II)=WC(I)
4060 WB(II)=WD(I)
4061 PRINT WA(II),WB(II),II
4070 II=II+1
4080 NEXT I
4090 INPUT K0,JJ
4091 REM 2*JJ IS THE LARGEST POWER OF Y
4092 REM JJ<=0 AS DEFINED BY DIMA)
4093 A=0
4100 FOR I=1 TO JJ+1
4110 FOR J=1 TO JJ+2
4120 FOR K=K0 TO II-1
4121 IF J=JJ+2 THEN 4141
4130 A(I,J)=A(I,J)+ABS(WB(K))*^(2*(I+J-2))
4132 GOTO 4150
4141 A(I,J)=A(I,J)+WA(K)*ABS(WB(K))*^(2*I-2)
4150 NEXT K
4160 NEXT J
4170 NEXT I
4175 NN=JJ+1
4179 FOR I=1 TO JJ+1
4180 XM=ABS(A(I,I))
4200 L=I
4210 KK=I+1
4220 FOR K=KK TO NN
4230 IF XM>ABS(A(K,I)) THEN 4260
4240 XM=ABS(A(K,I))

```

```

4250 L=K
4260 NEXT K
4270 FOR J=1 TO NN+1
4280 B=X(I,J)
4290 X(I,J)=X(L,J)
4300 X(L,J)=B
4310 NEXT J
4320 M=NN+1
4330 X(I,M)=X(I,M)/X(I,I)
4340 IF M=I THEN 4370
4350 M=M-1
4360 GOTO 4330
4370 IF I<=1 THEN 4400
4380 N=1
4390 GOTO 4440
4400 N=I
4410 N=N+1
4420 IF N=I THEN 4410
4430 IF N>NN THEN 4490
4440 M=NN+1
4450 X(N,M)=X(N,M)-X(N,I)*X(I,M)
4460 IF M=I THEN 4410
4470 M=M-1
4480 GOTO 4450
4490 NEXT I
4500 PRINT X(1:JJ+1, JJ+2)
4509 INPUT MK
4510 FOR I=K0 TO MK
4520 MC(I)=0
4530 FOR J=1 TO JJ+1
4540 MC(I)=MC(I)+X(J, JJ+2)*ABS(X(I,J))^(2*J-2)
4550 NEXT J
4551 PRINT MC(I), MB(I)
4560 NEXT I
4565 PRINT R0, " US ", S0, " MN=", MN, " MX=", MX, " AVERAGED IN ", JA, " S"

```



```

4570 WAIT
4575 GRAPH WC(MN:MX)
4580 WAIT
4583 GOSUB 5000
4585 FOR I=MN TO MX
4590 WC(I)=0
4595 FOR J=1 TO JJ+1
4600 WC(I)=WC(I)+AK(J,JJ+2)*ABS(WX(I))^(2*J-2)
4605 NEXT J
4610 NEXT I
4624 PRINT "MAKE SURE RIGHT DISC IS IN DX1"
4625 WAIT
4626 GOSUB 2000
4627 PRINT AK(1:JJ+1,JJ+2)
4628 WC(213)=AK(1,JJ+2)
4630 GRAPH WAK(MN:MX),WC(MN:MX)
4635 WAIT
4640 END
5000 FOR I=511 TO 0 STEP -1
5010 WX(I)=5.35E-03*(I-213)
5020 NEXT I
5030 RETURN

```

```

READY
*

```

APPENDIX I

COMPUTER PROGRAM "ABEL8"

```

5 DIM R(101),AL(101),T(101),TT(101)
6 DIM A(7),P(7),C(7,7),L(7),HK(7)
7 DIM AA(7)
10 INPUT T0,P0,PP,A,RA,P,RP
11 AA=A
15 INPUT RN,RX
17 PI=3.14159
18 R(0)=RN
20 FOR I=0 TO 10
21 M=0
22 Z=RA
25 X=SQR(Z^2-R(I)^2)
30 GOSUB 1000
31 FOR J=1 TO 7
32 L(J)=-X^(2*J-1)/PI
33 NEXT J
34 GOSUB 2000
35 Z=RP
36 X=SQR(Z^2-R(I)^2)
37 FOR J=1 TO 7
38 HK(J)=-X^(2*J-1)/PI
39 NEXT J
40 GOSUB 1000
41 GOSUB 3000
45 T(I)=2.68E-03*RN+5.8E-03*P0/T0
46 GOSUB 4000
47 R(I+1)=R(I)*(RX-RN)/10
48 A=AA
50 NEXT I
53 PRINT T0,P0,PP,A,RA,P,RP
55 FOR I=0 TO 10
56 PRINT R(I),AL(I),T(I),TT(I)
60 NEXT I
62 WAIT

```

```

63 PAGE
65 GRAPH AL(0:10)
66 WAIT
67 PAGE
70 GRAPH T(0:10)
72 WAIT
73 PAGE
75 GRAPH TT(0:10)
80 WAIT
85 END
1000 C=0
1001 IF M=0 THEN 1008
1002 A=P
1008 M=1
1009 FOR J=1 TO 7
1010 C(J,1)=Z^(2*J-2)*AK(J)*2*J
1015 IF J=1 THEN GOTO 1612
1020 IF J=2 THEN GOTO 1522
1030 IF J=3 THEN GOTO 1432
1040 IF J=4 THEN GOTO 1342
1050 IF J=5 THEN GOTO 1252
1060 IF J=6 THEN GOTO 1162
1072 C(7,2)=-4*Z^10*AK(7)*14
1073 C(7,3)=8*Z^8*AK(7)*14
1074 C(7,4)=-64/7*Z^6*AK(7)*14
1075 C(7,5)=384/63*Z^4*AK(7)*14
1076 C(7,6)=-512/231*Z^2*AK(7)*14
1077 C(7,7)=3872/9009*AK(7)*14
1078 GOTO 1612
1162 C(6,2)=-10/3*Z^8*AK(6)*12
1163 C(6,3)=16/3*Z^6*AK(6)*12
1164 C(6,4)=-32/7*Z^4*AK(6)*12
1165 C(6,5)=128/63*Z^2*AK(6)*12
1166 C(6,6)=-256/693*AK(6)*12
1167 GOTO 1612

```



```

1252 C(5,2)=-8/3*Z^6*A(5)*10
1253 C(5,3)=16/5*Z^4*A(5)*10
1254 C(5,4)=-64/35*Z^2*A(5)*10
1255 C(5,5)=128/315*A(5)*10
1256 GOTO 1612
1342 C(4,2)=-6/3*Z^4*A(4)*8
1343 C(4,3)=8/5*Z^2*A(4)*8
1344 C(4,4)=-16/35*A(4)*8
1345 GOTO 1612
1432 C(3,2)=-4/3*Z^2*A(3)*6
1433 C(3,3)=8/15*A(3)*6
1434 GOTO 1612
1522 C(2,2)=-2/3*A(2)*4
1523 GOTO 1612
1612 NEXT J
1613 RETURN
2800 AL(I)=0
2801 FOR J=1 TO 7
2810 FOR K=1 TO 7
2820 AL(I)=AL(I)+L(K)*C(J,K)
2830 NEXT K
2840 NEXT J
2850 RETURN
3800 N=0
3801 FOR J=1 TO 7
3810 FOR K=1 TO 7
3820 N=N+K*K)*C(J,K)
3830 NEXT K
3840 NEXT J
3850 RETURN
4800 TT(I)=6.277E-03*PP/T(I)
4810 IF TT(I)*3800 THEN GOTO 4890
4820 TT(I)=4.985E-03*PP/T(I)
4830 IF TT(I)>4500 THEN GOTO 4890
4840 TT(I)=0

```

4090 RETURN

READY
*